Optical Three-Dimensional Image Matching using Holographic Information

by

Taegeun Kim

Dissertation submitted to the Faculty of
Virginia Polytechnic Institute and State University
in partial fulfillment of the requirements for the degree of

Doctor of Philosophy
in
Electrical and Computer Engineering

Dr. Ting-Chung Poon, Chairman

Dr. A. Lynn Abbott

Dr. Ioannis M. Besieris

Dr. Leonard A. Ferrari

Dr. Guy Indebetouw

July 19, 2000

Blacksburg, Virginia

Keywords: 3-D image recognition, Optical Scanning Holography, Holographic correlation, Phase-only holographic information

Optical Three-Dimensional Image Matching using Holographic Information

by

Taegeun Kim

Ting-Chung Poon, Chairman

Electrical and Computer Engineering Department

(ABSTRACT)

We present a three-dimensional (3-D) optical image matching technique and location extraction techniques of matched 3-D objects for optical pattern recognition. We first describe the 3-D matching technique based on two-pupil optical heterodyne scanning. A hologram of the 3-D reference object is first created and then represented as one pupil function with the other pupil function being a delta function. The superposition of each beam modulated by the two pupils generates a scanning beam pattern. This beam pattern scans the 3-D target object to be recognized. The output of the scanning system gives out the 2-D correlation of the hologram of the reference object and that of the target object. When the 3-D image of the target object is matched with that of the reference object, the output of the system generates a strong correlation peak. This theory of 3-D holographic matching is analyzed in terms of two-pupil optical scanning. Computer simulation and optical experiment results are presented to reinforce the developed theory.

The second part of the research concerns the extraction of the location of a 3-D image matched object. The proposed system basically performs a correlation of the hologram of a 3-D reference object and that of a 3-D target object, and hence 3-D matching is possible. However, the system does not give out the depth location of matched 3-D target objects

directly because the correlation of holograms is a 2-D correlation and hence not 3-D shift invariant. We propose two methods to extract the location of matched 3-D objects directly from the correlation output of the system. One method is to use the optical system that focuses the output correlation pattern along depth and arrives at the 3-D location at the focused location. However, this technique has a drawback in that only the location of 3-D targets that are farther away from the 3-D reference object can be extracted. Thus, in this research, we propose another method in which the extraction of a location for a matched 3-D object is possible without the aforementioned drawback. This method applies the Wigner distribution to the power fringe-adjusted filtered correlation output to extract the 3-D location of a matched object. We analyze the proposed method and present computer simulation and optical experiment results.

Acknowledgments

I wish to express my sincere thanks to my advisor, Dr. Ting-Chung Poon for his guidance, support and encouragement throughout my graduate studies. Special thanks also to Dr. Guy J. Indebetouw for his insightful comments and discussions of my graduate studies. Thanks also goes to Dr. A. Lynn Abbott, Dr. Ioannis M. Besieris and Dr. Leonard A. Ferrari for graciously serving on my Ph.D. advisory committee.

Many people have helped me throughout my program of study. I wish to thank to my fellow graduate students at the Optical Image Processing Laboratory, Virginia Tech for their advice, consultation and lasting friendships.

Finally, I wish to thank to my parents (Pyung Kwang Kim, Ae Sook Kim), sister (Jae Hee Kim) and grandmother (Soon Lim Cho) for their endless support and encouragement.

This research is supported by the National Science Foundation (ECS-9810158). Material support was also provided by Hamamatsu Corporation and Hamamatsu Photonics.

Table of Contents

List of Figures

List of Tables

Chapter 1: Introduction

The main objective of this research is to investigate a three-dimensional (3-D) image matching technique and two methods for extracting locations of pattern-matched objects [1,2,3,4]. 3-D pattern recognition has been one of the most challenging problems in the pattern recognition area, due to the desires to endow pattern recognition systems with robust visual capabilities and a variety of applications [5]. Our real spatial world is 3-D, and thus 3-D information about objects can give a pattern recognition system more robust visual capabilities. 3-D pattern recognition finds a variety of applications in the areas of industrial inspections, 3-D microscopy, medical imaging and recognition, robotics vision, 3-D data acquisition and processing, and optical remote sensing [5,6].

Matching two images and learning the location of a pattern-matched object are two essential roles of correlation in various schemes of pattern recognition [7,8,9] and target tracking [8,10]. These two essential operations in two-dimensional (2-D) pattern recognition have been achieved by conventional optical correlation, rooted in the 1960's [11,12]. Two-dimensional pattern recognition has been rejuvenated in the past decades due to the advancement of the development of spatial light modulators [13]. However, matching 3-D images and extracting the 3-D location of the 3-D image-matched object is still difficult, which makes the pattern recognition and target tracking in 3-D space remain formidable tasks.

For a higher order correlation operation, trans-dimensional mapping and matching the dimension-reduced signals has been proposed [14]. Especially for 3-D correlation, 3-D to 2-D planar encoding and matching was proposed [15]. However, these two proposed techniques are restricted to 3-D correlation of the given 3-D information of objects, and require a lot of 2-D sampling images for high resolution performance. In 3-D image recognition, the extraction of 3-D information about objects is another critical issue because conventional imaging systems are restricted to two dimensions. Most recently, an

interesting idea for 3-D correlation has been proposed, in which 3-D information about an object is extracted by moving a CCD camera transversely. The 3-D information is processed by 2-D optical Fourier transformations. However, this proposed technique also requires many 2-D images and a 3-D discrete Fourier transformation [16].

The difficulties of matching a 3-D object and learning its location are due mainly to visual systems that are restricted to the sensing and processing of information which can be displayed as 2-D projections [5]. In this research, we propose an optical technique based on two-pupil optical heterodyne scanning in which the proposed optical system can sense 3-D information about objects as a form of holographic information, and processes the 3-D information by performing essentially the correlation of two pieces of holographic information pertaining to two 3-D objects, a 3-D reference object and a 3-D target object to be matched. In the technique, there is no need to record 2-D images for 3-D object representation because the depth information about an object is contained as a form of fringe pattern on the hologram. 3-D matching is achieved only by 2-D optical correlation of holograms of a reference object and a target object.

Chapter 2 presents a 3-D optical image matching system based on two-pupil optical heterodyne scanning. In section 2.1, we briefly review two-pupil optical heterodyne scanning. This section also serves to define most of the symbols, notations, and definitions used in subsequent sections. Section 2.2 develops the 3-D optical image matching system based on two-pupil optical heterodyne scanning, whereby the technique for correlating two sets of holographic information is developed. Section 2.3 discusses the necessary pupils to implement the idea for optical 3-D image matching. In section 2.4, computer simulation results of 3-D optical image matching are presented. Section 2.6 presents the physical interpretation of the proposed optical matching system in terms of masks.

The other essential role in correlation is to learn the shifted location of a pattern-matched object. However, the correlation output does not give a strong correlation peak when the location of the 3-D target object is shifted along the depth direction because the

holographic correlation is basically a 2-D correlation process. In fact, the correlation peak is smeared out or broadened by a convolution process, reminiscent of defocused imaging in coherent optical systems. To achieve z- or depth- invariance, and extract the 3-D location of the pattern-matched 3-D object from the output of the 3-D holographic correlation, we propose two methods. One is to focus the correlation output along the depth, and then the correlation peak is focused at the shifted depth location if the 3-D pattern of the target object is matched with that of the reference object. Because the output of the location-shifted 3-D pattern-matched object is the defocused correlation pattern along the depth, the depth location is achieved by focusing the correlation output along the depth direction. The transverse location of the pattern-matched object is achieved from the shifted location of the focused correlation peak. This focusing process can be performed by an optical system that is proposed in section 2.5, or digitally with the digitized correlation output. However, the proposed system has a drawback in that only 3-D targets that are located farther away from the 3-D reference object can be shift invariantly detected. In addition, the method employs a manual and semi-manual process that is tedious and time consuming. The other way to extract the 3-D location of the 3-D pattern-matched object directly from the correlation output without a focusing process is to filter the correlation output by using a power fringe adjusted filter and the Wigner distribution. Since holography is widely used in imaging and information systems, the needs for the analysis of holographic information have increased, and therefore several techniques are proposed in the analysis of fringe patterns, especially in the area of particle field holography [17-20]. In chapter 3, we propose a technique that extracts the 3-D location of a 3-D image-matched object using a power fringe adjusted filter [21,22] and the Wigner distribution [23, 24]. Power fringe adjusted filtering is a widely used filtering method to sharpen the correlation peak, whereas the Wigner distribution is a signal transformation for a time-frequency analysis in signal processing, which yields the frequency contents of a signal at different time instants. We analyze the holographic

correlation pattern that has a fringe pattern (spatial frequency contents) at a different location (spatial instant). A brief review of Wigner distribution is given in section 3.1. The Wigner analysis of defocused correlation output and computer simulation results are presented in section 3.2 and section 3.3.

In the realization of the proposed technique, the feasibility in implementation and the robustness of the system are very critical issues. Thus, chapter 4 introduces a real-only hologram and a phase-only hologram as a mask in matching stage to improve the feasibility in implementation and robustness of the system. Chapter 5 presents experimental results to reinforce the proposed technique.

Chapter 2: 3-D holographic image matching system

This chapter presents a real-time optical technique for matching 3-D objects. The goal is to match 3-D objects, i.e., objects of three spatial coordinates, in a hybrid optical/electronic system. In essence, the proposed hybrid system performs correlation of two pieces of holographic information pertaining to the two 3-D objects, a 3-D reference object and a 3-D target object, to be matched and hence 3-D image matching is made possible. Since the depth information of an object is encoded as a form of fringe pattern on the hologram, 3-D image matching now can be achieved by 2-D optical correlation of holograms of the 3-D reference object and the 3-D target object. The proposed technique is based on a two-pupil optical heterodyne scanning technique. A hologram of the 3-D reference object is first created which is then used to spatially modulate one of the pupils of the optical system, with the other pupil being a point source. A 3-D target object to be recognized is then 2-D scanned by optical beams modulated by the two pupils, and the result of the 2-D scan pattern effectively displays the correlation between the holographic information of the 3-D reference object and that of the 3-D target object. A strong correlation peak results if their holographic information is matched.

Section 2.1 presents the transfer function of the two-pupil optical heterodyne scanning system. This section also serves to define most of the symbols, notations, and definitions used in subsequent sections. Section 2.2 develops the 3-D matching technique based on the two-pupil optical heterodyne scanning system by means of its transfer function. Section 2.3 presents the possible optical methods to implement the pupils in the matching stage. Section 2.4 presents and discusses the computer-simulation results.

The 3-D shift invariance of a matching system is practically important. The proposed 3-D holographic matching system achieves 3-D image matching by the direct correlation of holograms. Even though holograms have whole 3-D information of objects as a form of fringe pattern, the fringe pattern varies according to the depth locations of objects. Thus

the direct correlation between the hologram of a reference object and that of a target object does not give out the correlation peak. In other words, this system is not invariant to the shift of a target object along the z-axis. Section 2.5 analyzes the z-invariance and provides a solution. Finally, in the section 2.6 physical interpretation of the 3-D holographic matching system is presented.

2.1 Two-pupil optical heterodyne scanning: Introduction and Background

The two-pupil optical heterodyne scanning system is an incoherent image processing system. The conventional incoherent image processing system manipulates the intensity of an image. Thus the point spread function (PSF) of the system is restricted to positive real numbers. However, in the two pupil optical heterodyne scanning system, the PSF of the system is extended to complex numbers by utilizing the interferometric interaction of the two pupil with shifted temporal frequency [25-31]. This makes possible to extract and process the holographic information of objects using two-pupil optical heterodyne scanning.

A typical two-pupil heterodyne optical scanning system is shown in fig. (2.1-1) [25-31]. Beam splitters BS and BS1 and mirrors M and M1 form the Mach-Zenhner interferometer. A collimated laser at temporal frequency ω_0 is used to illuminate the pupil, $p_1(x, y)$. The other pupil, $p_2(x, y)$, is illuminated by the laser of temporal frequency ω_o + Ω. The laser's temporal frequency offset of Ω is introduced by an acousto-optic frequency shifter (AOFS) as shown in the fig. (2.1-1) [32]. The two pupils are located at the front focal planes of lenses L1 and L2, both with focal length f. The two pupils are then combined by beam splitter BS1 to focus the light onto the 2-D scanning mirrors, which are located on the back focal plane of lenses L1 and L2. The combined optical scanning field at z away from the focal plane of the two lenses are then given by

$$P_{1z}\left(\frac{k_o x}{f},\frac{k_o y}{f}\right) exp[j\omega_o t] + P_{2z}\left(\frac{k_o x}{f},\frac{k_o y}{f}\right)exp[j(\omega_o+\Omega)t] , \qquad (2.1\text{-}1)$$

where $P_{iz}(\frac{k_o x}{f},\frac{k_o y}{f})$ is the field distribution z away from the scanning mirrors and is given by through Fresnel diffraction [33,34,35]:

$$P_{iz}\left(\frac{k_o x}{f},\frac{k_o y}{f}\right)= P_i\left(\frac{k_o x}{f},\frac{k_o y}{f}\right) \otimes h(x,y;z),\ i = 1,2. \qquad (2.1\text{-}2)$$

In Eq. (2.1-2), $P_i(\frac{k_o x}{f},\frac{k_o y}{f})$ is the field distribution in the back focal plane of lenses L_1 and L_2, and is given, aside from some inessential constant and a phase factor, by

$$P_i\left(\frac{k_o x}{f},\frac{k_o y}{f}\right)= \int\int p_i(x',y')\, exp\left[j\frac{k_o}{f}(xx'+yy')\right]dx'dy' \qquad (2.1\text{-}3)$$

$$= \mathcal{F}\{p_i(x,y)\}_{k_x=\frac{k_o x}{f},\ k_y=\frac{k_o y}{f}}$$

where $\mathcal{F}$ denotes the optical Fourier-transform operation and is defined as

$\mathcal{F}\{u(x,y)\}_{k_x,k_y} = \int\int u(x,y)\, exp(jk_x x + jk_y y)dxdy = U(k_x,k_y)$ with k_x and k_y denoting spatial frequencies, and with the upper case function U denoting the transform of the lower case function u. The term $h(x,y;z)$ is the free-space impulse response [35] and, aside from some phase constant, is given by

$$h(x,y;z)= \frac{jk_o}{2\pi z}exp\left[-j\frac{k_o}{2z}\left(x^2+y^2\right)\right] \qquad (2.1\text{-}4)$$

with k_o denoting the wave number of the light, and finally, the symbol $\otimes$ in Eq. (2.1-2) denotes the 2-D convolution operation defined as:

$$g_1(x,y) \otimes g_2(x,y) \;=\; \int\int g_1(x',y')g_2(x-x',y-y')dx'dy'. \qquad (2.1\text{-}5)$$

Returning to Eq. (2.1-1), the combined optical field or the scanning pattern is used to 2-D scan an object amplitude transparency $\Gamma_o(x,y;z)$ located a distance z away from the scanning mirrors, as shown in fig.$(2.1\text{-}1)$. The photodetector, which responds to the incident intensity of the optical transmitted field or scattered field, generates a current that is given by

$$i(x,y;z) = \int\int_A \left| \left[P_{1z}\left(\frac{k_o\,x'}{f},\frac{k_o\,y'}{f}\right) exp(j\omega_o t) \right.\right. \qquad (2.1\text{-}6)$$

$$\left.\left. + P_{2z}\left(\frac{k_o\,x'}{f},\frac{k_o\,y'}{f}\right) exp[j(\omega_o+\Omega)t] \right] \times \Gamma_o(x+x',y+y';z) \right|^2 dx'dy'.$$

Note that the integration is over the area A of the photodetector, that $x = x(t)$ and $y = y(t)$ represent the instantaneous position of the scanning pattern, and the shifted coordinates of Γ_o represent the action of scanning. The heterodyne current at temporal frequency Ω of Eq. (2.1-6), after a band pass filter (BPF) tuned at frequency Ω, becomes

$$i_\Omega(x,y;z) = Re\left[\int\int_A P_{1z}^{*}\left(\frac{k_o\,x'}{f},\frac{k_o\,y'}{f}\right) P_{2z}\left(\frac{k_o\,x'}{f},\frac{k_o\,y'}{f}\right) \right. \qquad (2.1\text{-}7)$$

$$\left. |\Gamma_o(x+x',y+y';z)|^2 dx'dy' exp(j\,\Omega t) \right],$$

where we adopted the convention for phasor ψ_p as $\psi\,(x,y,t) = Re[\psi_p(x,y,t)exp(j\Omega t)]$, where $Re[.]$ denotes the real part of Eq. $(2.1\text{-}7)$ which can be written as:

$$i_{\Omega}(x,y) = Re\left[i_{\Omega_p}(x,y;z)exp(j\,\Omega t)\right], \tag{2.1-8}$$

where

$$i_{\Omega_p}(x,y;z)= \int\int_A P_{1z}^{*}\left(\frac{k_0\,x'}{f},\frac{k_0\,y'}{f}\right)\,P_{2z}\left(\frac{k_0\,x'}{f},\frac{k_0\,y'}{f}\right)|\Gamma_o(x+x',y+y';z)|^2dx'dy'$$

is the output phasor which denotes the amplitude and the phase information of the heterodyne current which constitutes the scanned and processed version of the object $|\Gamma_o|^2$. Defining the correlation operation as:

$$g(x,y)\odot h(x,y)\;=\;\int\int g^{*}(x',y')h(x+x',y+y')dx'dy', \tag{2.1-9}$$

we can now re-write the output phasor as:

$$i_{\Omega_p}(x,y;z)=\;P_{1z}\left(\frac{k_0\,x}{f},\frac{k_0\,y}{f}\right)\,P_{2z}^{*}\left(\frac{k_0\,x}{f},\frac{k_0\,y}{f}\right)\odot|\Gamma_o(x,y;z)|^2. \tag{2.1-10}$$

Note that, as in conventional optical scanning systems, only the intensity distribution, i.e., $|\Gamma_o|^2$ is processed, hence the optical system is incoherent [25-31].

We shall now define the optical transfer function (OTF) of the system as:

$$OTF_{\Omega}(k_x,k_y;z) = \mathcal{F}\left\{i_{\Omega_p}(x,y;z)\right\}/\mathcal{F}\left\{|\Gamma_o(x,y;z)|^2\right\}. \tag{2.1-11}$$

Substituting Eq. (2.1-10) into Eq. (2.1-11), we have

$$OTF_{\Omega}(k_x,k_y;z)\;=\mathcal{F}^{*}\left\{\;P_{1z}\left(\frac{k_0\,x}{f},\frac{k_0\,y}{f}\right)\,P_{2z}^{*}\left(\frac{k_0\,x}{f},\frac{k_0\,y}{f}\right)\right\}. \tag{2.1-12}$$

In terms of the pupils p_1 and p_2, we substitute Eq. (2.1-2) and Eq. (2.1-3) into Eq. (2.1-12) to obtain [26]

$$OTF_{\Omega}(k_x, k_y; z) = exp\left[j\frac{z}{2k_o}\left(k_x^2 + k_y^2\right)\right] \tag{2.1-13}$$

$$\times \int\int p_1^*(x', y')p_2\left(x' + \frac{f}{k_o}k_x\ , y' + \frac{f}{k_o}k_y\right) exp\left[j\frac{z}{f}\ (x'k_x + y'k_y)\right] dx'dy'.$$

This equation states that OTF_{Ω} of the system can be modified according to the selection of the two pupils. Now, by using Eq. (2.1-11) and re-writing Eq. (2.1-8) in terms of OTF_{Ω}, we have

$$i_{\Omega}(x, y; z) = Re\left[i_{\Omega_p}(x, y; z) exp(j\Omega t)\right] \tag{2.1-14}$$

$$= Re\left[\mathcal{F}^{-1}\left\{ \mathcal{F}\left\{ |\Gamma_o(x, y; z)|^2 \right\} \times OTF_{\Omega}(k_x, k_y; z)\right\} exp(j\Omega t)\right].$$

By defining the point spread function of the optical heterodyne scanning system as $h_{\Omega}(x, y; z) = \mathcal{F}^{-1}\{\ OTF_{\Omega}\}$, we can now re-write Eq. (2.1-14) in the spatial domain as:

$$i_{\Omega}(x, y; z) = Re\left[|\Gamma_o(x, y; z)|^2 \otimes h_{\Omega}(x, y; z)\, exp(j\Omega t)\right]. \tag{2.1-15}$$

Equation (2.1-14) or (2.1-15) represents the scanned and the processed output current modulated by a temporal carrier at frequency Ω. We can demodulate and extract the in-phase and the quadrature-phase components of the output current by mixing it with

$cos(\Omega t)$ and $sin(\Omega t)$, and hence the idea of parallel processing. The demodulation system is shown in fig. (2.1-2), and the two outputs can be shown and given as:

$$i_c(x,y;z) = Re\left[\mathcal{F}^{-1}\left\{\mathcal{F}\left\{|\Gamma_o|^2\right\} \times OTF_\Omega\right\}\right] = Re\left[|\Gamma_o|^2 \otimes h_\Omega(x,y;z)\right] \quad (2.1\text{-}16a)$$

and

$$i_s(x,y;z) = Im\left[\mathcal{F}^{-1}\left\{\mathcal{F}\left\{|\Gamma_o|^2\right\} \times OTF_\Omega\right\}\right] = Im\left[|\Gamma_o|^2 \otimes h_\Omega(x,y;z)\right], \quad (2.1\text{-}16b)$$

where Im[.] denotes the imaginary part of Eqs.(2.1-16a,b), and the subscripts "c" and "s" represent the use of $cos\Omega t$ and $sin\Omega t$ for mixing, respectively, to extract the information from i_Ω.

In Eqs. (2.1-16a,b), the input object, $|\Gamma_o(x,y;z)|^2$, has been assumed to be an infinitely thin 2-D object located at z away from the focus of the spherical wave which is on the 2-D scanning mirrors as shown in fig.(2.1-1). To generalize Eqs. (2.1-16a,b) for 3-D objects, we need to integrate the equation over the depth, i.e., over z, of the 3-D object. Eqs. (2.1-16a,b) become

$$i_c(x,y) = Re\left[\int \mathcal{F}^{-1}\left\{\mathcal{F}\left\{|\Gamma_o(x,y;z)|^2\right\} \times OTF_\Omega\right\} dz\right], \quad (2.1\text{-}17a)$$

$$= Re\left[\int |\Gamma_o(x,y;z)|^2 \otimes h_\Omega(x,y;z) dz\right]$$

and

$$i_s(x,y) = Im\left[\int \mathcal{F}^{-1}\left\{\mathcal{F}\left\{|\Gamma_o(x,y;z)|^2\right\} \times OTF_\Omega\right\} dz\right]. \quad (2.1\text{-}17b)$$

$$= Im\left[\int |\Gamma_o(x,y;z)|^2 \otimes h_\Omega(x,y;z) dz\right].$$

Note that we have left the z dependence out of the left-hand side of Eqs. (2.1-17a,b) to emphasize that the recorded information is strictly 2-D even for 3-D objects. $i_c(x,y)$ or $i_s(x,y)$ represents the scanned and processed information and can be stored as a 2-D record if these currents are stored in synchronization with the signals used to drive the scanning mirrors. The complex hologram is synthesized in a digital computer with the stored holographic recordings of $i_c(x,y)$ and $i_s(x,y)$. The complex hologram is given as:

$$H_{\Gamma_o} = i_c(x,y) + j\, i_s(x,y) \tag{2.1-18}$$

$$= \int |\Gamma_o(x,y;z)|^2 \otimes h_\Omega(x,y;z) dz.$$

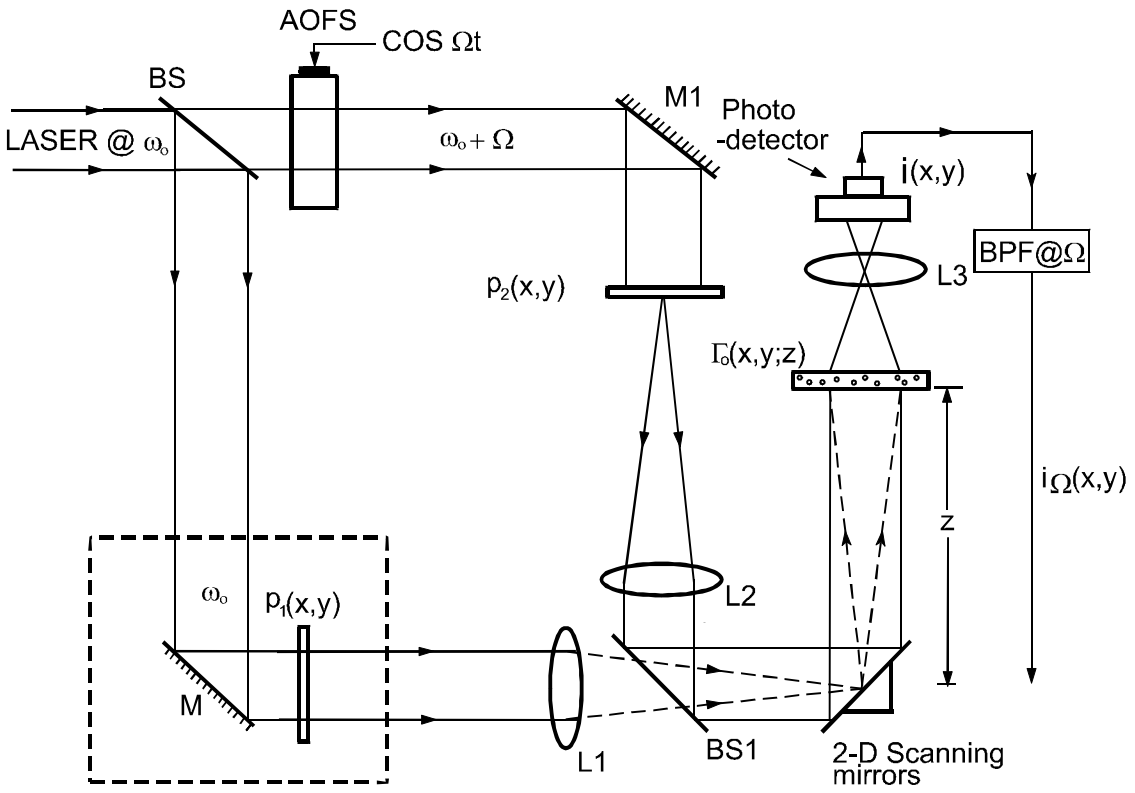

Figure (2.1-1): Two-pupil optical heterodyne scanning system. (BPF @ Ω: bandpass filter tuned at frequency Ω, BS, BS1: beam splitters, AOFS: acousto-optic frequency shifter, M,M1: mirrors, L1,2,3: lenses)

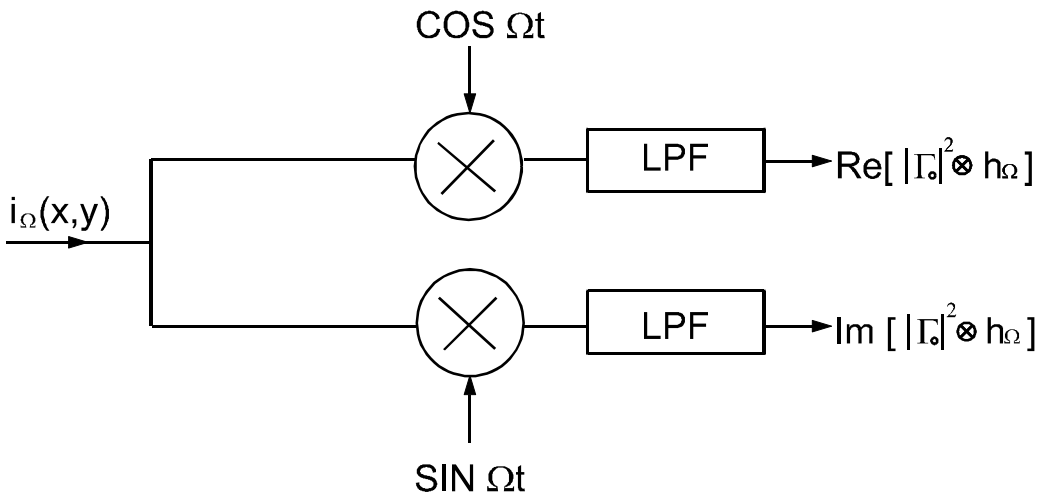

Figure (2.1-2): Parallel processing for obtaining the in-phase and quadrature-phase information of the scanned signal simultaneously. (LPF: lowpass filter)

2.2 Matching of 3-D object

The proposed 3-D matching technique is divided into two steps: a) construction of reference holograms and b) correlation of two sets of holographic information by 2-D scanning a 3-D target object. The technique is based on optical heterodyne scanning described in the last section. We shall now describe the two steps separately.

2.2.1 Construction of reference holograms

To construct the hologram of the 3-D reference object, the two pupils are chosen such that $p_1(x, y)$= 1 and $p_2(x, y)$= $\delta(x, y)$ as illustrated in fig. (2.1-1). With this choice of the pupils, the OTF of the scanning system, according to Eq. (2.1-13), becomes

$$OTF_{\Omega}(k_x, k_y;z) = exp\left[- j\frac{z}{2k_o}\left(k_x^2 + k_y^2\right)\right] = OTF_{osh}(k_x, k_y;z)\ , \qquad (2.2\text{-}1)$$

where the subscript "osh" denotes that the particular achieved OTF is for holographic recording [26]. What is being recorded in two dimensions is a hologram, $t(x, y)$. We shall use equation (2.1-17a) as an example. $i_c(x, y)$ now becomes a hologram and is given by

$$t(x, y) = Re\left[\int \mathcal{F}^{-1}\left\{ \mathcal{F}\left\{|\Gamma_o(x, y; z)|^2\right\} \times OTF_{osh}(k_x, k_y;z)\right\}dz\right] \qquad (2.2\text{-}2)$$

$$= Re\left[\int \mathcal{F}^{-1}\left\{\mathcal{F}\left\{|\Gamma_o(x, y; z)|^2\right\} \times exp\left[- j\frac{z}{2k_o}\left(k_x^2 + k_y^2\right)\right]\right\}dz\right]\ .$$

From the above equation, it is clear that holographic recording process in the frequency domain can be interpreted as the object's spectrum along its depth (z) is being processed by the OTF of the form given by Eq. (2.2-1). To clearly see why this

corresponds to holographic recording, we re- write Eq. (2.2-2) in terms of convolution and we have

$$t(x,y) = Re\left[\int |\Gamma_o|^2 \otimes h^*(x,y;z)dz\right], \tag{2.2-3}$$

where interestingly Eq. (2.2-3) can be written in terms of $h(x,y;z)$ which is the free-space impulse response defined in Eq. (2.1-4). Eq. (2.2-3) can be re-written in terms of correlation as:

$$t_{sin}(x,y) = Re\left[\int h(x,y;z) \odot |\Gamma_o|^2 dz\right] \tag{2.2-4}$$

$$= \int \frac{k_o}{2\pi z} sin\left[\frac{k_o}{2z}\left(x^2 + y^2\right)\right] \odot |\Gamma_o|^2 \, dz \, .$$

In writing the last step of Eq. (2.2-4), since $|\Gamma_o|^2$ represents intensity distribution which is strictly positive, the Re-operation has been distributed to the function h. The subscript "sin" in the left side of the equation denotes a sine function is involved in the calculation of the correlation integral.

If we let $|\Gamma_o|^2 = \delta(x - x_o, y - y_o, z - z_o)$, $t_{sin}(x,y) \sim sin\left\{\frac{k_o}{2z_o}\left[(x - x_o)^2 + (y - y_o)^2\right]\right\}$, which is the hologram of an offset delta function. Equation (2.2-4) is a very important result. In optical scanning holography, 3-D holographic recording process can be thought of as a 2-D transverse correlation between the real part of the free-space impulse response, $\frac{k_o}{2\pi z} sin\left[\frac{k_o}{2z}(x^2 + y^2)\right]$, and the 3-D object, $|\Gamma_o(x,y;z)|^2$. The resulting correlation is then integrated along the depth of the object to obtain the hologram of the whole object. To put Eq. (2.2-4) into a wider context, the Re - operation can be replaced by Im - operation. This corresponds to the use of Eq. (2.1-17b) as an output:

$$t_{cos}(x,y) = Im\left[\int h(x,y;z) \odot |\Gamma_o|^2 dz\right] \qquad (2.2\text{-}5)$$

$$= \int \frac{k_0}{2\pi z} cos\left[\frac{k_0}{2z}\left(x^2 + y^2\right)\right] \odot |\Gamma_o|^2 dz$$

$$= \frac{k_0}{2\pi z_0} cos\left\{\frac{k_0}{2z_0}\left[(x - x_0)^2 + (y - y_0)^2\right]\right\}$$

for $|\Gamma_o|^2 = \delta(x - x_o, y - y_o, z - z_o)$ again. We shall call $t_{sin}(x,y)$ and $t_{cos}(x,y)$ the sine-Fresnel zone plate (sine-FZP) hologram and cosine-FZP hologram of the object $|\Gamma_o|^2$, respectively. Indeed, due to the fact that holographic information is available in electronic form as given by $i_\Omega(x,y)$ as shown in fig.(2.1-1), we can have a sine-FZP hologram and cosine-FZP hologram simultaneously through parallel processing as shown in fig.(2.1-2). As it turns out that the sine- and cosine-FZP holograms are important for the implementation of complex pupil functions for 3-D optical image recognition, to be discussed in section 2.3.

2.2.2 Correlation of two sets of holographic information

From the last section, we see that holographic recording can be analyzed by using an OTF approach and the OTF is expressed in terms of the two pupil functions as shown in Eq. (2.1-13) in general. By particularly choosing $p_1 = 1$ and $p_2 = \delta(x,y)$, we have the type of OTF [see Eq. (2.2-1)] capable of performing holographic recording.

To be more general, we now choose $p_2 = \delta(x,y)$ and keep $p_1(x,y)$ as is. The OTF of the system becomes, according to Eq. (2.1-13):

$$\text{OTF}_\Omega(k_x, k_y; z) = exp\left[-j\frac{z}{2k_o}(k_x^2 + k_y^2)\right] \times p_1^*\left(-\frac{f}{k_o}k_x, -\frac{f}{k_o}k_y\right). \qquad (2.2\text{-}6)$$

The 2-D record is then, according to Eq. (2.1-17a), i.e., using Re [.] as an example:

$$i_c(x,y) = Re\left[\int \mathcal{F}^{-1}\left\{\mathcal{F}\{T(x,y;z)\} \times exp\left[-j\frac{z}{2k_o}\left(k_x^2 + k_y^2\right)\right]\right.\right. \qquad (2.2\text{-}7)$$

$$\left.\left. \times\, p_1^*\left(-\frac{f}{k_o}k_x,\, -\frac{f}{k_o}k_y\right)\right\} dz\right],$$

where we have assumed that $|\Gamma_o|^2 = T(x,y;z)$ is the 3-D target object to be recognized. Now, we have seen that $\int \mathcal{F}\{T(x,y;z)\} \times exp[-j\frac{z}{2k_o}(\ k_x^2\ +\ k_y^2)]\, dz$ contains holographic information of $T(x,y;z)$ [see Eq. (2.2-2)]. If we now assume p_1 carries the holographic information of a 3-D reference object, $R(x,y;z)$, we then have

$$p_1\left(-\frac{f}{k_o}k_x,\ -\frac{f}{k_o}k_y\right) = \int \mathcal{F}\{R(x,y;z)\}\ exp\left[-j\frac{z}{2k_o}\left(k_x^2 + k_y^2\right)\right] dz. \quad (2.2\text{-}8)$$

Substituting Eq. (2.2-8) into Eq. (2.2-7), we have 2-D recording of the form

$$i_c(x,y) = Re\left\{\mathcal{F}^{-1}\left[\left(\int \mathcal{F}\{T(x,y;z)\}\ exp\left[-j\frac{z}{2k_o}\left(k_x^2 + k_y^2\right)\right] dz\right)\right.\right. \qquad (2.2\text{-}9)$$

$$\left.\left. \times \left(\int \mathcal{F}\{R(x,y;z)\} exp\left[-j\frac{z}{2k_o}\left(k_x^2 + k_y^2\right)\right] dz\right)^*\right]\right\}.$$

Using the correlation property, i.e., $\mathcal{F}^{-1}\{F^*G\} = \mathcal{F}^{-1}\{F\} \odot \mathcal{F}^{-1}\{G\} = f \odot g$, Eq. (2.2-9) becomes

$$i_c(x,y) = Re\left\{\left(\int \mathcal{F}^{-1}\left\{\mathcal{F}\{R(x,y;z)\}\ exp\left[-j\frac{z}{2k_o}\left(k_x^2 + k_y^2\right)\right]\right\}dz\right) \quad \text{(2.2-10a)}$$

$$\odot \left(\int \mathcal{F}^{-1}\left\{\mathcal{F}\{T(x,y;z)\}\ exp\left[-j\frac{z}{2k_o}\left(k_x^2 + k_y^2\right)\right]\right\}dz\right)\Bigg\}$$

$$= Re[H_R(x,y) \odot H_T(x,y)],$$

where $H_R(x,y) = \int h(x,y;z) \odot R(x,y;z)dz$

and $H_T(x,y) = \int h(x,y;z) \odot T(x,y;z)dz$. From the inspection of Eq. (2.2-4) and Eq. (2.2-5), $H_R(x,y)$ and $H_T(x,y)$ represent the complex hologram of $R(x,y;z)$ and $T(x,y;z)$ being obtained by optical scanning holography, respectively. By the same token, when Eq. (2.1-17b) is used, Eq. (2.2-10a) becomes

$$i_s(x,y) = Im[H_R(x,y) \odot H_T(x,y)]. \quad \text{(2.2-10b)}$$

Eqs. (2.2-10a,b) are the major result of the research. $i_c(x,y)$ or $i_s(x,y)$ given in Eqs.(2.2-10a,b) is the display of a 2-D pattern which basically represents the correlation of holograms of two 3-D objects, T and R. Only when the two sets of holographic data are identical, i.e., $H_R(x,y) = H_T(x,y)$, we have a strong correlation peak on the pattern and hence a match of the two 3-D objects is performed. The 3-D target object has to match with the 3-D reference object throughout the depth in order to produce a sharp correlation peak, and hence a true 3-D matching is achieved. We do not need to record 2-D images of the 3-D objects to be matched, but a single hologram of the reference 3-D object is required to perform 3-D matching.

2.3 Pupil implementation for 3-D optical image matching

In the last section, we discuss that the target object $T(x, y; z)$ to be recognized is 2-D scanned with the two pupils setting as $p_2 = \delta(x, y)$ and $p_1(x, y)$ has a functional form as that given by Eq. (2.2-8), a holographic information of R. Let us now specify p_1. We re-write Eq. (2.2-8) as:

$$p_1\left(-\frac{f}{k_o}k_x, -\frac{f}{k_o}k_y \right) = \int \left[\mathcal{F}\{h(x, y; z) \odot R(x, y; z)\}_{k_x, k_y} \right] dz. \qquad (2.3\text{-}1)$$

Substituting $x = -\frac{f}{k_o}k_x$ and $y = -\frac{f}{k_o}k_x$ into the above equation, we have

$$p_1(x, y) = \int [\mathcal{F}\{h(x, y; z) \odot R(x, y; z)\}_{k_x = -k_o x/f,\, k_y = -k_o y/f}] dz \qquad (2.3\text{-}2)$$

$$= \mathcal{F}\left\{ \int h(x, y; z) \odot R(x, y; z) dz \right\}_{k_x = -k_o x/f,\, k_y = -k_o y/f}$$

Note that $\int h(x, y; z) \odot R(x, y; z)\, dz = H_R(x, y)$ is the complex hologram of the reference object R. This can be conveniently achieved by optical scanning holography as discussed in section 2.2.1. To be more precise, Eq. (2.2-4) and Eq. (2.2-5) can be added to give a complex hologram, $H_R(x, y)$, of the reference object R as follows:

$$H_R(x, y) = t_{cos}(x, y) + j\, t_{sin}(x, y) \sim \int h(x, y; z) \odot R(x, y; z)\, dz \qquad (2.3\text{-}3)$$

for $|\Gamma_o|^2 = R(x, y; z)$, where $t_{cos}(x, y)$ and $t_{sin}(x, y)$ in this case are called the cosine- and sine-FZP holograms of the reference object R.

Note that the holographic data is complex in general, and in principle complex data can be fabricated onto a mask using diffractive optical elements (DOE's) by photolithography. To achieve Fourier transformation as shown in Eq.(2.3-2), the DOE can be put in the front focal plane of a lens of focal lens f and illuminated by laser light of wavelength λ. In the back focal plane of the lens, we would then achieve our designed pupil in Eq.(2.3-2), but without the negative signs as indicated by the substitutions in Eq.(2.3-2). To take the negative signs into account, we just need to rotate the DOE by 180º before the optical Fourier transformation. Fig. (2.3-1) illustrates the implementation of the function p_1 , and this implementation replaces the part of the system outlined by the dotted line in fig.(2.1-1), in order to turn the two-pupil heterodyne scanning system into a 3-D object recognition system. Note that in fig. (2.3-1), the coordinates of DOE have negative signs which represent 180º in-plane rotation of its coordinates with respect to those in p_1. In summary, for 3-D optical image recognition, the scanning system shown in fig.(2.1-1) will have p_2 = δ(x,y), and p_1 is specified by Eq. (2.3-2). The target object $T(x, y; z)$ to be recognized, located at z, will be 2-D scanned and a strong correlation peak will occur when $R = T$.

For real-time applications, implementation of the pupil through the use of spatial light modulators is needed. We shall discuss the use of SLMs for a proposed implementation. The idea is illustrated in fig. (2.3-2). The two holograms are in the front focal plane of the Fourier transform lens, and the beam splitter is used to combine the two holograms. In front of the cosine-FZP hologram, we put a microscope glass plate which can be rotated through some angle θ. Through a proper rotation and thereby a proper thickness of the glass, a 90^o laser light phase shift between the two holograms can be achieved. At the back focal plane of the lens, we then have a pupil p_1 generated by complex hologram of the form

$$p_1(x,y) \sim \quad \mathcal{F}\{[b_s + t_{sin}(x,y)] + e^{j\pi/2}[b_c + t_{cos}(x,y)]\}\Big|_{k_x=\frac{-k_O x}{f},\, k_y=\frac{-k_O y}{f}} \qquad (2.3\text{-}4)$$

$$= \mathcal{F}\Big\{\big[b_s + e^{j\pi/2}b_c\big] + Re\Big[\int h(x,y;z_R) \odot R(x,y;z_R)dz\Big]$$

$$+ j\,Im\Big[\int h(x,y;z_R) \odot R(x,y;z_R)dz\Big]\Big\}\Big|_{k_x=\frac{-k_O x}{f},\, k_y=\frac{-k_O y}{f}}$$

$$= \mathcal{F}\Big\{\big[b_s + e^{j\pi/2}b_c\big] + \Big[\int h(x,y;z_R) \odot R(x,y;z_R)dz\Big]\Big\}\Big|_{k_x=\frac{-k_O x}{f},\, k_y=\frac{-k_O y}{f}}$$

where b_s and b_c are the bias for the SLMs which can only displays real and positive images. Note that the pupil in Eq. (2.3-4) is exactly the same form of the one given by Eq. (2.3-2), except for the complex constant, that is required for 3-D matching. Hence, the dashed portion of fig. (2.1-1) will be replaced by fig. (2.3-2) for complex hologram implementation of pupil p_1.

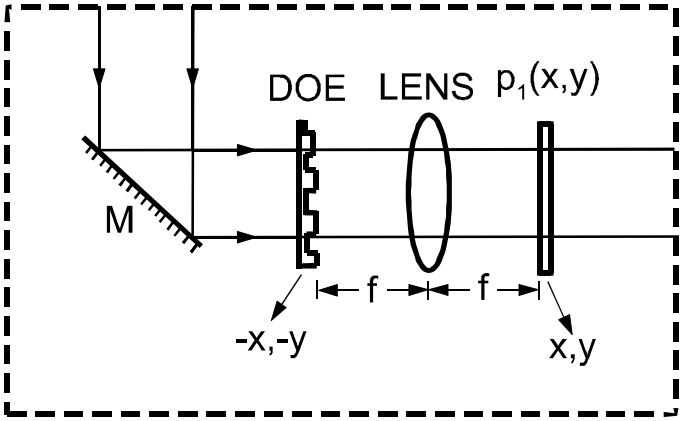

Figure (2.3-1): Implementation of complex pupil function through the use of diffractive optical element (DOE) for 3-D image recognition.

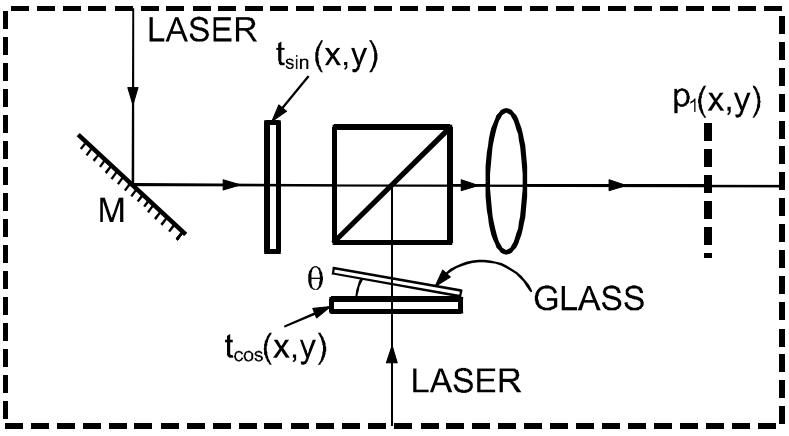

Figure (2.3-2): Implementation of complex pupil using the sine-FZP hologram and the cosine-FZP hologram.

2.4 Simulation results

Fig. (2.4-1a) shows a $1\,\text{cm} \times 1\,\text{cm} \times 3\,\text{cm}$ reference object, R, consisting of a "triangle" and a "square," separated by 3 cm along the depth of the object. Figs. (2.4-1b,c) plot the cosine-FZP hologram and the sine-FZP hologram of the reference object R as calculated by Eq. (2.3-3), with $z = 26$ cm for the "triangle" and 29 cm for the "square" of the 3-D reference object. The used wavelength of light is 0.6μm for h. The scanned area of the hologram is $1\,\text{cm} \times 1\,\text{cm}$. Physically, these holograms would correspond to the scanning of R, with its front face located 26 cm away from the scanning mirrors. Again, the pupils have been chosen such that $p_1(x,y) = 1$ and $p_2(x,y) = \delta(x,y)$ for holographic recording as described in section 2.2.1.

The holograms shown in figs. (2.4-1b,c) now will be used for the pupil specified by Eq. (2.3-2), which will result in the output calculated according to Eq. (2.2-10a) [alternatively, one can use Eq. (2.2-10b) for the output (see fig.(2.1-2) for parallel processing discussion)] :

$$t(x,y) = Re\left[\left\{\int h(x,y;z) \odot R(x,y;z)dz\right\} \odot \left\{\int h(x,y;z) \odot T(x,y;z)dz\right\}\right] \quad (2.4\text{-}1)$$

This output corresponds to the 2-D scanning of a 3-D target object, T, with the hologram of a 3-D reference object, R, used to form the pupil. Fig. (2.4-1d) shows the plotting of Eq. (2.4-1) when $T = R$, where R is the object shown in fig. (2.4-1a).

With the same reference object as shown in fig. (2.4-1a), Figs. (2.4-2a,b,c,d) show the results of another 3-D target object to be scanned. Fig. (2.4-2a) shows the target object and its front face is again 26 cm away from the scanning mirrors in the simulations. Note that the target has the same 2-D patterns as those in the reference object, but located at different depths. Figs. (2.4-2b,c) show the cosine-FZP hologram and the sine-FZP

hologram of the target object, $T(x, y)$. Fig.(2.4-2d) shows the correlation output according to Eq. (2.4-1). Note that the amplitude axis of fig. (2.4-2d) has been normalized by the peak value of fig. (2.4-1d). The lack of a strong correlation peak in fig. (2.4-2d) clearly indicates a mis-match of the two 3-D objects. It is important to point out that the holograms shown in figs. (2.4-1b,c) and figs.(2.4-2b,c) are very similar and yet when they are correlated with the reference hologram as our proposed system effectively performs, we do not find a match for the two 3-D objects shown in figs. (2.4-1a) and (2.4-2a). The reason is that since we are really correlating two holographic data sets, the depth information is as important as the planar distributions. In order to have a strong correlation peak, the 3-D objects have to be matched precisely throughout the whole 3-D volume.

Finally, in fig. (2.4-3a) and figs. (2.4-3b,c) we show another target object and its holograms. The matching outputs between fig. (2.4-1a), the reference, and fig. (2.4-3a), the target, are shown in fig. (2.4-3d). Clearly, no correlation peak is observed in fig. (2.4-3d). Note that in this case, the "X" and the "O" of the 3-D object are located at the same distance of the "triangle" and the "square", respectively.

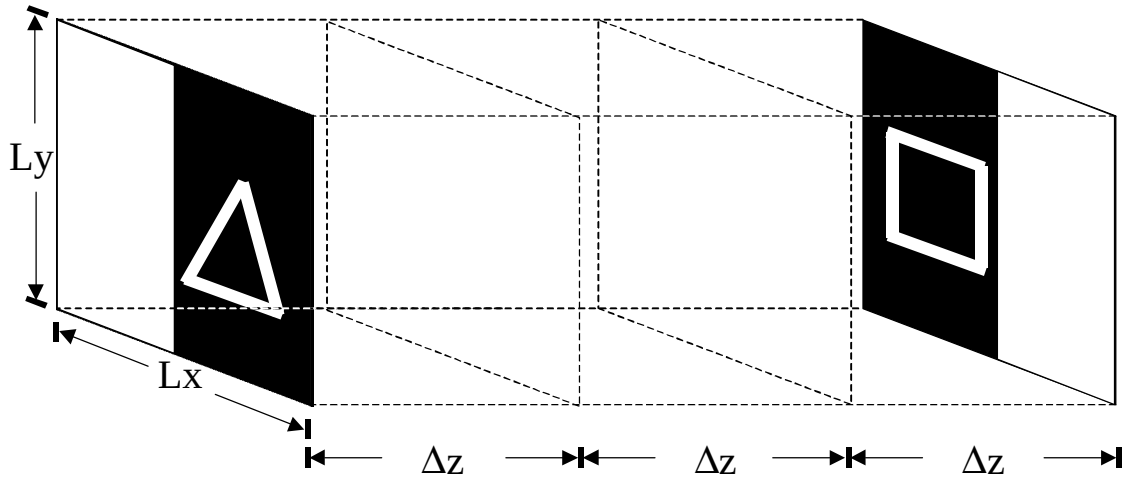

Figure (2.4-1a): 3-D reference object R, with $L_x = L_y \ = 1\,cm,\ \triangle\, z = 1\,cm.$

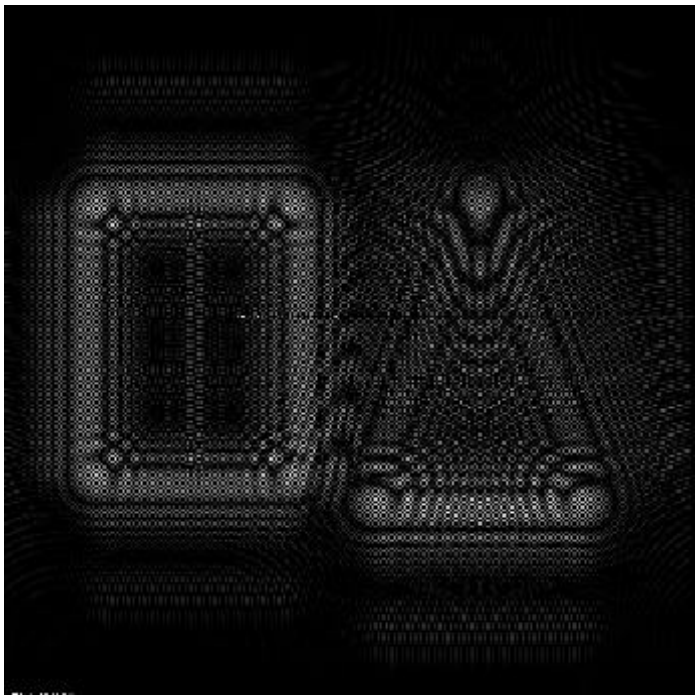

Figure (2.4-1b): Cosine-FZP hologram of the 3-D reference object. (the scanned area is 1 cm $\times$ 1 cm)

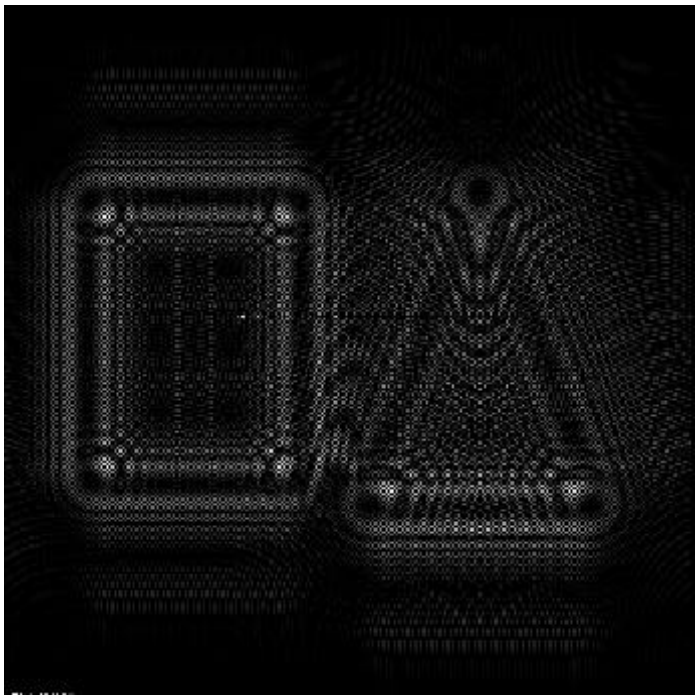

Figure (2.4-1c) Sine-FZP hologram of the 3-D reference object. (the scanned area is 1cm $\times$ 1cm)

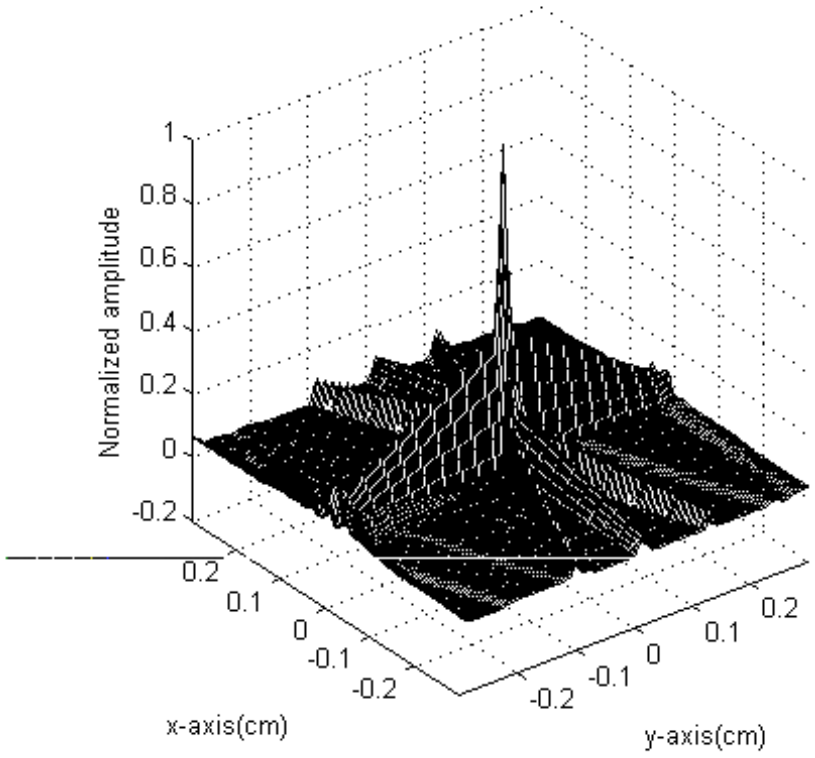

Figure (2.4-1 d): Correlation output (0.4 cm $\times$ 0.4 cm) when the target object T, is matched with the reference object R.

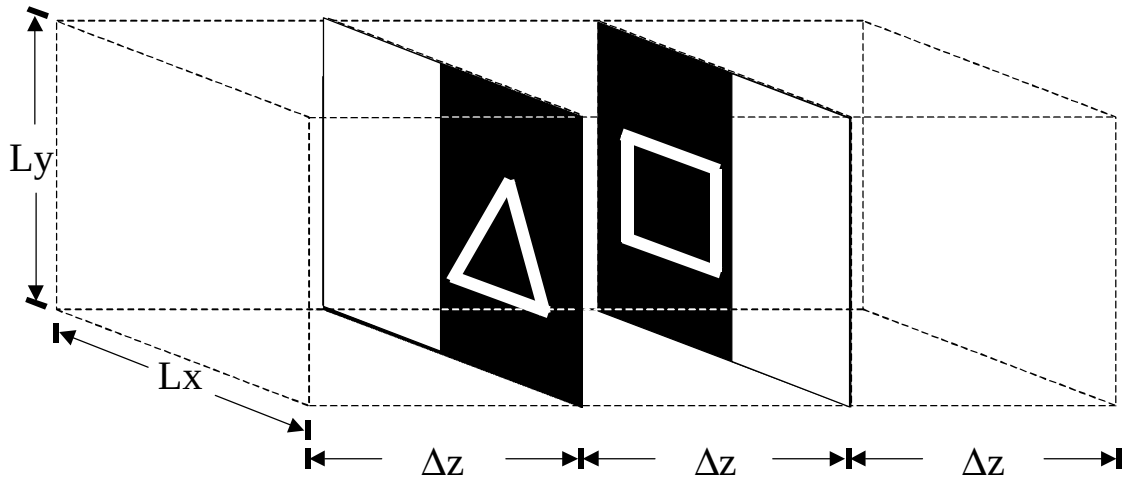

Figure (2.4-2a): 3-D target object T.

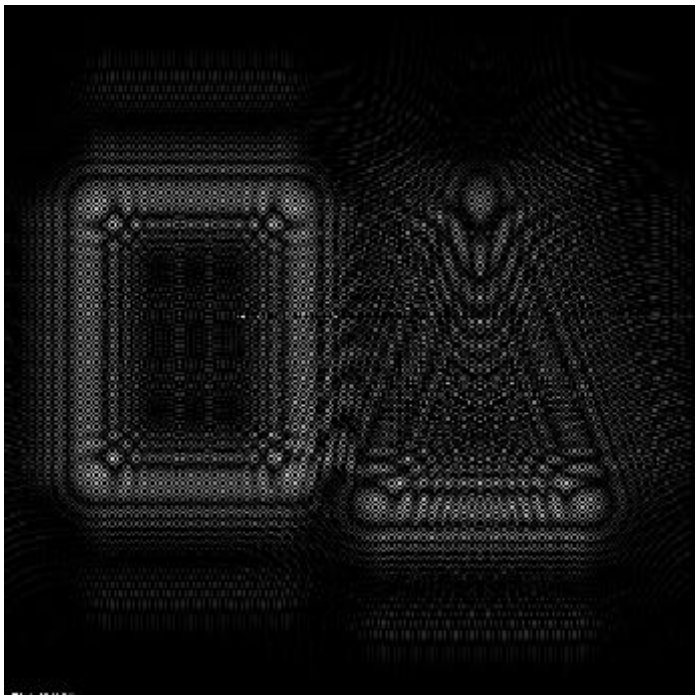

Figure (2.4-2b): Cosine-FZP hologram of the 3-D target object shown in fig. (2.4-2a).

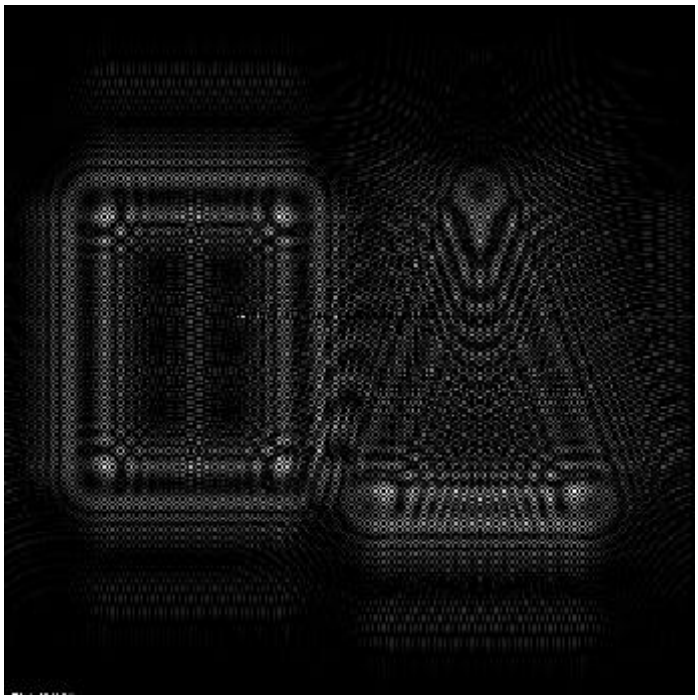

Figure (2.4-2c): Sine-FZP hologram of the 3-D target object shown in fig. (2.4-2a).

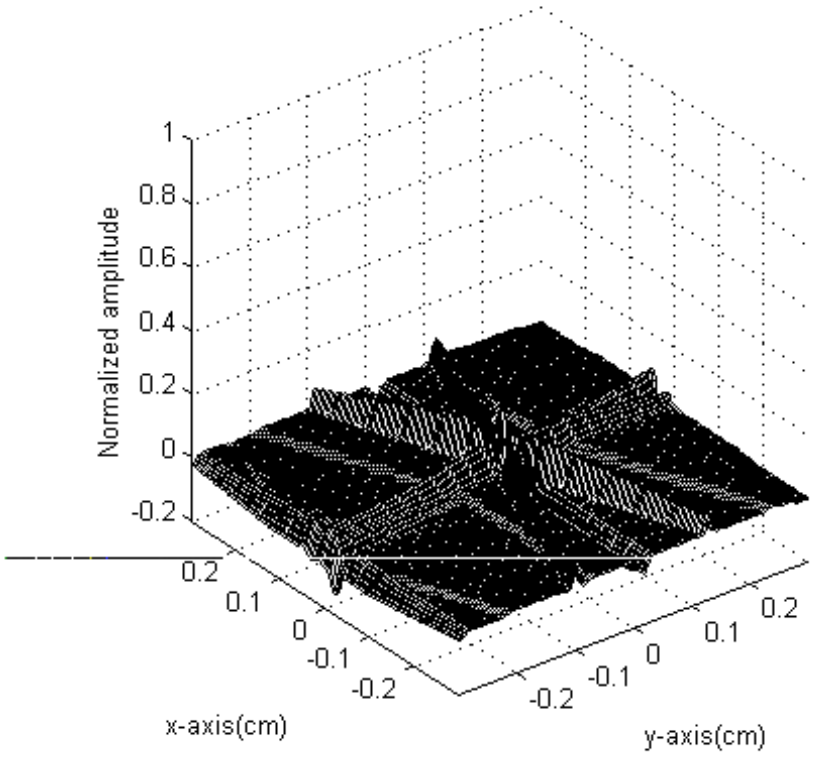

Figure (2.4-2d): Correlation output when the target object in fig. (2.4-2a) is scanned. The reference object is shown in fig. (2.4-1a).

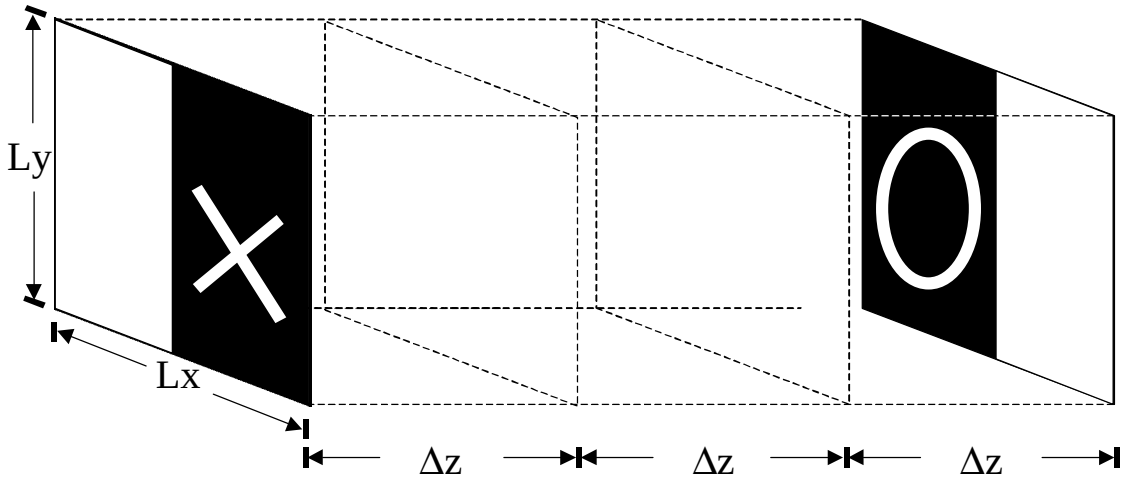

Figure (2.4-3a): 3-D target object T.

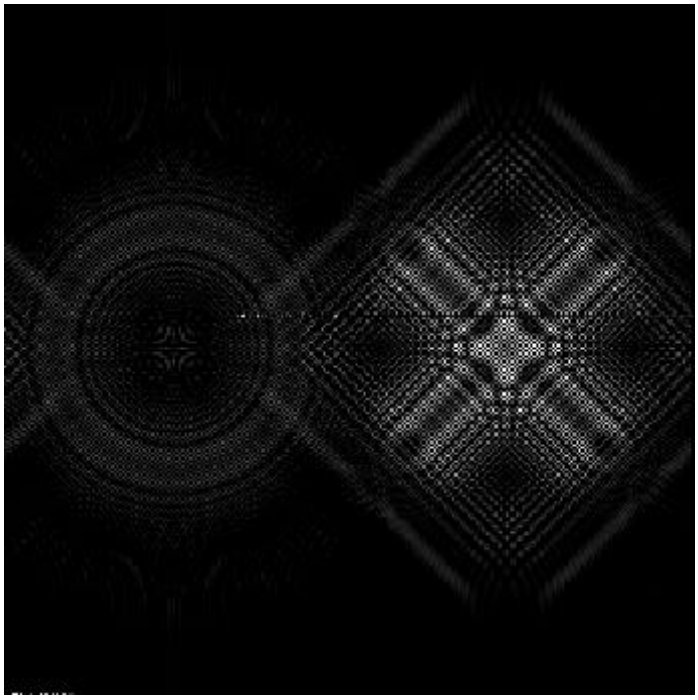

Figure (2.4-3 b): Cosine-FZP hologram of the 3-D target object shown in fig. (2.4-3a).

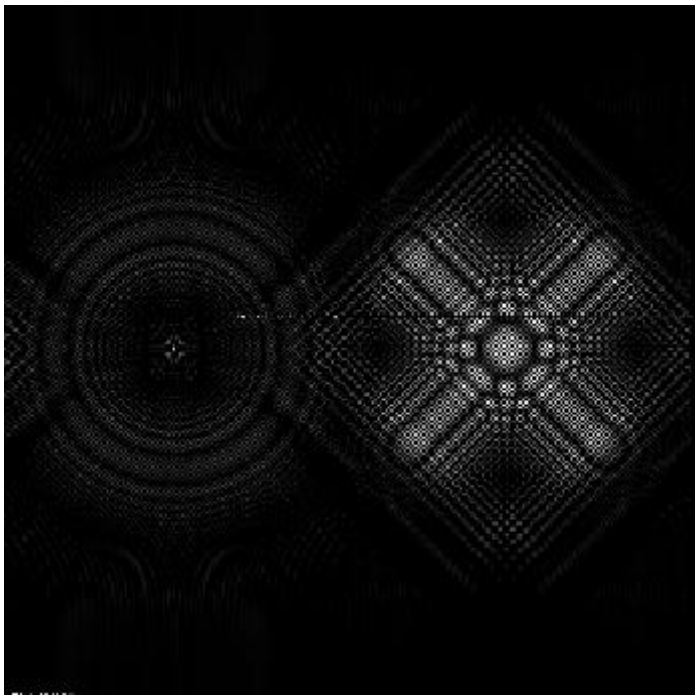

Figure (2.4-3c): Sine-FZP hologram of the 3-D target object shown in fig. (2.4-3a).

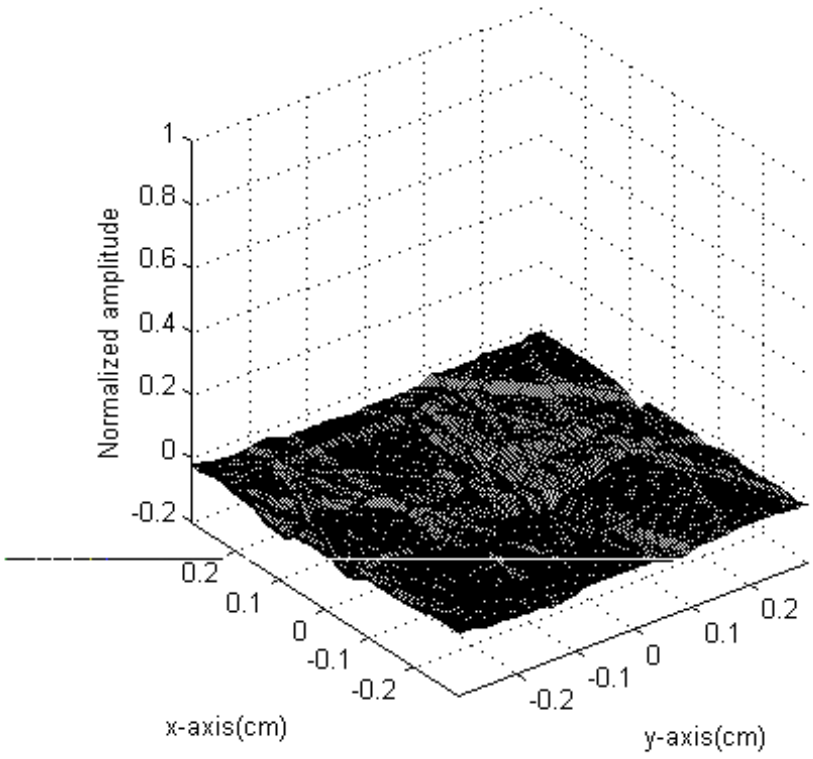

Figure (2.4-3d): Correlation output when the target object in fig. (2.4-3a) is scanned. The reference object is shown in fig. (2.4-1a).

2.5 3-D shift invariance

3-D shift invariance in 3-D image matching is practical important and the extraction of location is the other essential role of image matching. The proposed system so far is not invariant to the target object shift along the z-axis, and thus we can not extract the 3-D location of the matched 3-D object.

In this section, we analyze z-invariance and provide solutions to extract the 3-D location of the matched 3-D object. Let the target 3-D object shifted along $x, y,$ and z by an amount $\Delta x, \Delta y,$ and $\Delta z, i.e.,$ we let $T(x, y; z) = T(x - \Delta x, y - \Delta y; z - \Delta z)$. Eq. (2.2-10a) becomes

$$i_c(x, y) = Re\left[H_R(x, y) \odot \left\{\int h(x, y; z) \odot T(x\text{-}\Delta x, y\text{-}\Delta y; z\text{-}\Delta z)dz\right\}\right] \quad (2.5\text{-}1)$$

$$= Re\left[H_R(x, y) \odot \left\{\int h(x, y; z\text{+}\Delta z) \odot T(x\text{-}\Delta x, y\text{-}\Delta y; z)dz\right\}\right]$$

After some manipulations, Eq. (2.5-1) can be cast into the following form involving convolution:

$$i_c(x, y) = Re\left[\left\{H_R(x, y) \odot \left[\int h(x, y; z) \odot T(x\text{-}\Delta x, y\text{-}\Delta y; z)dz\right]\right\} \otimes h^*(x, y; \Delta z)\right] \quad (2.5\text{-}2a)$$

$$= Re[\{H_R(x, y) \odot H_T(x\text{-}\Delta x, y\text{-}\Delta y)\} \otimes h^*(x, y; \Delta z)].$$

Similarly, Eq. (2.2-10b) becomes

$$i_s(x, y) = Im[\{H_R(x, y) \odot H_T(x\text{-}\Delta x, y\text{-}\Delta y)\} \otimes h^*(x, y; \Delta z)]. \quad (2.5\text{-}2b)$$

Now, if we add the correlation results from Eqs. (2.5-2a,b) to form a complex correlation, we have

$$i(x,y) = i_c(x,y) + j\, i_s(x,y) \qquad (2.5\text{-}3)$$

$$= H_R(x,y) \odot H_T(x\text{-}\Delta x, y\text{-}\Delta y) \otimes h^*(x,y;\Delta z).$$

Equation (2.5-3) states that if the 3-D target object $T(x,y;z) = R(x\text{-}\Delta x, y\text{-}\Delta y; z\text{-}\Delta z)$, i.e., it is the same as the 3-D reference object but shifted along $\Delta x, \Delta y$ and Δz, the correlation peak is located at Δx and Δy and the peak is broadened by the convolution of $h^*(x,y;\Delta z)$ due to the longitudinal shift of the target object. Fig. (2.5-1) plots the absolute value of Eq. (2.5-3) which shows a broadened correlation output when the 3-D target object shown in fig. (2.4-1a) is now located 51 cm away from the scanning mirrors and where the 3-D reference object is the same as the target object but located at 26 cm away.

To extract the information of Δz optically, the system shown in fig. (2.5-2) is proposed. The functional distribution of $i(x,y)$ in Eq.(2.5-3) would be placed as the form of a complex transparency, on the input plane and illuminated uniformly by a laser. A z-translated CCD camera detects the diffraction pattern and produces a 2-D output. When the distance from the input plane to the CCD camera is $z = \Delta z$, the output of the shifted CCD camera gives the 3-D coordinates of the shifted correlation peak. Mathematically, it is clear from Eq. (2.5-3) that $i(x,y) \otimes h(x,y;\Delta z)$ due to diffraction gives $H_R(x,y) \odot H_T(x\text{-}\Delta x, y\text{-}\Delta y)$ as $h(x,y;\Delta z) \otimes h^*(x,y;\Delta z) \sim \delta(x,y)$. Fig. (2.5-3) gives the intensity distribution of the correlation output as the CCD camera moves from $z = 10\,cm$ to $35\,cm$. Note that when $z = 25\,cm$ (51 cm - 26 cm), we have the sharp correlation peak as expected.

However, when the CCD camera is at $z = -\Delta z$, $h^*(x, y; \Delta z) \otimes h(x, y; -\Delta z)$ would not give a delta function as an output and hence the z-invariance of the proposed technique works only if the target 3-D object is located behind the 3D reference object. In addition, the use of CCD camera employs a z-scanning which is tedious and time consuming. Thus we propose a computation method to extract the 3-D location of the image matched 3-D object directly from the correlation output. We first apply the concept of power fringe-adjusted filtering, commonly used in the context of joint-transform correlation systems [21,22], to sharpen the defocused correlation peak obtained from Eq. (2.5-3). We then perform Wigner analysis on the sharpen correlation to extract the location of the correlation peak.

Section 3.1 gives the fundamental definitions and some related properties of the Wigner distribution. The location extraction of the matched 3-D object using power fringe adjusted filtering and Wigner distribution is presented in section 3.2. Computer simulation results are included in section 3.3.

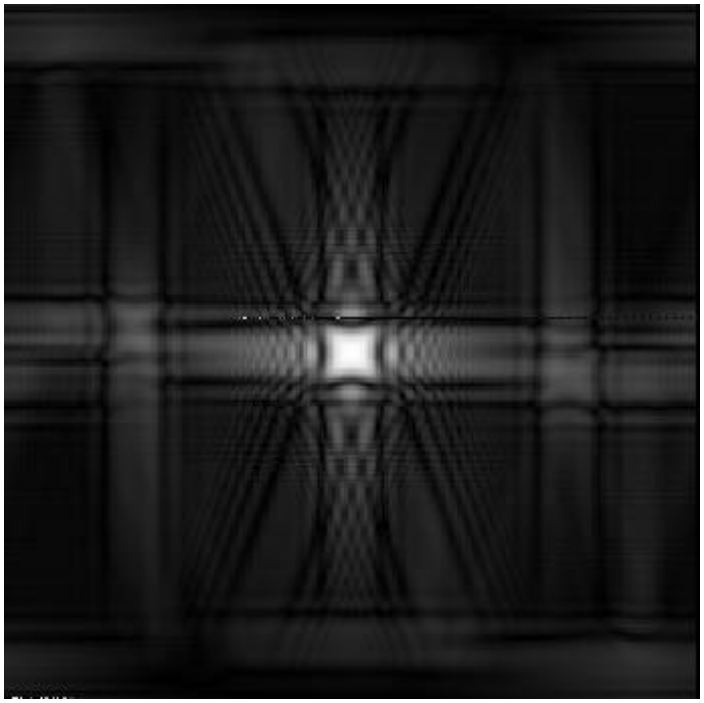

Figure (2.5-1): Correlation output when the 3-D target object and the 3-D reference object are displaced along the depth (z-direction), but otherwise the target object and the reference are the same.

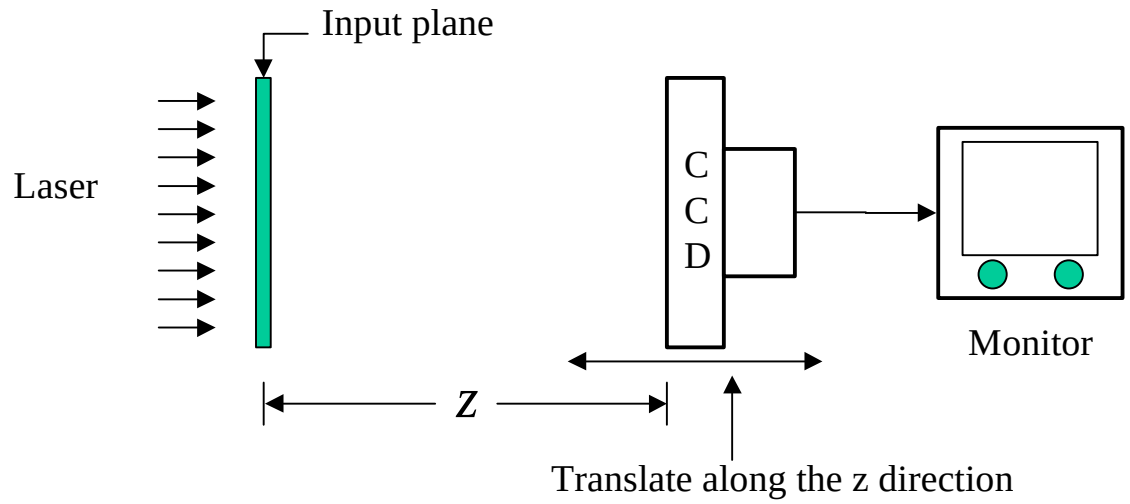

Figure (2.5-2): Optical system capable of extracting the depth difference between the 3-D target and the 3-D reference object.

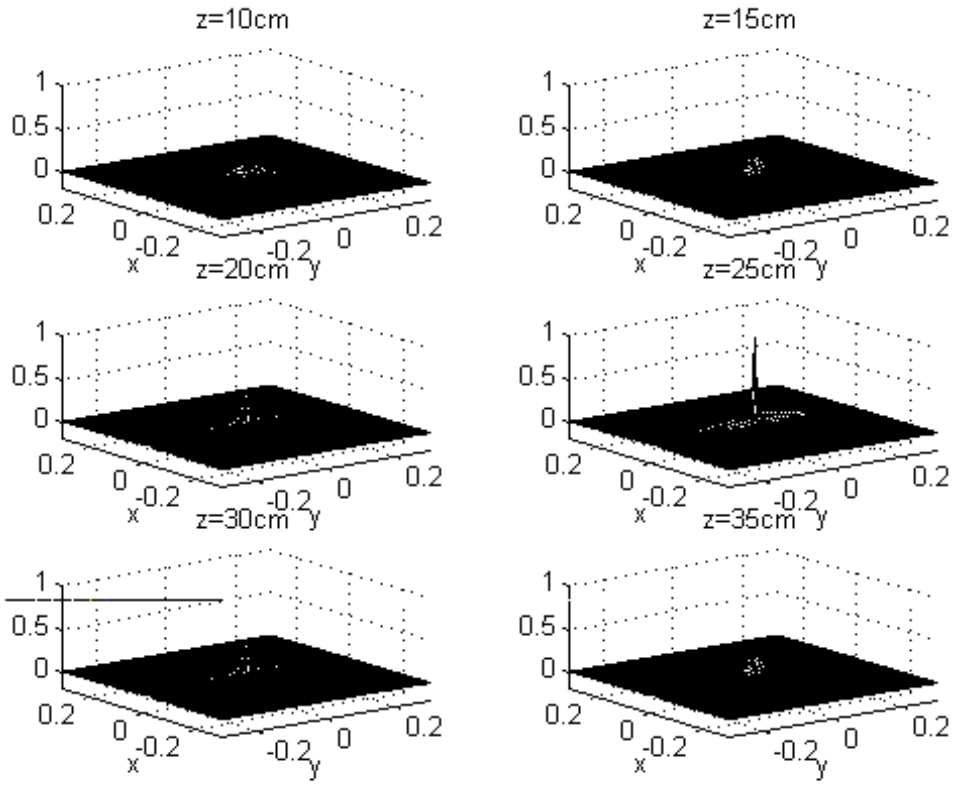

Figure (2.5-3): Correlation outputs as observed by the CCD camera when the camera is translating along the z-direction. The two 3-D objects are located at different places in depth by 25 cm, but otherwise they are the same. Note the strong correlation peak at z = 25 cm.

2.6 Physical interpretation

In the previous sections, we developed the optical 3-D matching system based on two pupil heterodyne scanning system. The two pupil analysis interprets the proposed optical system in terms of a linear system's transfer function. However, it is not easy to get physical insight directly from that interpretation. Thus, in this section, we present the proposed optical system in terms of masks to get the physical insight of the system.

Fig. (2.6-1) shows the optical heterodyne scanning system. In this figure, the pupils and lens are substituted by masks. In other words, the spatial distribution of the scanning beam is modulated directly by the masks. A rigorous mathematical analysis of the optical system, that is based on the spatial frequency domain analysis and the synthesis of optical transfer function (OTF), has been developed in the previous sections. This section presents an intuitive and physical description of the system. In fig. (2.6-1), the laser beam generated by HeNe laser is split into two paths by a beam splitter. The temporal frequency of each beam is shifted by an acousto-optic frequency shifter, operating at frequency Ω. These beams are collimated by beam expanders BE1 and BE2. Each collimated beam is modulated spatially by masks, m_1 and m_2 respectively, and are combined by a beam splitter, BS1. The intensity pattern of the combined beam, $I_s(x, y; z)$ at a distance z away from the masks is given by

$$I_s(x, y; z) = | m_{1z}(x, y)exp[j(\omega_o + \Omega)t] + m_{2z}(x, y)exp(j\omega_o t)|^2, \qquad (2.6\text{-}1)$$

where $m_{1z}(x, y)$ and $m_{2z}(x, y)$ are respectively diffracted patterns of masks $m_1(x, y)$ and $m_2(x, y)$, that are given by

$$m_{iz}(x, y) = m_i(x, y) \otimes h(x, y; z);\ i=1, 2, \qquad (2.6\text{-}2)$$

where $h(x, y; z)$ is called the free space impulse response, and is given by

$$h(x,y;z)= \frac{jk_o}{2\pi z} exp\left[-j\frac{k_o}{2z}\left(x^2+y^2\right)\right],$$

with k_o representing the wave number of the scanning beam and $\otimes$ denoting the 2-D convolution operation, which is defined as:

$$g_1(x,y) \otimes g_2(x,y) \;=\; \int\int g_1(x',y')g_2(x-x',y-y')dx'dy'. \qquad (2.6\text{-}3)$$

When the 3-D intensity pattern of the combined beam, $I_s(x,y;z)$ scans on the object amplitude transparency, $I_o(x,y;z)$, located z away from the masks as shown in fig. (2.6-1), the total intensity passes through $I_o(x,y;z)$ is given by

$$I(x,y) = \int\int I_s(x',y';z)\; I_o(x+x',y+y';z)dx'dy', \qquad (2.6\text{-}4)$$

$$= I_s(x,y;z) \odot I_o(x,y;z).$$

Note that the total intensity that passes through the object intensity transparency is proportional to the correlation between the scanning beam and the object amplitude transparency. The symbol $\odot$ in Eq. (2.6-4), denotes the 2-D correlation operation that is defined as:

$$g(x,y) \odot h(x,y) \;=\; \int\int g^*(x',y')h(x+x',y+y')dx'dy'. \qquad (2.6\text{-}5)$$

The total intensity is collected and transformed to an electric signal by the photo-detector. The current output that is proportional to the total intensity consists of a DC term and heterodyne term with temporal frequency at Ω.

The in-phase and the quadrature-phase components of the heterodyne term of the output current are extracted by respectively multiplying it with $sin(\Omega t)$, $cos(\Omega t)$, and low-pass filtering. These are given by

$$Re\{m_{1z}(x', y')\, m^*_{2z}(x', y')\} \odot I_o(x, y; z), \tag{2.6-6a}$$

and

$$Im\{m_{1z}(x', y')\, m^*_{2z}(x', y')\} \odot I_o(x, y; z). \tag{2.6-6b}$$

where $Re[.]$ and $Im[.]$ represent the real part of and the imaginary part of the cross term of the scanning beam respectively.

Note that the undesirable space-variant DC terms have been eliminated due to the heterodyne photo detection. The two outputs respectively represent the correlation between the real part of, and the imaginary part of the product of the diffraction patterns of each mask, and the object intensity. For a general 3-D object that is distributed along z as well as $x - y$ distribution, equations $(2.6\text{-}6a,b)$ are integrated along the depth z due to the superposition. These are given by

$$i_r(x, y) = \int Re\{m_{1z}(x, y)\, m^*_{2z}(x, y) \odot I_o(x, y; z)\}\, dz, \tag{2.6-7a}$$

and

$$i_i(x, y) = \int Im\{m_{1z}(x, y)\, m^*_{2z}(x, y) \odot I_o(x, y; z)\}\, dz, \tag{2.6-7b}$$

respectively.

2.6.1 Recording stage of the holographic information of objects

Fig. (2.6-2) shows the optical system in the recording stage of holographic information of an object. Here, we choose masks, $m_1(x,y)$=$\delta(x,y)$ and $m_2(x,y)$=1 and then scan a reference object, $R(x,y;z)$ i.e., we let $I_o(x,y;z) = R(x,y;z)$. The diffracted pattern from the first mask, $m_1(x,y)$=$\delta(x,y)$ is the sperical wave, $m_{1z}(x,y) = \frac{jk_o}{2\pi z} exp\Big[- j\Big\{ \frac{(x^2+y^2)k_o}{2z} \Big\}\Big]$ and the diffracted pattern from the second mask, $m_2(x,y)$=1, is the plane wave, $m_{2z}(x,y) = 1$. Thus, 3-D distribution of the scanning beam pattern is the Fresnel zone pattern. That is given by

$$m_{1z}(x,y)\, m^{*}_{2z}(x,y) = \frac{jk_o}{2\pi z} exp\Big[- j\frac{(x^2+y^2)k_o}{2z} \Big], \qquad (2.6\text{-}8)$$

One output of the system is the correlation between the real part of the Fresnel zone pattern and the intensity distribution of the object, that corresponds to the cosine hologram of the object as in Eq. (2.6-7a). The other output of the system is the correlation between the imaginary part of the Fresnel zone pattern and the intensity distribution of the object, that corresponds to the sine hologram of the object as in Eq. (2.6-7b). Thus, the outputs of the system are cosine and sine holograms of the reference object. These are given by

$$i_r(x,y) \;=\; \int \frac{k_o}{2\pi z} cos \left[\frac{k_o}{2z} \left(x^2 + y^2 \right) \right] \odot R(x,y;z)\, dz, \qquad (2.6\text{-}9a)$$

$$i_i(x,y) \;=\; \int \frac{k_o}{2\pi z} sin \left[\frac{k_o}{2z} \left(x^2 + y^2 \right) \right] \odot R(x,y;z)\, dz. \qquad (2.6\text{-}9b)$$

These output currents of the system are stored in a digital computer using an analog-to-digital converter. In the digital computer, the complex hologram is achieved by adding two holograms in a complex manner:

$$H_R(x,y) = i_r(x,y;z) + j\, i_i(x,y;z) \tag{2.6-10}$$

$$= \int j\frac{k_o}{2\pi z} exp\left[\frac{-jk_o}{2z}\left(x^2+y^2\right)\right] \odot R(x,y;z)dz.$$

Note that the complex hologram of an object has the depth information of the object as a form of fringe pattern.

2.6.2 3-D image matching stage

After the complex hologram of the object is recorded as described in section 2.6.1, the object is removed. We shall call the hologram as a reference hologram as the object being recorded is the reference object. The reference hologram will be used to match a 3-D target.

In the matching stage, a target object, $T(x,y;z)$, now is placed z away from the masks of the scanning system. Let $m_1(x,y) = H_R(x,y)$, and keep $m_2(x,y)$=1 as in the holographic recording stage, and then the target object, $T(x,y;z)$ is scanned by the system.

The diffracted pattern from the first mask, $m_1(x,y) = H_R(x,y)$, is the reconstructed image of the reference hologram. That is given by

$$m_{1z}(x,y) = \left\{\int \frac{jk_o}{2\pi z} exp\left[\frac{-jk_o}{2z}\left(x^2+y^2\right)\right] \odot R(x,y;z)\, dz\right\} \otimes h(x,y;z). \tag{2.6-11}$$

The diffracted pattern from the second mask, $m_2(x,y)$=1, is the plane wave, $m_{2z}(x,y) = 1$. Thus, 3-D distribution of the scanning beam is the reconstructed image of the reference hologram. That is given by

$$m_{1z}(x,y)\, m_{2z}^{*}(x,y) = \left\{ \int \frac{jk_o}{2\pi z} exp\left[\frac{-jk_o}{2z}\left(x^2+y^2\right)\right] \odot R(x,y;z)\, dz \right\} \quad (2.6\text{-}12)$$

$$\otimes\, h(x,y;z).$$

Note that the 3-D distribution of the scanning beam is the same as the actual intensity distribution of the reference object as shown in fig. (2.6-3), in which the dotted line represents the reconstructed field of the reference object.

According to Eqs. (2.6-7a,b), the output currents are given by

$$i_r(x,y;z) = Re[m_{1z}(x,y)\, m_{2z}^{*}(x,y)] \odot T(x,y;z)\,, \quad (2.6\text{-}13a)$$

$$= Re[H_R(x,y) \otimes h(x,y;z)] \odot T(x,y;z),$$

$$= Re\left[\left\{ \frac{jk_o}{2\pi z} exp\left[\frac{-jk_o}{2z}\left(x^2+y^2\right)\right] \odot R(x,y;z) \right\} \otimes h(x,y;z) \right] \odot T(x,y;z),$$

$$= Re\left[\left\{ \frac{jk_o}{2\pi z} exp\left[\frac{-jk_o}{2z}\left(x^2+y^2\right)\right] \odot R(x,y;z) \right\} \right.$$

$$\left. \odot \left\{ \frac{jk_o}{2\pi z} exp\left[-j\frac{k_o}{2z}\left(x^2+y^2\right)\right] \odot T(x,y;z) \right\} \right],$$

$$= Re[H_R(x,y) \odot H_T(x,y)],$$

$$= c_r(x,y)\,,$$

$$i_i(x,y;z) = Im[m_{1z}(x,y)\, m_{2z}^{*}(x,y)] \odot T(x,y;z)\,, \quad (2.6\text{-}13b)$$

$$= \quad Im[H_R(x,y) \otimes h(x,y;z)] \odot T(x,y;z),$$

$$= \; Im\left[\left\{\frac{jk_o}{2\pi z} exp\left[\frac{-jk_o}{2z}\left(x^2+y^2\right)\right] \odot R(x,y;z)\right\} \otimes h(x,y;z)\right] \odot T(x,y;z),$$

$$= Im\left[\left\{\frac{jk_o}{2\pi z} exp\left[\frac{-jk_o}{2z}\left(x^2+y^2\right)\right] \odot R(x,y;z)\right\},\right.$$

$$\left. \odot \left\{\frac{jk_o}{2\pi z} exp\left[-j\frac{k_o}{2z}\left(x^2+y^2\right)\right] \odot T(x,y;z)\right\}\right],$$

$$= Im[H_R(x,y) \odot H_T(x,y)],$$

$$= \quad c_i(x,y).$$

where $H_T(x,y)$ is the complex hologram of the target object, $T(x,y)$.

The complex correlation is achieved by adding two correlations in a complex manner:

$$\begin{aligned} c(x,y) \; &= \; c_r(x,y) \; + j\, c_i(x,y), \\ &= \; H_R(x,y) \odot \; H_T(x,y). \end{aligned} \tag{2.6-14}$$

Equations (2.6-14) demonstrates that the system can perform correlation of two holographic information, and hence 3-D image matching is possible.

2.6.2.1 Matched case with the same location

Let us consider the case that the target object, which has the same intensity pattern as the reference object, is placed at the same location as the reference object, i.e., $T(x,y;z) = R(x,y;z)$ as shown in fig. (2.6-4). Since the identical target object is located at the same location as the reference object, the hologram of the target object is the same as the hologram of the reference object, that is $H_T(x,y) = H_R(x,y)$ in Eq. (2.6-14). Thus the correlation in Eq. (2.6-14) gives a strong correlation peak at the origin. That is given by

$$c(x,y) = H_R(x,y) \odot H_R(x,y), \qquad (2.6\text{-}15)$$
$$= A_c(x,y).$$

where $A_c(x,y)$ represents the auto-correlation between the identical holograms; thus, $A_c(x,y)$ has the maximum value at the origin.

This corresponds to the following physical interpretation. First, the scanning beam pattern represented as a dotted line in fig. (2.6-4), scans the target object that is represented as a solid line in fig. (2.6-4). When the scanning mirrors face the target object, the scanning beam pattern overlaps the target object as shown in fig. (2.6-4). Thus, we get the maximum reflected light. That corresponds to the strong correlation peak at the origin in Eq. (2.6-15).

2.6.2.2 Matched case with a transversely shifted location

Let us consider the case that the target object which has the same intensity pattern as the reference object, is placed at the shifted location along the transverse direction, i.e., $T(x,y;z) = R(x-\Delta x, y-\Delta y; z)$ as shown in fig. (2.6-5). Since the identical target object is placed at the transversely shifted location, the hologram of the target object is the same as the hologram of the reference object except shifted location. That is $H_T(x,y) = H_R(x-\Delta x, y-\Delta y)$ in Eq. (2.6-14). Thus the correlation in Eq. (2.6-14) gives the strong correlation peak at that shifted location. That is given by

$$c(x,y) = H_R(x,y) \odot H_R(x-\Delta x, y-\Delta y), \qquad (2.6\text{-}16)$$
$$= A_c(x-\Delta x, y-\Delta y).$$

where the auto-correlation, $A_c(x,y)$ is shifted by Δx and Δy along transverse direction. Thus, we get the strong correlation peak at the shifted location. The shifted location of the correlation peak gives to the shifted location of the target object.

This corresponds to the following physical interpretation. First, the scanning beam pattern represented as a dotted line in fig. (2.6-5), scans the target object represented as a solid line in fig. (2.6-5). When the scanning mirrors face the target object, the scanning beam pattern overlaps the target object as shown in fig. (2.6-5). Thus, we get the maximum reflected light. That corresponds the strong correlation peak at shifted location in Eq. (2.6-16). In this case, the maximum correlation peak is achieved when the scanning mirrors face the shifted location of the target object with respect to the location of the reference object. The shifted location of the scanning mirrors corresponds the shifted location of the correlation peak.

2.6.2.3 Matched case with a longitudinally shifted location

Let us consider the case that the target object which has the same intensity pattern as the reference object is placed at the shifted location along the longitudinal direction, i.e., $T(x,y;z) = R(x,y;z+\Delta z)$ as shown in fig. (2.6-6). Unlike the transversely shifted case in the section 2.6.2.2, the hologram of the identical target object with its shifted location along depth direction is not just the shifted version of the reference hologram. Because the fringe pattern in a hologram depends on the depth location, the fringe pattern of the hologram of the target object is different from that of the reference hologram. Thus, direct correlation between the hologram of the target object and that of the reference object does not give the strong correlation peak. However, the hologram of the target object is just the defocused version of the hologram of the reference object. That is given by

$$H_T(x,y) = \int h(x,y;z) \odot T(x,y;z) dz, \tag{2.6-17}$$

$$= \int h(x,y;z+\Delta z) \odot R(x,y;z+\Delta z) dz,$$

$$= \left\{ \int h(x,y;z) \odot R(x,y;z) dz \right\} \otimes h^*(x,y;\Delta z)$$

$$= H_R(x,y) \otimes h^*(x,y;\Delta z).$$

Thus, the output of the system, the correlation between the hologram of the target object and that of the reference object is the defocused auto-correlation. That is given by

$$\begin{aligned} c(x,y) &= H_R(x,y) \odot H_T(x,y), \\ &= H_R(x,y) \odot \{H_R(x,y) \otimes h^*(x,y;\Delta z)\}, \\ &= \{H_R(x,y) \odot H_R(x,y)\} \otimes h^*(x,y;\Delta z), \\ &= Ac(x,y) \otimes h^*(x,y;\Delta z). \end{aligned} \tag{2.6-18}$$

Note that the strong correlation peak is achieved by focusing the defocused correlation output by using the technique in section 2.5.

This corresponds to the following physical interpretation. First, the scanning beam pattern that is represented as a dotted line in fig. (2.6-6), scans the target object that is represented as a solid line in fig. (2.6-6). When the scanning mirrors scans the target object, the intensity of the reflected light is the correlation between the diffracted beam pattern from the reconstruction of the reference hologram, and the matched target object.

Even though it does not give out the maximum reflection like the previous cases, it corresponds to the defocused correlation. Thus, by using the focusing process of the section 2.5, the strong correlation peak can be achieved.

2.6.2.4 Mismatched case

Let us consider the case that the target object which has a different intensity pattern than the reference object; in other words, the 3-D image of the target object is not matched with that of the reference object, it is placed as shown in fig. (2.6-7). Since the 3-D image of the target object is not matched with that of the reference object, the hologram of the target object is different from the hologram of the reference object. That is $H_T(x,y) \neq H_R(x,y)$ in Eq. (2.6-14). Thus the correlation in Eq. (2.6-14) does not give the strong correlation peak.

This corresponds to the following physical interpretation. First, the scanning beam represented as a dotted line in fig. (2.6-7), scans the target object represented as a solid line in fig. (2.6-7). Even though the scanning mirrors face the target object, the scanning beam pattern does not overlap the target object as shown in fig. (2.6-7). Thus, a small part of the scanning beam is reflected, which is smaller than the maximum reflected light as in matched case. That corresponds to the no-correlation peak in the output.

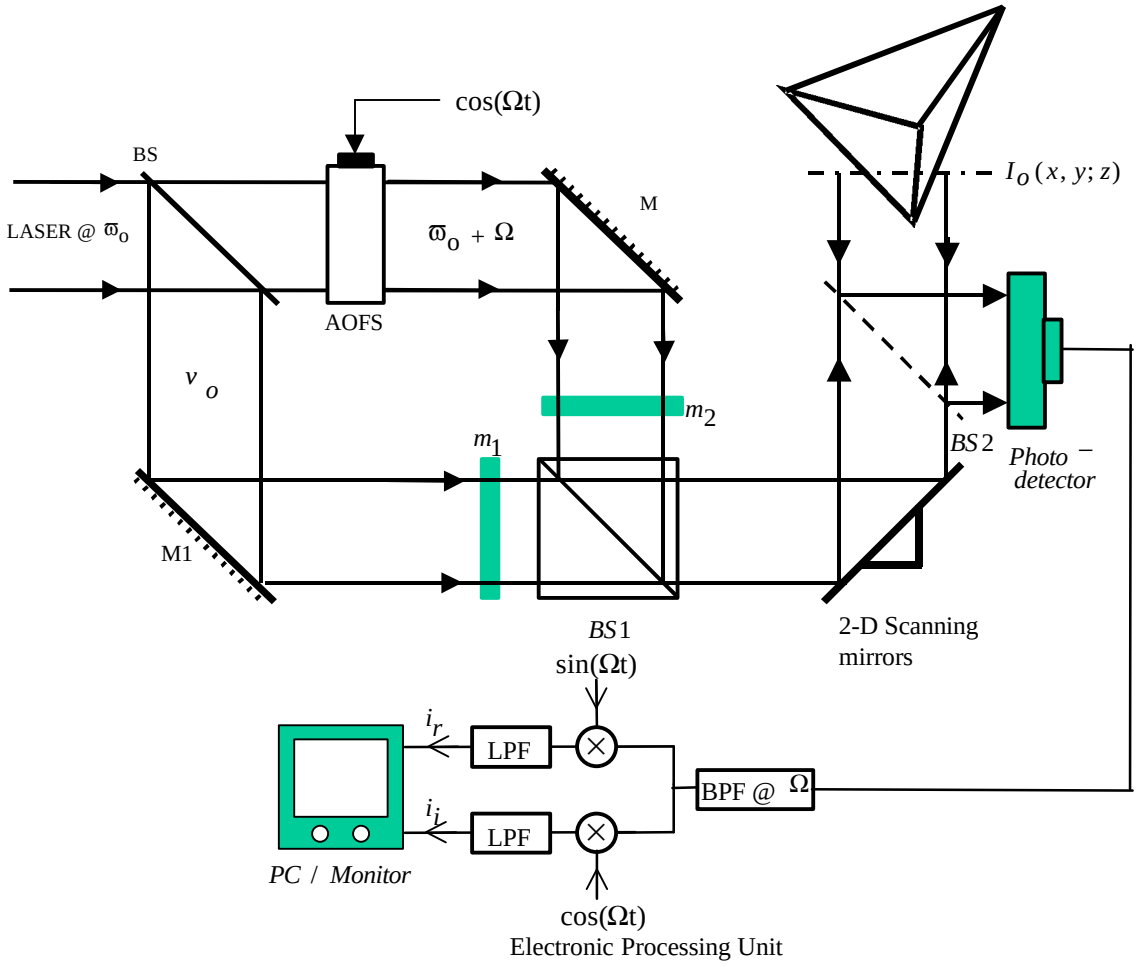

Figure (2.6-1): Optical scanning holography system.
(BS, BS1, $BS2$: beam splitters, M,M1: mirrors, m_1,m_2: masks, AOFS: acousto-optic frequency shifter; BPF@Ω: bandpass filter tuned at frequency Ω; LPF: low pass filter)

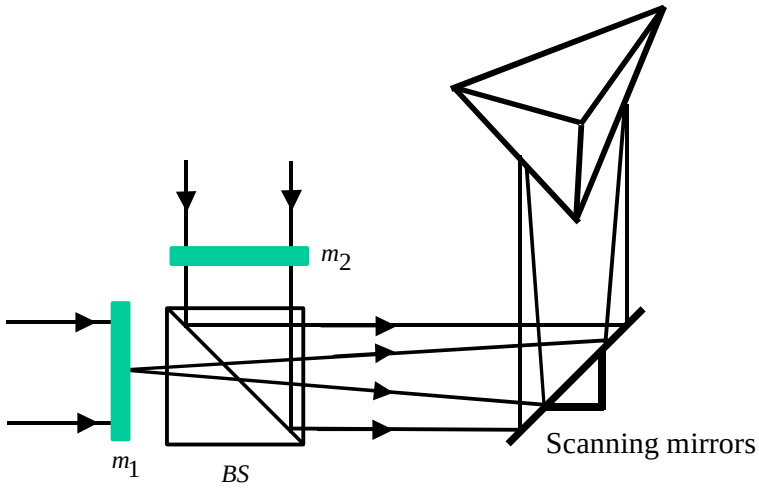

Figure(2.6-2): Recording stage of the holographic information of objects.
(BS: beam splitter, m_1,m_2: masks)

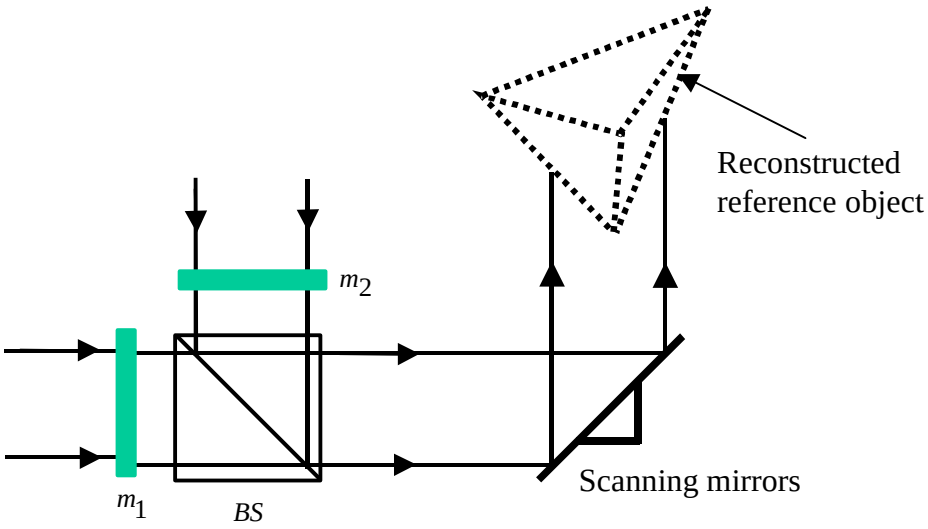

Figure (2.6-3): Scanning beam pattern in matching stage.
(BS: beam splitter, m_1,m_2: masks)

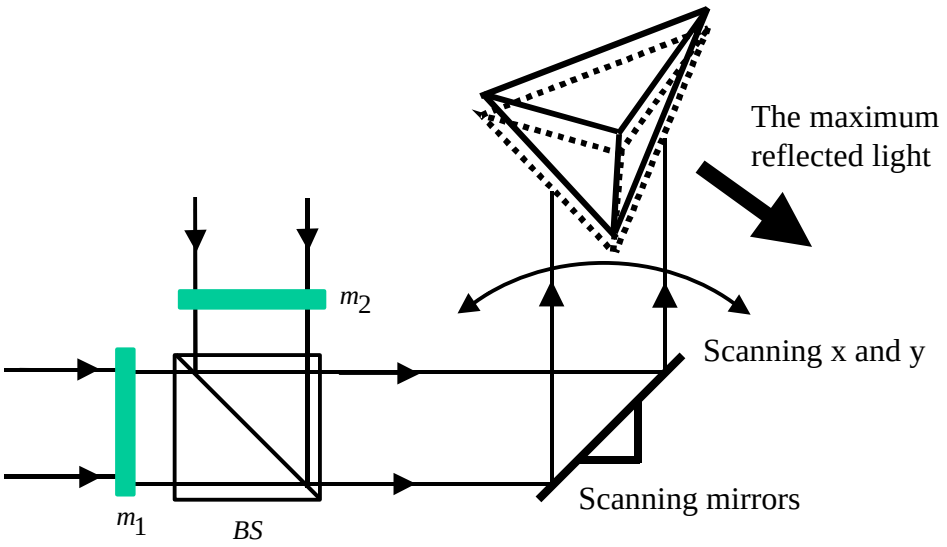

Figure (2.6-4): Scanning the matched target object is placed at the same location.
(BS: beam splitter, m_1,m_2: masks)

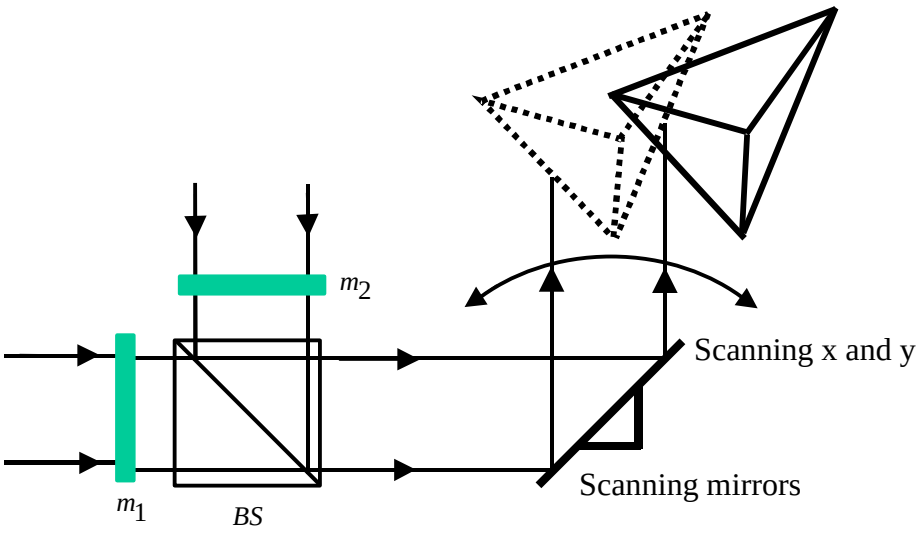

Figure (2.6-5) Scanning the matched target object is placed at the transversely shifted location. (BS: beam splitter, m_1,m_2: masks)

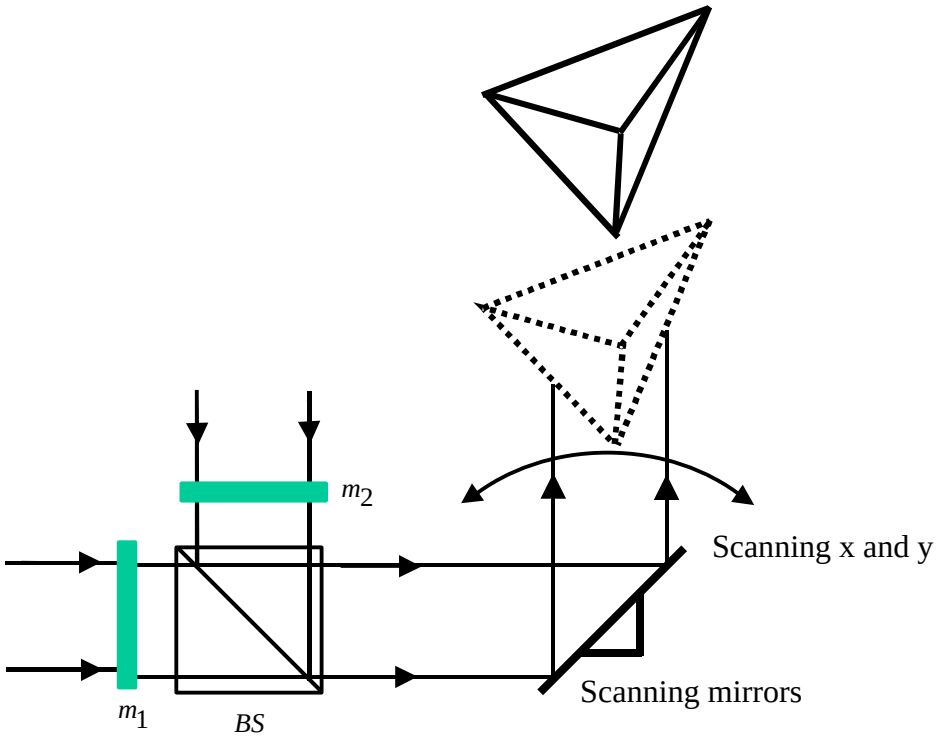

Figure (2.6-6): Scanning the matched target object is placed at the longitudinally shifted location. (BS: beam splitter, m_1,m_2: masks)

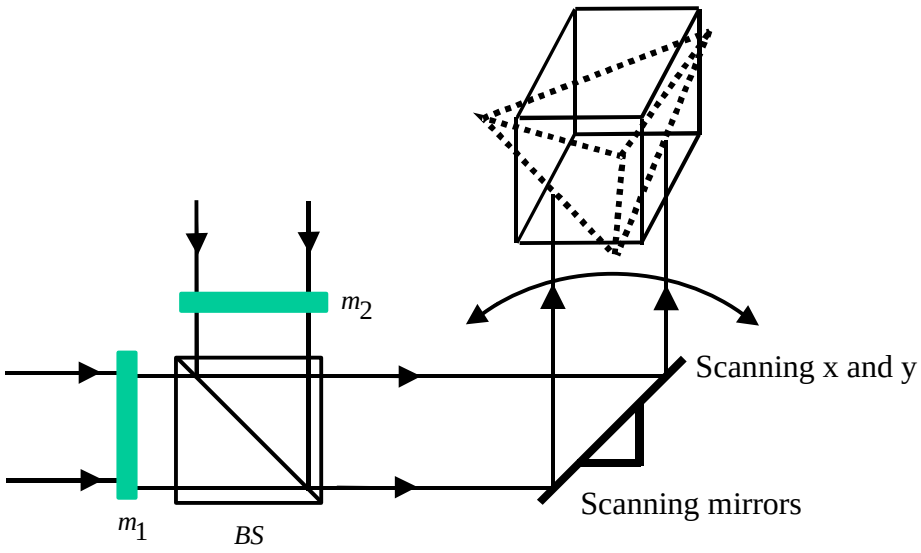

Figure (2.6-7) Scanning the mis-matched target object.
(BS: beam splitter, m_1,m_2: masks)

Chapter 3: 3-D location extraction of image matched 3-D object

In chapter 2, 3-D image matching technique was presented. The optical system basically performs a correlation of the holographic information of a 3-D reference object and that of a 3-D target object, and hence 3-D matching is possible. However, the correlation output does not give a strong correlation peak when the location of the 3-D target is shifted along the depth direction because the holographic correlation is basically a 2-D correlation process. In fact, the correlation peak is smeared out or broadened by a convolution process, reminiscent of defocused imaging in coherent optical systems [1].

To achieve z- or depth- invariance, it has been proposed that the "defocused" correlation would first be presented as a complex transparency and illuminated by a laser. A z-translated CCD camera would detect the diffraction pattern and give the 3-D coordinates of the shifted target object [1]. However, the proposed system has a drawback in that only 3-D targets that are located farther away from the 3-D reference object can be shift invariantly detected. In addition, the method employs a manual and semi-manual process that is tedious and time consuming.

Holography is widely used in optical imaging and information systems, and the needs for the analysis of holographic information have been increased. There are several techniques in the analysis of fringe patterns of holograms, especially in the field of particle field holography [17-20]. This chapter presents a digital signal analysis technique that extracts the 3-D location of the matched object. This technique is based on the power fringe-adjusted filtering [21,22] and Wigner analysis [23,24]. Power fringe adjusted filtering is a widely used filtering method to sharpen the correlation peak in pattern recognition, whereas the Wigner distribution is a signal transformation for space-frequency analysis in signal processing, which yields the frequency contents of the signal at different space instant. A brief review of the Wigner distribution is given in section 3.1. In

section 3.2, we discuss the Wigner analysis of power fringe-adjusted filtering of defocused correlation. In section 3.3, we present computer simulation results.

3.1 Wigner distribution [17,23,24]

The information about the 3-D location of the image matched object is contained in the correlation output as a form of fringe pattern that is the spatial frequency varying signal against the space. The Wigner distribution is a signal transformation that is convenient for such a time-frequency (or a space-frequency) analysis because the Wigner distribution yields the time (space) variation of the frequency components of a signal. Only the basic definitions and properties of discrete Wigner distribution that are used in this paper are discussed here. The complete set of properties of the Wigner distribution was formulated by Claasen and Mecklenbrauker [23, 24]. The auto-Wigner distribution of signal $f(t)$ is defined by

$$W_f(t,w) = \int_{-\infty}^{\infty} f\left(t+\frac{\tau}{2}\right) f^*\left(t-\frac{\tau}{2}\right) exp(-jw\tau) d\tau \qquad (3.1\text{-}1)$$

The auto-Wigner distribution of complex-valued discrete signals $f(n)$ is given by

$$W_f(n,\theta) = 2\sum_{k=-\infty}^{\infty} exp(-j2k\theta) f(n+k) f^*(n-k), \qquad (3.1\text{-}2)$$

where k and n are discrete variables and θ is a continuous variable.

The following are the properties of the discrete-time (discrete-space) Wigner distribution, that are used in this paper:

1. $Periodicity\, with\, repect\, to\, the\, continuous\, frequency\, variable$

The discrete-time (discrete-space) Wigner distribution is a function of the discrete-time (discrete-space) variable n and the continuous frequency variable θ. The discrete-time (discrete-space) Wigner distribution is periodic with a period π with respect to the continuous frequency variable θ:

$$W_f(n,\theta) = W_f(n,\theta+\pi),\ \forall\ n,\theta. \tag{3.1-3}$$

2. $Finite\, duration$

When the signal is limited in time (space), the Wigner distribution is also limited:

$$f(n) = 0, \quad n < n_a\ or\ n > n_b \Rightarrow W_f(n,\theta) = 0, \quad n < n_a\ or\ n > n_b \tag{3.1-4}$$

3. $Band\, limitted\, signals$

Since the Wigner distribution is repeated with respect to the frequency variable θ with a period π, frequency components that are π apart have same influence on the Wigner distribution, which causes aliasing. However, if the spectrum of the signal is non zero only in an interval of a duration less than π, aliasing is prevented. Comparing the band limit to the Nyquist criteria for the Fourier spectrum of a discrete signal, the non zero frequency interval of duration is twice as small as the Nyquist criteria. Therefore twice the sampling rate of the Nyquist rate is required to prevent aliasing.

Due to the properties of the Wigner distribution, the discrete Wigner distribution of a signal which has the finite extend confined to the interval $[0\ N-1]$, is also confined at the

same extend of the signal, i.e., $W_f(n,\theta) = 0$ for $n < 0$ or $n > N$, and the frequency variable, θ, is also a periodic function with a period π. Therefore the discrete Wigner distribution is fully determined for the intervals $n \in [0, N-1]$ and $\theta \in$ (-π/2 π/2]. Discretizing $W_f(n,\theta)$ about θ with a sampling interval $\Delta\theta=\frac{\pi}{N}$ in the interval (-π/2 π/2], we get the discrete Wigner distribution:

$$W_f\left(n, \frac{\pi}{N}m\right) = 2\sum_{k=-\infty}^{\infty} exp\left(-j\frac{2\pi}{N}km\right) f(n+k)f^*(n-k) \qquad (3.1\text{-}5)$$

where m is an integer variable satisfying $-N/2+1 \le m \le N/2$.

Note that the sequence of duration is finite, i.e. $-N/2+1 \le k \le N/2-1$, therefore the equation $(3.1\text{-}5)$becomes

$$W_f\left(n, \frac{\pi}{N}m\right) = 2\sum_{k=-N/2+1}^{N/2-1} f(n+k)f^*(n-k)exp\left(-j\frac{2\pi}{N}km\right) \qquad (3.1\text{-}6)$$

Defining a new sequence $z_n(k)$ by

$$z_n(k) = \begin{cases} 2\,f(n+k)\,f^*(n-k) & 0 \le k \le \frac{N}{2}-1 \\ 0 & k = \frac{N}{2} \\ 2\,f(n+k-N)\,f^*(n-k+N) & \frac{N}{2}+1 \le k \le N-1 \end{cases} \qquad (3.1\text{-}7)$$

The Eq.$(3.1\text{-}6)$becomes

$$W_f\left(n, \frac{\pi}{N}m\right) = \sum_{k=0}^{N-1} z_n(k)exp\left(-j\frac{2\pi}{N}km\right).$$

The N-points discrete Fourier transform, $W(m)$, of the sequence $z_n(k)$ is defined by

$$W(m) = \sum_{k=0}^{N-1} z_n(k) exp\left(- j\frac{2\pi}{N} km \right) \tag{3.1-8}$$

where $m \in \{0, 1, ..., N-1\}$.

From the periodicity of the discrete Fourier transformation, the discrete Wigner distribution is given by

$$W_f\left(n, \frac{\pi}{N} m\right) = \begin{cases} W(m) & 0 \le m \le \frac{N}{2} \\ W(m+N) & \frac{-N}{2} + 1 \le m \le -1 \end{cases} \tag{3.1-9}$$

Note that a discrete Wigner distribution can be achieved by the discrete Fourier transformation of the sequence, $z_n(k)$ at each value of n, and the discrete Fourier transformation can be performed effectively by the use of Fast Fourier Transformation (FFT) algorithms.

3.2 Power fringe-adjusted filtering and Wigner analysis of the 3-D holographic matching

3.2.1 Power fringe-adjusted filtering of the 3-D holographic matching

The 3-D holographic correlation output between a 3-D reference object and a z-shifted 3-D target object has a broad correlation peak as calculated by Eq. (2.5-3), which makes the system a poor discriminator. We shall employ the concept of the power fringe-adjusted filtering to sharpen the peak. The proposed filter is defined as:

$$F(k_x, k_y) = \frac{1}{|\mathcal{F}\{H_R\}|^2 + \delta} \tag{3.2-1}$$

where δ is a small value of either a constant or, some function of k_x or k_y. δ is added to

overcome the possible pole problems of the filter [21,22]. The filtered correlation in the frequency domain is given by the product of the Fourier transformation of the Eq. (2.5-3) and the power fringe- adjusted filter. Thus the power fringe-adjusted (PFA) - filtered correlation in the frequency domain is given by

$$C_{pfa}(k_x, k_y) = \mathcal{F}\{c(x,y)\} \times F(k_x, k_y) = \frac{\mathcal{F}^*\{H_R\}\mathcal{F}\{H_T\}H^*(k_x, k_y; \Delta z)}{|\mathcal{F}\{H_R\}|^2 + \delta} \quad (3.2\text{-}2)$$

When the 3-D target object is the same as the 3-D reference object but shifted by $\Delta x, \Delta y$ and Δz, i.e., $T(x,y;z) = R(x - \Delta x, y - \Delta y; z - \Delta z)$, the power fringe-adjusted filtered correlation in the frequency domain is

$$C_{pfa}(k_x, k_y) = \frac{|\mathcal{F}\{H_R\}|^2}{|\mathcal{F}\{H_R\}|^2 + \delta} exp(j(\Delta x k_x + \Delta y k_y))H^*(k_x, k_y; \Delta z) \quad (3.2\text{-}3)$$

$$\simeq exp(j(\Delta x k_x + \Delta y k_y))H^*(k_x, k_y; \Delta z).$$

as $\mathcal{F}\{H_T\} = \mathcal{F}\{H_T(x - \Delta x, y - \Delta y)\} = \mathcal{F}\{H_R(x,y)\}exp(j(\Delta x k_x + \Delta y k_y))$. Note that the power fringe-adjusted filtered correlation in the space domain is the shifted Fresnel zone pattern given by the inverse Fourier transformation of Eq. (3.2-3):

$$c_{pfa}(x,y) = \mathcal{F}^{-1}\{C_{pfa}(k_x, k_y)\} = \delta(x - \Delta x, y - \Delta y) \otimes h^*(x, y; \Delta z) \quad (3.2\text{-}4)$$

$$= h^*(x - \Delta x, y - \Delta y; \Delta z)$$

$$= \frac{-jk_0}{2\pi\Delta z} exp\left[j\frac{k_0}{2\Delta z}((x - \Delta x)^2 + (y - \Delta y)^2)\right]$$

according to the definition in Eq. (2.1-4). This power fringe adjusted filtering can be performed either by conventional coherent optical processors or digital computers.

3.2.2 Wigner analysis of 3-D holographic matching

The information of the 3-D shifted location of the pattern-matched object is contained in the output correlation as a form of fringe pattern that is the space-frequency characteristic (fringe pattern) of the space signal (the image). The Wigner distribution is a signal transformation that is convenient for such a time-frequency (or a space-frequency) analysis because Wigner distribution yields the time (space) variation of the frequency components of a signal. The Wigner distribution of a function displays the instantaneous frequency curve of the function in the time-frequency (space-frequency) plane.

Because the local frequency of the chirp signal $f(t) = exp(j\alpha t^2/2)$ is a monotonically increasing function along the time axis, the Wigner distribution of the signal gives a line impulse on the time-frequency domain with the slope of the instantaneous frequency on the time-frequency plane. This is given by

$$W_f(t,\omega) = 2\pi\delta(\omega - \alpha t) \tag{3.2-5}$$

The power fringe adjust filtered holographic correlation of the 3-D pattern-matched object is a form of 2-D chirp type signal given by Eq. (3.2-4), thus the absolute value of continuous Wigner distribution of the power fringe adjusted filtered correlation output, $c_{pfa}(x,y)$, about x for any given y value, $y = y'$, is given by

$$\left|W_{h^*_{\Delta z}}(x,\omega;y')\right| = \left| -\, j\frac{1}{2\pi}\left(\frac{k_o}{\Delta z}\right)^2 \delta\left(\omega - \frac{k_o}{\Delta z}(x - \Delta x)\right)\right. \tag{3.2-6}$$

$$\left. \times\, exp\left[-\, j\frac{k_o}{2\Delta z}(y' - \Delta y)^2\right]\right|$$

$$= \left| \frac{1}{2\pi} \left(\frac{k_o}{\Delta z} \right)^2 \delta \left(\omega - \frac{k_o}{\Delta z} (x - \Delta x) \right) \right|$$

Note that the absolute value of the Wigner distribution of the power fringe-adjusted filtered correlation is the desired line impulse on the space-frequency plane. This line impulse intersects with the $x - axis$, and the intersection point is Δx which is the shifted location of the 3-D target along the x-axis. Furthermore, the slope of the line impulse is inversely proportional to the shifted location along the $z - axis$, that is -$k_o/2\Delta z$. Therefore, if the wave length λ is known ($k_o = \lambda/2\pi$), the shifted location is known by directly measuring the slope of the line.

When the 3-D target is not matched with the 3-D image of the reference object, we do not observe the line impulse in the Wigner distribution. In the same manner, the shift along the y − axis can be obtained by the Wigner distribution of the y − axis. This implies that the complete location of the 3-D shifted target object can be directly calculated from the power fringe-adjusted filtered correlation, and the Wigner analysis of correlation output reveals the 3-D location of the 3-D target object.

3.3. Application and computer simulation results

Fig. (2.4-1a) shows a 1 cm $\times$ 1 cm $\times$ 3 cm 3- D reference object, R, consisting of a "triangle" and a "square," separated by 3 cm along the depth of the object. Holograms of R are then calculated according to Eqs. (2.2-4) and (2.2-5) with z = 26 cm for the triangle and z = 29 cm for the square of the 3-D object. The used wavelength of light is 0.6μm. Subsequently, a complex hologram of the reference object can be calculated according to Eq. (2.3-3). Figs. (3.3-1a,b) display the correlation output given by the real and the imaginary part of Eq. (2.5-3) when $T(x,y;z) = R(x-\Delta x, y-\Delta y; z-\Delta z)$ for $\Delta x = -0.3\ cm$, $\Delta y = 0$, and $\Delta z = -1cm$, i.e., the 3-D target object is identical to the 3-D reference object, but otherwise displaced away from the original 3-D reference object's location. Physically these outputs correspond to the 2-D scanning of the 3-D target object with the pupil specified by Eq. (2.2-8). The center of the correlation is at $\Delta x = -0.3\ cm$, $\Delta y = 0$ as evident from the figures. The central areas of the correlation are broaden or defocused by the convolution of $h^*(x,y;\Delta z)$ due to the shift of the target object along the depth. Since the 3-D target object is matched with the 3-D reference object, the power fringe-adjusted filtered output is given by Eq. (3.2-4). Fig. (3.3-2a) and Fig. (3.3-2b) show the real and the imaginary part of Eq. (3.2-4). The Wigner distribution of the power fringe-adjusted filtered correlation along the $x-$ axis is shown in Fig. (3.3-3). The intersection between the line impulse, $\left|\frac{1}{2\pi}\left(\frac{k_o}{\Delta z}\right)^2 \delta\left(k_x - \frac{k_o}{\Delta z}(x-\Delta x)\right)\right|$, and the x-axis gives Δx, i.e., the x location of the 3-D target object. The slope of the line impulse gives Δz, i.e., the z location of the 3-D target object as expected. The y location, Δy, can be extracted with the same process along the $y-$ axis.

Fig. (2.4-2a) shows the target object that consists of two slices that are the same with the 3-D reference object but located at different depths within the 3-D volume of the object. Again, its front face is 26 cm away from the scanning mirrors in the simulations.

Figs. (3.3-4a,b) respectively show the real and the imaginary part of the power fringe-adjusted filtered correlation. In this case, since the 3-D target object and the 3-D reference object are not matched, there are no distinct chirp-type pattern on the fringe-adjusted correlation as it is evident from fig. (3.3-5) which shows the Wigner distribution, along the $x-$ axis, of the filtered correlation. Note that in this case, we cannot observe the line impulse in the Wigner distribution because the 3-D the target object shown in Fig. (2.4-2a) is not matched with the 3-D reference object shown in fig. (2.4-1a).

In our last simulations, fig. (2.4-3a) shows the target object whose depth location of the 2-D patterns are the same with the reference object but the 2-D patterns are different with the reference object. The real and the imaginary part of the power fringe-adjusted filtered correlation output are shown in figs. (3.3-6a,b), respectively. The Wigner distribution of the filtered correlation with this target object is shown in fig. (3.3-7). We again do not observe the line impulse as expected.

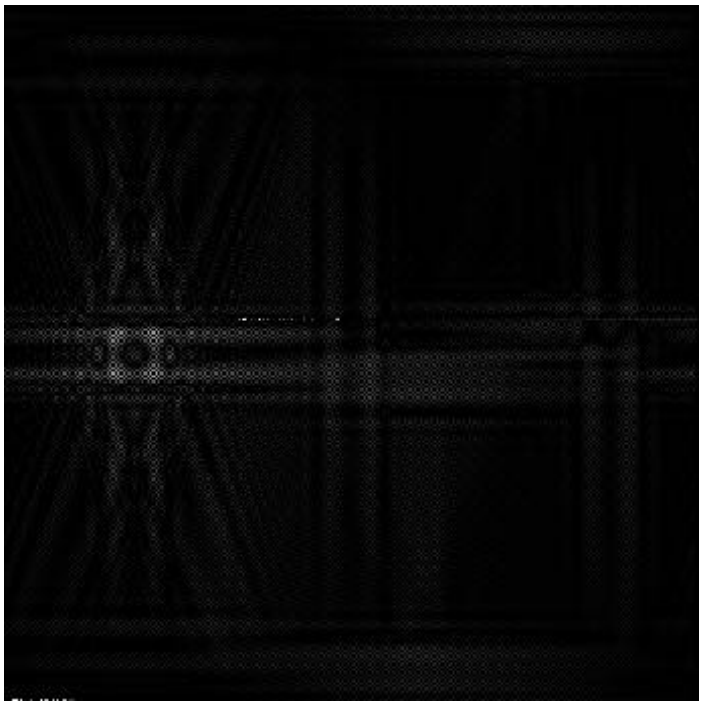

Figure (3.3-1a): Real part of the correlation output when the matched 3-D target object and the 3-D reference object are displaced ($\Delta x = -0.3\ cm$, $\Delta y = 0$, and $\Delta z = -1cm$): the origin of the $xy-$ axes is at the center of the figure.

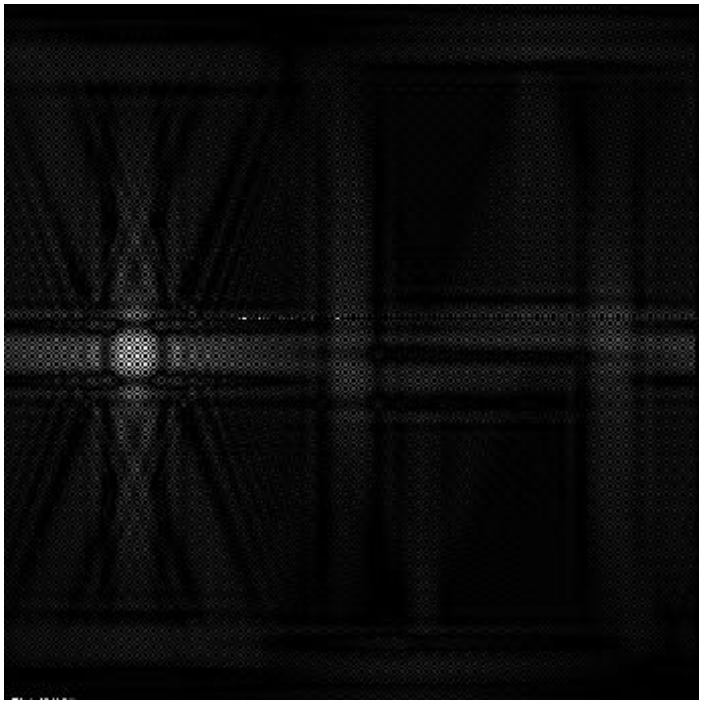

Figure (3.3-1b): Imaginary part of the correlation output when the matched 3-D target object and the 3-D reference object are displaced ($\Delta x = -0.3\ cm$, $\Delta y = 0$, and $\Delta z = -1cm$): the origin of the $xy-$ axes is at the center of the figure.

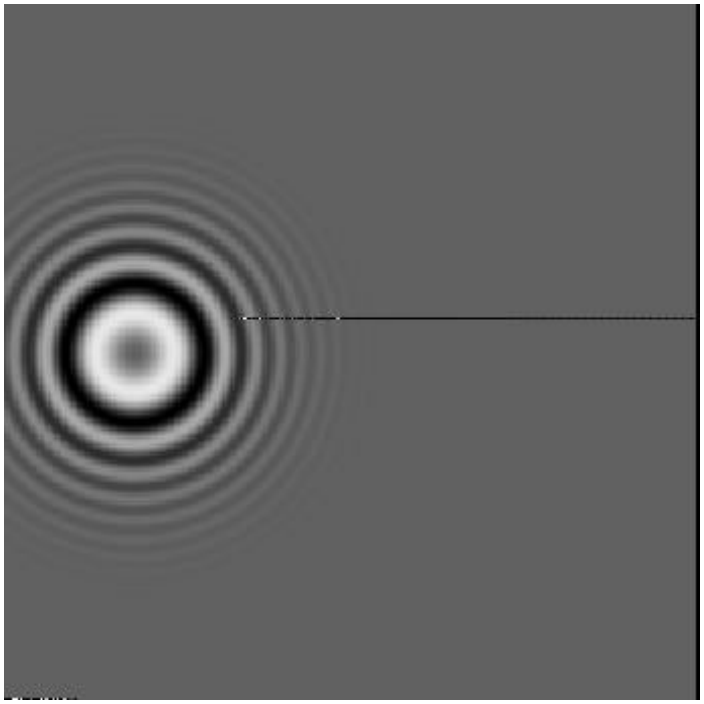

Figure (3.3-2a): Real part of the fringe adjusted-filtered correlation output when the 3-D target object and the 3-D reference object are displaced; otherwise the target object and the reference object is identical.

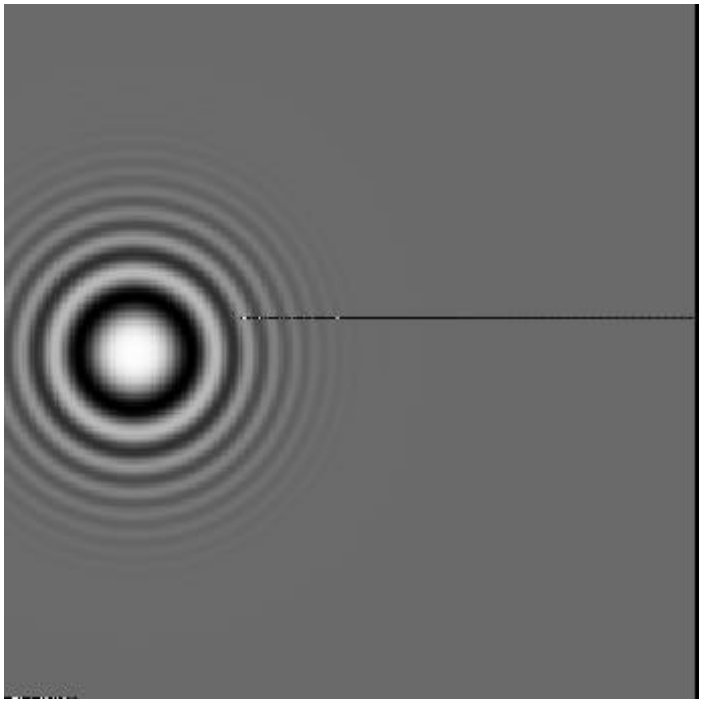

Figure (3.3-2b): Imaginary part of the fringe adjusted-filtered correlation output when the 3-D target object and the 3-D reference object are displaced; otherwise the target object and the reference object is identical.

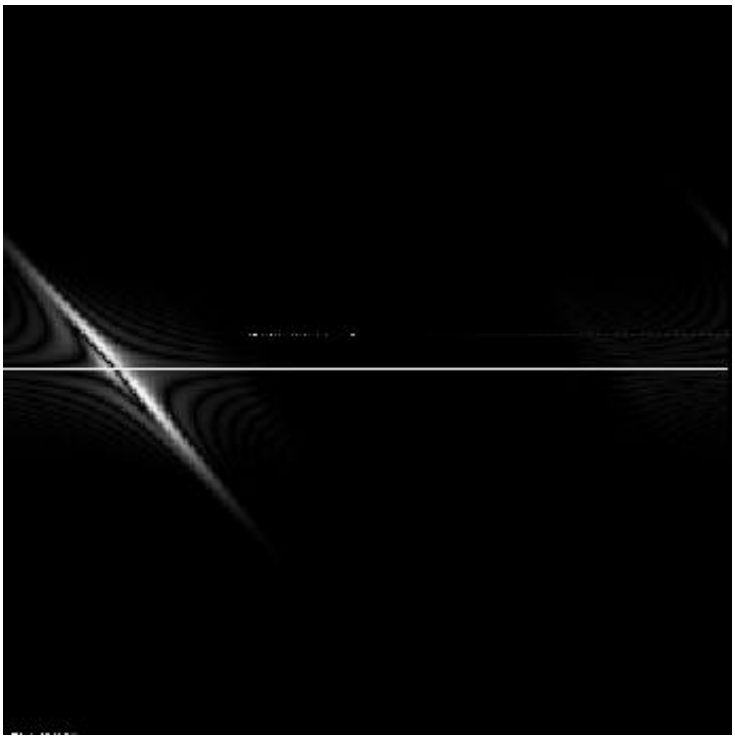

Figure (3.3-3): Magnitude of the Wigner distribution of the power fringe-adjusted filtered correlation output.

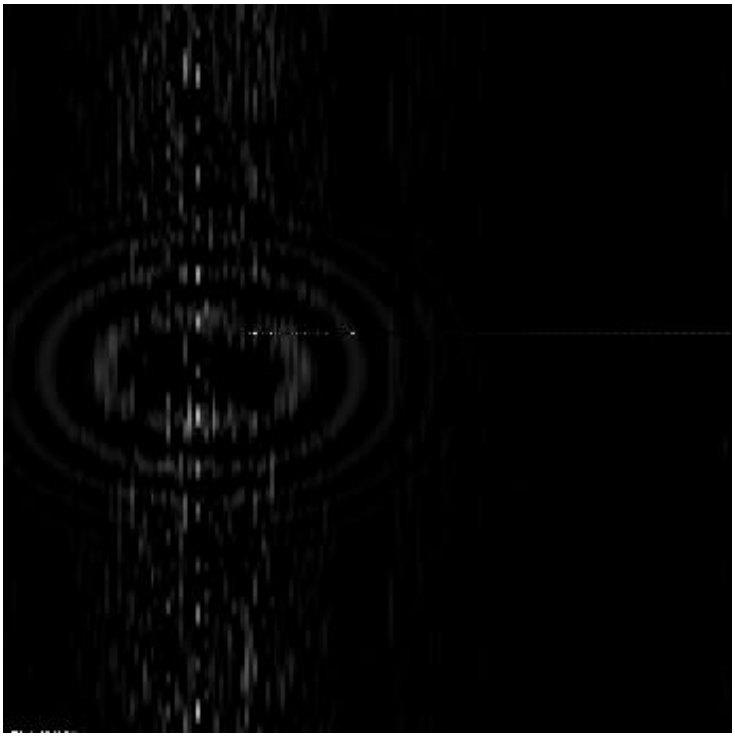

Figure (3.3-4a): Real part of the fringe adjusted-filtered correlation output when the 3-D target object consisted of two slices that are the same with the reference object but located at different depths within the 3-D volume.

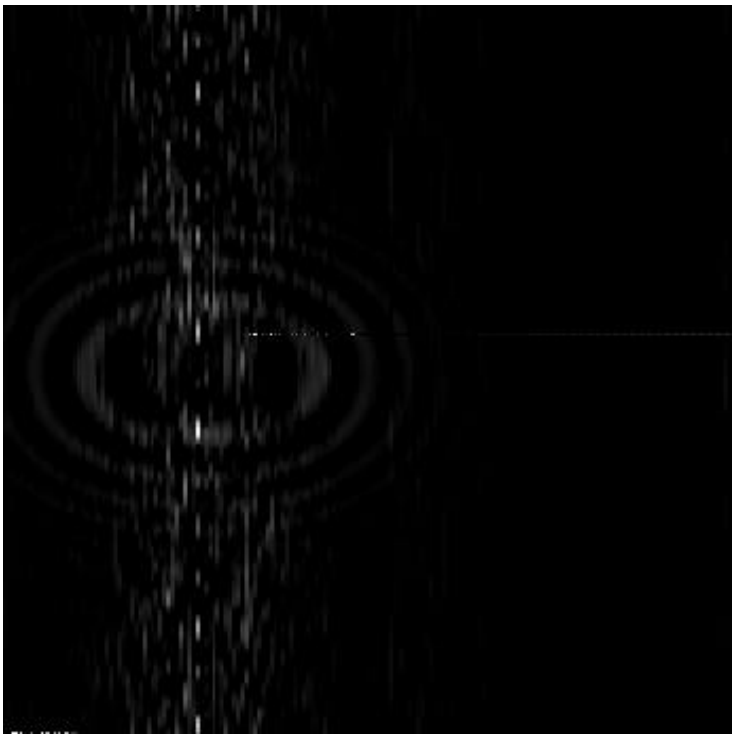

Figure (3.3-4b): Imaginary part of the fringe adjusted-filtered correlation output when the 3-D target object consisted of two slices that are the same with the reference object but located at different depths within the 3-D volume.

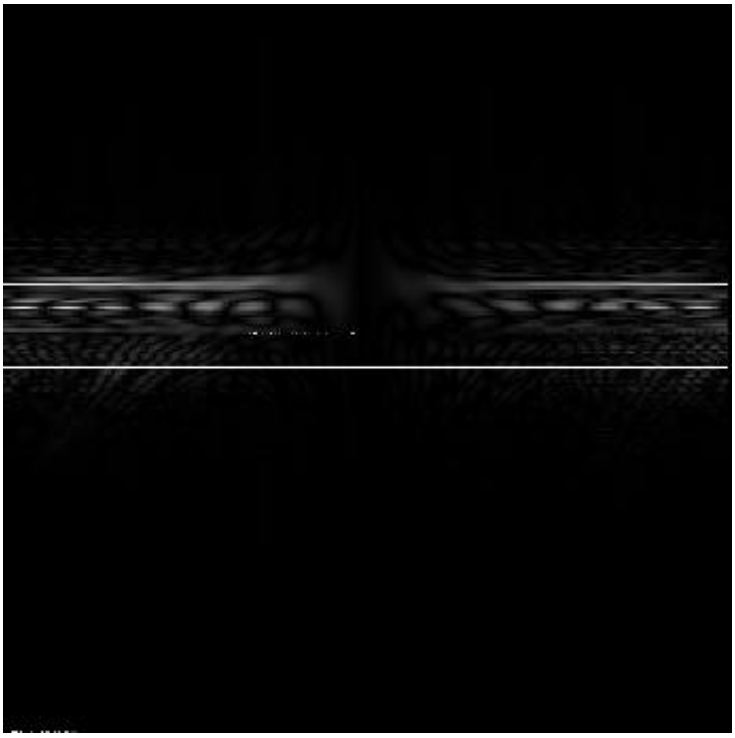

Figure (3.3-5): Magnitude of the Wigner distribution of the power fringe adjusted-filtered output of the correlation output when the 3-D target object consisted of two slices that are the same with the reference object but located at different depths.

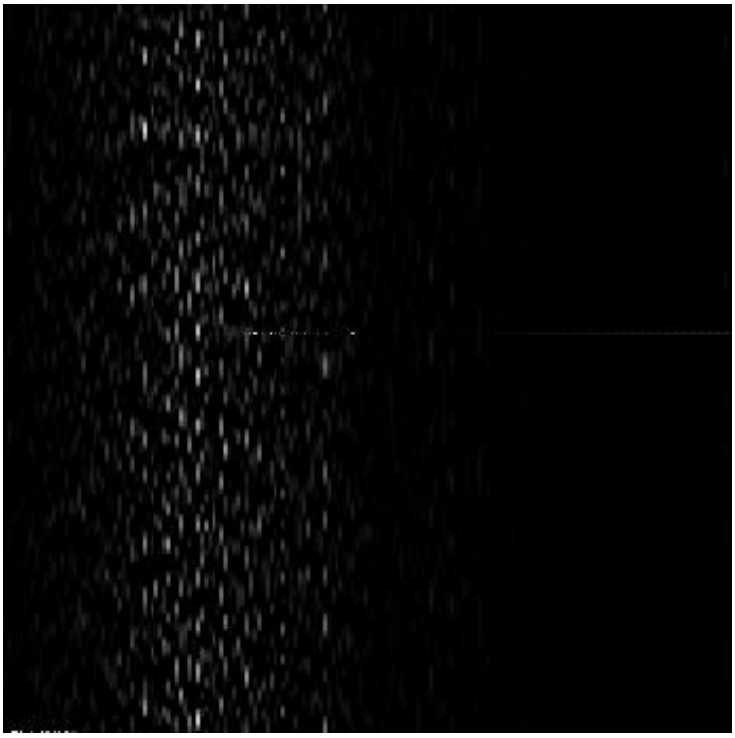

Figure (3.3-6*a*): Real part of the fringe adjusted-filtered correlation output when the 3-D target object consists of two slices whose depth location of the 2-D patterns are the same with the reference object but the 2-D patterns are different with the reference object.

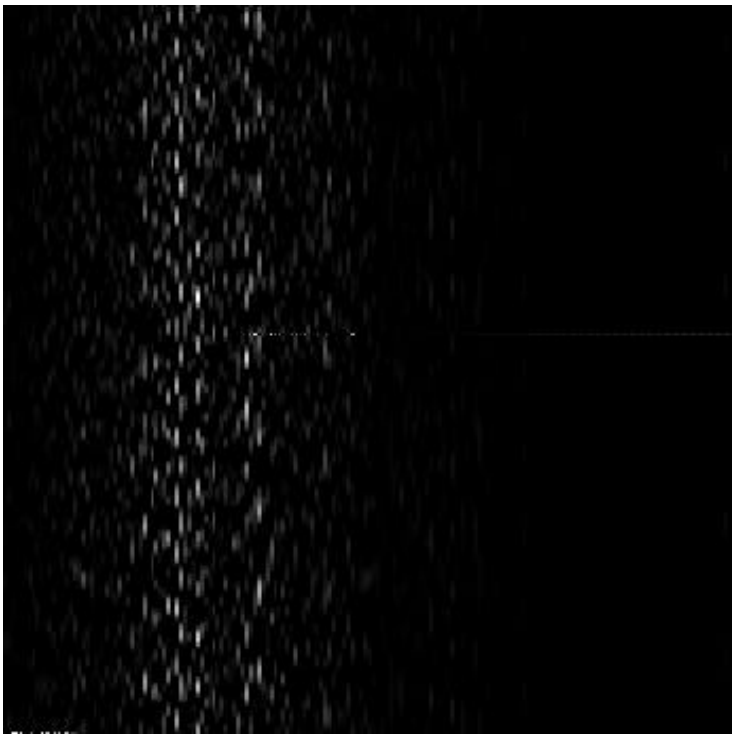

Figure (3.3-6b): Imaginary part of the fringe adjusted-filtered correlation output when the 3-D target object consists of two slices whose depth location are the same with the reference object but the 2-D patterns are different with the reference object.

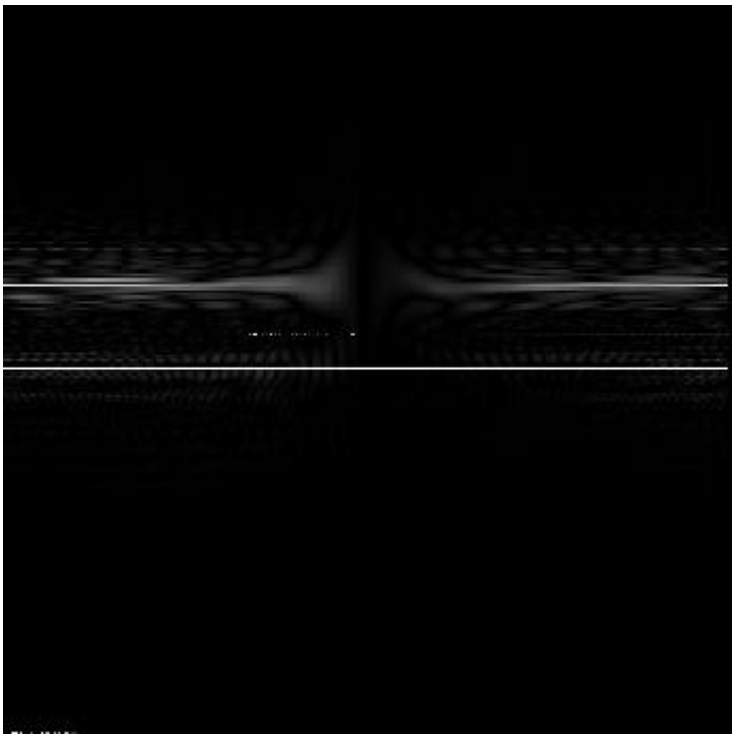

Figure (3.3-7): Magnitude of the Wigner distribution of the power fringe adjusted-filtered output of the correlation output when the 3-D target object consists of two slices whose depth location of the 2-D patterns are the same with the reference object but the 2-D patterns are different with the reference object shown in fig. (2.4-1a).

Chapter 4: Feasibility in implementation and the robustness of the system

In the realization of the proposed technique, the feasibility in implementation and the robustness of the system are very critical issues. Chapter 4 introduces a real-only hologram and a phase-only hologram as a mask in matching stage to improve the feasibility in implementation and the robustness of the system.

4.1 Real-only hologram modulation scheme

There are several possible spatial modulation schemes for the scanning beam of the 3-D holographic image matching system. One is to modulate the scanning beam using the complex hologram of the reference object as a mask. However, in practical implementation, making a complex mask is difficult because it requires the fabrication of diffractive optical elements (DOE's) or careful alignment of two real masks with phase difference as shown in fig. (2.3-1a,b). Thus, a real-only hologram is proposed as another possible spatial modulation scheme. Instead of a complex hologram of the reference object, the real-only hologram of the reference object is proposed to modulate the scanning beam of the system. The complex hologram of the reference object is achieved by adding the two outputs of the system in a complex manner as in Eq. (2.6-10).

The real-only hologram is defined by the real part of the complex hologram, that is the cosine hologram of the reference object as in Eq. (2.6-9a). The real-only hologram of the reference object is given by

$$i_r(x,y) = \int \frac{k_o}{2\pi z} cos\left[\frac{k_o}{2z}\left(x^2+y^2\right)\right] \odot R(x,y;z)\, dz = H_R^r(x,y). \quad (4.1\text{-}1)$$

Note that the real-only hologram of the reference object has the depth information of the 3-D reference object as a form of the fringe pattern by correlating the 3-D object with the real part of the Fresnel zone pattern.

For 3-D matching, we choose the real-only hologram of the reference object that is given by Eq. (4.1-1), as one of the masks of the heterodyne scanning system, i.e., we let $m_1(x,y) = H_R^r(x,y)$ with the other mask being a plane wave, i.e., $m_2(x,y) = 1$. Note that, since the real-only hologram is achieved with a conventional intensity transparency, it is easy to implement the 3-D image matching system with the real-only hologram.

The diffracted pattern from the first mask, $m_1(x,y) = H_R^r(x,y)$, is the reconstructed image of the real-only reference hologram. That is given by

$$m_{1z}(x,y) = \left\{ \int \frac{k_o}{2\pi z} cos\left[\frac{k_o}{2z}\left(x^2 + y^2\right)\right] \odot R(x,y;z)\, dz \right\} \otimes h(x,y;z)\,. \qquad (4.1\text{-}2)$$

The diffracted pattern from the second mask, $m_2(x,y)$=1, is the plane wave, $m_{2z}(x,y) = 1$. Thus, 3-D distribution of the scanning beam is the reconstructed image of the real-only reference hologram. That is given by

$$m_{1z}(x,y)\, m_{2z}^*(x,y) = \left\{ \int \frac{k_0}{2\pi z} cos\left[\frac{k_o}{2z}\left(x^2 + y^2\right)\right] \odot R(x,y;z)\, dz \right\} \qquad (4.1\text{-}3)$$

$$\otimes h(x,y;z).$$

Then, a target object, $T(x,y;z)$ is scanned by the scanning beam given by Eq.(4.1-3). According to (2.6-13a), the in-phase output of the heterodyne scanning system represents the correlation between the real-only hologram of the reference object and that of the target object:

$$i(x,y) = \; Re[m_{1z}(x,y)\; m^{*}_{2z}(x,y)] \odot T(x,y;z) \qquad (4.1\text{-}4)$$

$$= \; Re\left[\left\{\int \frac{k_0}{2\pi z} cos\left[\frac{k_o}{2z}\left(x^2+y^2\right)\right] \odot R(x,y;z)\, dz\right\} \otimes h(x,y;z)\right] \odot T(x,y;z),$$

$$= \left[\int \frac{k_0}{2\pi z} cos\left[\frac{k_o}{2z}\left(x^2+y^2\right)\right] \odot R(x,y;z) dz\right]$$

$$\odot \left[\int \frac{k_0}{2\pi z} cos\left[\frac{k_o}{2z}\left(x^2+y^2\right)\right] \odot T(x,y;z) dz\right]$$

$$= H^r_R(x,y) \odot H^r_T(x,y),$$

where $H^r_T(x,y) = \left[\int \frac{k_o}{2\pi z} cos\,[\frac{k_o}{2z}(x^2+y^2)] \odot I_t(x,y;z) dz\right]$ is the real-only hologram of the target object.

Note that, because the real-only holograms of the two identical objects have the same 2-D pattern, the heterodyne scanning system gives a correlation peak when the 3-D image of the 3-D target object is matched with that of the 3-D reference object. However, for the matched case with longitudinally shifted location, the Wigner distribution gives the cross delta line as shown in fig. (4.1-1) because the real-only hologram is a two side band signal. The fig. (4.1-1) shows the computer simulation results of the Wigner distribution for real-only hologram case with the same reference object as in section 3.3.

Thus, with real-only hologram, we can not determine whether the matched object is shifted close to the scanning mirrors or far away from the scanning mirrors. This is the one draw back in 3-D image marching system with the real-only hologram, compared to that with the complex hologram.

4.1.1 Computer simulation results with a real-only mask

Fig. (2.4-1a) shows a 1 cm $\times$ 1 cm $\times$ 3 cm 3-D reference object, R, consisting of a "triangle" and a "square," separated by 3 cm along the depth of the object. Fig. (2.4-1b) plots the real-only hologram of the reference object, R as calculated by Eq. (2.6-9a), with $z =$ 26 cm for the "triangle" and 29 cm for the "square" of the 3-D reference object. The

used wavelength of light is 0.6μm for h. The scanned area of the hologram is 1 cm $\times$ 1 cm. Physically, the hologram would correspond to the scanning of R, with its front face located 26 cm away from the scanning mirrors. Again, the masks have been chosen such that $m_1(x,y)$= $\delta(x,y)$ and $m_2(x,y)$=1 for holographic recording as described in section 2.6.

The real-only hologram shown in fig.(2.4-1b) now will be used for the one mask specified by $m_1(x,y) = H_R^r(x,y)$, which will result in the output calculated according to Eq. (4.1-4) :

$$i(x,y) = \left[\int \frac{k_0}{2\pi z} cos\left[\frac{k_o}{2z}\left(x^2 + y^2\right)\right] \odot R(x,y;z)dz\right] \qquad (4.1\text{-}5)$$

$$\odot \left[\int \frac{k_0}{2\pi z} cos\left[\frac{k_o}{2z}\left(x^2 + y^2\right)\right] \odot T(x,y;z)dz\right]$$

$$= H_R^r(x,y) \odot H_T^r(x,y),$$

This output corresponds to the 2-D scanning of a 3-D target object, O, with the real-only hologram of the 3-D reference object, R, used to form the mask. Fig. (4.1-2) shows the plotting of Eq. (4.1-5) when $T = R$, where R is the object shown in fig. (2.4-1a).

Fig.(2.4-2a) shows the target object and its front face is again 26 cm away from the scanning mirrors in the simulations. Note that the target has the same 2-D patterns as those in the reference object, but located at different depths. Fig. (2.4-2b) show the real-only hologram of the target object. Fig. (4.1-3) shows the correlation output according to Eq. (4.1-5). Note that the amplitude axis of fig. (4.1-3) has been normalized by the peak value of fig. (4.1-2). The lack of a strong correlation peak in fig. (4.1-3) clearly indicates that the two 3-D objects are not matched each other. It is important to point out that the holograms shown in figs. (2.4-1b) and (2.4-2b) are very similar. However, when the real-

only hologram of the target object is correlated with that of the reference hologram as our proposed system effectively performs, we do not find a match for the two 3-D objects shown in figs. (2.4-1a) and (2.4-2a). The reason is that since we are really correlating two holographic data sets, the depth information is as important as the planar distributions. In order to have a strong correlation peak, the 3-D objects have to be matched precisely throughout the whole 3-D volume.

Finally, in figs. (2.4-3a) and (2.4-3b) we show another target object and its real-only hologram. The correlation outputs between fig. (2.4-1b), the real-only hologram of the reference object, and fig. (2.4-3b), the real-only hologram of the target object, are shown in fig. (4.1-4). Clearly, no correlation peak is observed in fig. (4.1-4). Note that in this case, the "X" and the "O" of the 3-D object are located at the same distance of the "triangle" and the "square", respectively.

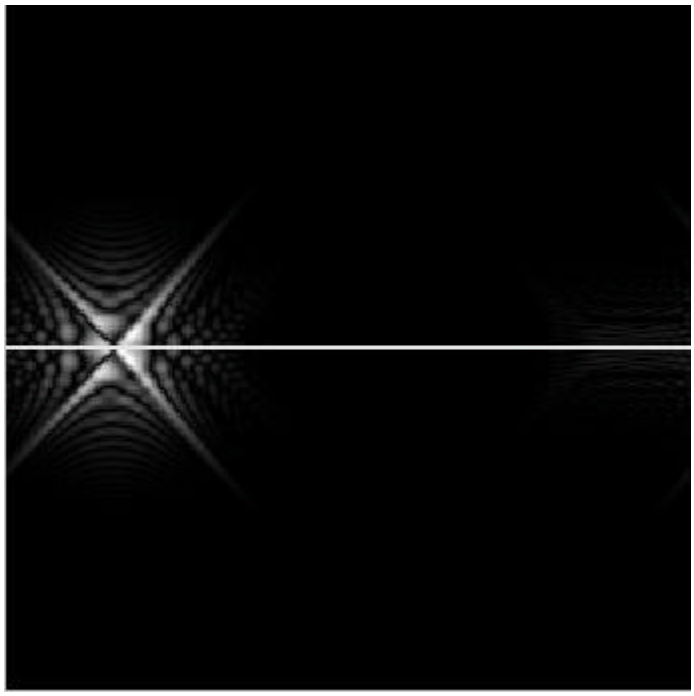

Figure (4.1-1): Magnitude of the Wigner distribution of power fringe-adjusted filter correlation with real-only hologram.

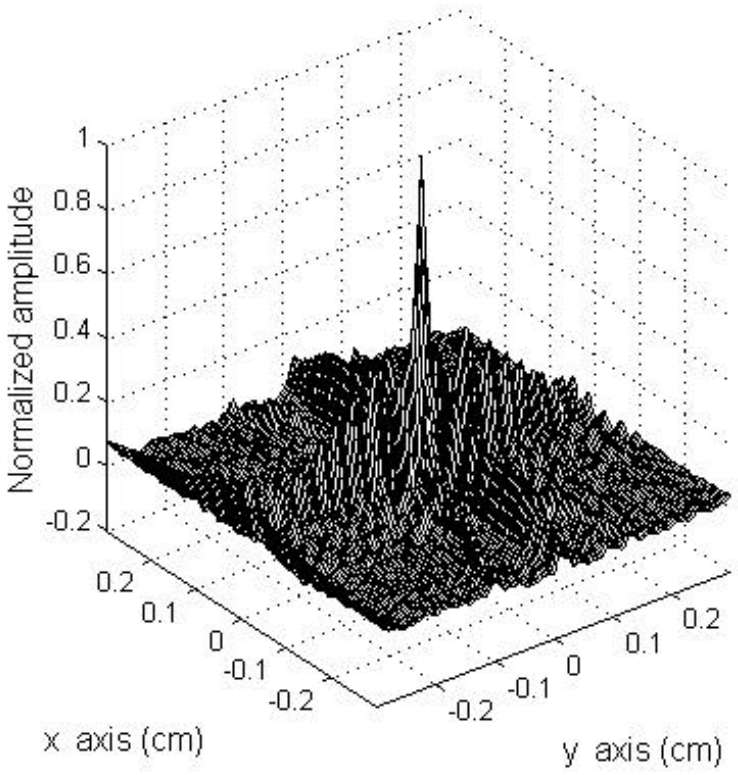

Figure (4.1-2): Correlation output (0.4 cm $\times$ 0.4 cm) with real-only hologram, when the target object T, is matched with the reference object R.

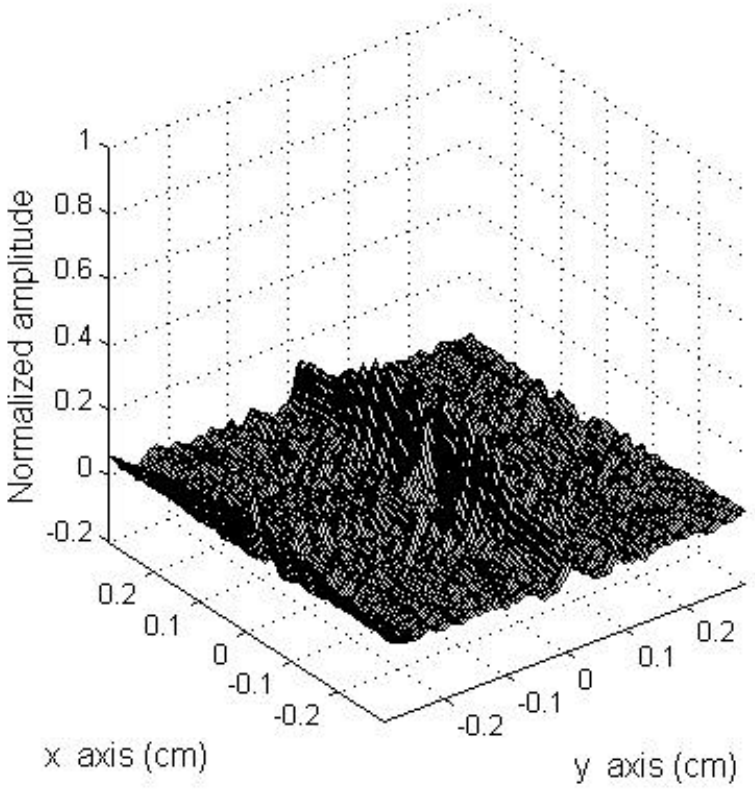

Figure (4.1-3): Correlation output with real-only hologram, when the target object in fig. (2.4-2 a) is scanned. The reference object is shown in fig. (2.4-1a).

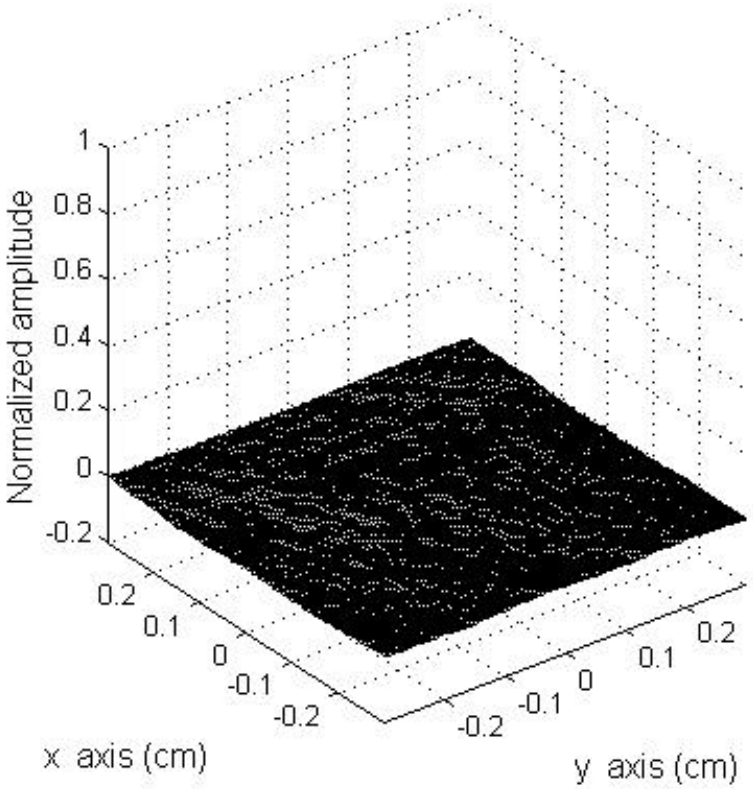

Figure (4.1-4): Correlation output with real-only hologram, when the target object in fig. (2.4-3a) is scanned. The reference object is shown in fig. (2.4-1a).

4.2 Phase-only hologram modulation scheme

Both proposed modulation schemes in section 4.1 suffer from a low power correlation signal. Because both the complex hologram and the real-only hologram block most light by amplitude, the intensity of the modulated scanning beam is small, and this generates a weak correlation signal against the system noise. If the correlation signal is small, compared to the noise level of the system, it is undetectable. Even though this can be overcome by increasing the intensity of the laser, the size and the power of the laser are limited in a real situation. Thus, increasing the power of the correlation signal with a given power of the laser is necessary to improve the robustness of the system.

4.21 Optical efficiency

Optical efficiency is a critical issue for the 3-D holographic correlation because the robustness of the 3-D holographic matching system about the noise of the system highly depends on the optical efficiency. The optical efficiency, or Horner efficiency means the ratio of the energy in correlation to the total energy of the input signal. That is defined as[37,38]:

$$\eta_H = \eta_M \frac{\int\int \left| f(x,y) \otimes g^*(x,y) \right|^2 dxdy}{\int\int \left| f(x,y) \right|^2 dxdy}. \qquad (4.2\text{-}1)$$

where $f(x,y)$ is any input function, $g(x,y)$ is a reference function, and η_M is the medium's efficiency.

In the 3-D holographic matching system, the hologram of the reference object and the hologram of the target object are the reference function and the target function, respectively.

Because the 3-D holographic image matching system uses the complex hologram of the reference object as one pupil in the frequency domain, most of the light is blocked by the amplitude of the hologram. Thus, the optical efficiency of the 3-D holographic matching system is insufficient.

The phase-only matched filtering technique was proposed to increase the optical efficiency of the conventional 2-D optical correlators [37,38]. The idea of the phase-only matched filtering technique originated from the fact that the phase information of the image in the frequency domain plays an important role in preserving the visual intelligibility of the image, compared to the intensity information of the image in the frequency domain [39]. In addition, a phase-only filter does not consume the power of the light because a phase-only object does not block the light, but merely changes the direction of the beam.

4.2.2 Phase-only hologram

This sub-section introduces the phase-only hologram, in which the 3-D information of a 3-D object is preserved because both the depth information and the transverse information of a 3-D object are contained in the phase term of a hologram.

The complex hologram of the reference object in the frequency domain is achieved by the Fourier transformation of the complex hologram which is achieved in the recording stage:

$$\mathcal{F}\{H_R(x,y)\} = \mathcal{F}\left\{\int j\frac{k_o}{2\pi z} exp\left[\frac{-jk_o}{2z}\left(x^2+y^2\right)\right] \odot R(x,y;z)dz\right\} \qquad (4.2\text{-}2)$$

$$= \int\left[\mathcal{F}^*\left\{j\frac{k_o}{2\pi z} exp\left[\frac{-jk_o}{2z}\left(x^2+y^2\right)\right]\right\} \times \mathcal{F}\{R(x,y;z)\}\right]dz$$

$$= \int \left[exp\left\{ j\frac{z}{2k_o}\left(k_x^2 + k_y^2\right)\right\} \mathcal{F}\{R(x,y;z)\}\right] dz,$$

where $\mathcal{F}$ denotes the Fourier transform operation and is defined as:

$\mathcal{F}\{u(x,y)\}_{k_x,k_y} = \int\int u(x,y)\, exp(jk_x x + jk_y y)dxdy = U(k_x,k_y)$ with k_x and k_y denoting the spatial frequencies, and with the upper case function U denoting the transform of the lower case function u.

Note that the Fourier transformation of an image is in general complex with $\mathcal{F}\{R(x,y;z)\}$ being represented as:

$$\mathcal{F}\{R(x,y;z)\} = A(k_x,k_y;z)exp(j\phi(k_x,k_y;z)) \qquad (4.2\text{-}3)$$

The phase, $\phi(k_x,k_y;z)$ is far more significant than its intensity, $A(k_x,k_y;z)$. In general, the phase information contains the locations of objects in them [39]. In particular, the information of the shifted location of an object is contained only in the phase by adding a linear phase term.

Thus, the hologram in frequency domain is expressed using the amplitude and phase parts of images with additional phase terms of the free space impulse response function, that is given by:

$$\mathcal{F}\{H_R(x,y)\} = \int \left[A(k_x,k_y;z)exp(j\phi(k_x,k_y;z))\, exp\left\{ j\frac{z}{2k_o}\left(k_x^2 + k_y^2\right)\right\}\right] dz \qquad (4.2\text{-}4)$$

$$= \int \left[A(k_x,k_y;z)\, exp\left\{ j\left[\phi(k_x,k_y;z) + \frac{z}{2k_o}\left(k_x^2 + k_y^2\right)\right]\right\}\right] dz$$

Note that the depth information of a 3-D object is contained in the phase of the hologram. Thus, the phase of the hologram in the frequency domain has both depth information and transverse information of the 3-D object.

We define a phase-only hologram in the frequency domain to be

$$\mathcal{F}\{H_R(x,y)\}_{\phi} = exp[j\,arg(\mathcal{F}\{H_R\})], \qquad (4.2\text{-}5)$$

where $arg(.)$ represents the argument operation of complex number.

Note that the phase-only hologram is composed of the unit amplitude and phase of the complex hologram in frequency domain. Because the spectral magnitude of an image tends to drop off at high frequencies, the phase only image is the high frequency enhanced version of the image. In it, lines, edges and other narrow events are emphasized without modifying their position [39]. Especially in the hologram, the holographic information is contained in the high frequencies of phase as a form of chirp type signal, as shown in Eq. (4.2-4). Thus, in the phase only hologram, the whole 3-D lines, edges and other narrow events are emphasized, and the matching accentuated narrow events will give better discrimination ability.

4.2.3 3-D image matching system with a phase-only hologram

In the phase-only 3-D holographic image matching system, the phase-only hologram of the reference object in the frequency domain is place, as the pupil, instead of the complex hologram. This increased the optical efficiency and sensitivity of the system.

Section 2.3 discussed that the target object $T(x,y;z)$ to be recognized is 2-D scanned, with the two pupils setting as $p_2 = \delta(x,y)$ and $p_1(x,y) = \mathcal{F}\{H_R\}$. Moreover, it has the same functional form as that given by Eq. (2.2-8), the complex hologram of the reference object. This section discusses the correlation between the phase-only hologram of the reference object and the complex hologram of the target object with high optical efficiency. We set the two pupils as $p_2 = \delta(x,y)$ and $p_1(x,y)$ equals the phase-only hologram of the reference object in the frequency domain, as given by Eq. (4.2-5). We rewrite Eq. (2.2-8) as

$$p_1\left(-\frac{f}{k_0}k_x,\ -\frac{f}{k_0}k_y\right)=exp[j\,arg(\mathcal{F}\{H_R\})] \qquad (4.2\text{-}6)$$

Note that the pupils of the phase-only 3-D holographic image matching system are realized by masks that are composed only of phase, when the delta pupil function, $p_2 = \delta(x,y)$ is realized by a focusing lens. Thus, 100 % of the light passes through the system, scans the target object. This gives high optical efficiency to the system which makes the system very robust about the noise.

Substituting Eq. (4.2-6) into Eq. (2.2-7),we have 2-D recording of the form:

$$i_c(x,y) = Re\left\{\mathcal{F}^{-1}\left[\left(\int\mathcal{F}\{T(x,y;z)\}\ exp\left[-j\frac{z}{2k_0}\left(k_x^2+k_y^2\right)\right]dz\right)\right.\right. \qquad (4.2\text{-}7)$$
$$\left.\left.\times\, exp[j\,arg(\mathcal{F}\{H_R\})]^*\right]\right\}.$$

Using the correlation property, i.e., $\mathcal{F}^{-1}\{F^*G\} = \mathcal{F}^{-1}\{F\}\odot\mathcal{F}^{-1}\{G\} = f\odot g$, Eq. (4.2-7) becomes:

$$i_c(x,y) = Re\left\{\left(\int\mathcal{F}^{-1}\left\{\mathcal{F}\{T(x,y;z)\}\ exp\left[-j\frac{z}{2k_0}\left(k_x^2+k_y^2\right)\right]\right\}dz\right)\right. \qquad (4.2\text{-}8)$$
$$\left.\odot\left(\mathcal{F}^{-1}\{exp[j\,arg(\mathcal{F}\{H_R\})]\}\right)\right\}$$

$$=Re[H_T(x,y)\odot H_{PR}(x,y)],$$

where $H_{PR}(x,y) = \mathcal{F}^{-1}\{exp[jarg(\mathcal{F}\{H_R\})]\}$ and

$H_T(x,y) = \int h(x,y;z)\odot T(x,y;z)dz.$

The $i_c(x,y)$ given in (4.2-8) is the display of a 2-D pattern which basically represents the correlation between the phase-only hologram of the reference object and the complex hologram of the target object. It is shown that the correlation between the phase-only

reference image and the target image gives the sharp correlation peak compared to the conventional correlation, with high robustness [37]. In the next section, we investigate the sensitivity and robustness of the 3-D holographic image matching system with phase-only pupil.

4.3 Robustness of the system

The robustness of the system is a critical issue in practical realization. The previous section showed that the system with a phase-only hologram as a pupil provides 100 % optical efficiency. It is obvious that this gives the strong signal compared to the complex and the real-only hologram cases. This makes the system with the phase-only hologram more robust to system noise that is attributed to the detector and optical components of the system itself [37]. Besides of this factor, this section considers the robustness of the proposed system against noise that is in the original input image, by means of computer simulations.

4.3.1 Computer simulations

For matched cases and mis-matched cases, 3-D image matching tests are performed with noise added, and without noise. Noise is added to the image of the target object, but not the holograms of the reference object, which are used to spatially modulate the scanning beam. Additive intensity noise is the intensity of a Gaussian noise having a zero mean and a standard deviation σ. The signal to noise ratio (SNR) that is related to Gaussian noise having standard deviation, σ, is given by SNR=1/σ [37]. Additive Gaussian noise is generated by a random number subroutine in the computer.

Fig. (4.3-1) shows a $1\,\text{cm} \times 1\,\text{cm} \times 3\,\text{cm}$ 3-D reference object, R, consisting of a "triangle" and a "circle," separated by 3 cm along the depth of the object. Figs. (4.3-2a,b) plot the cosine-FZP hologram and the sine-FZP hologram of the reference object, R, as

calculated by Eq. (2.3-3), with $z = 26$ cm for the "triangle" and 29 cm for the "circle" of the 3-D reference object. The wavelength of light that is used, is 0.6μm for h. The scanned area of the hologram is $1\,\text{cm} \times 1\,\text{cm}$. Physically, these holograms would correspond to the scanning of R, with its front face located 26 cm away from the scanning mirrors. Again, the masks have been chosen such that $m_1(x,y)$= 1 and $m_2(x,y)$= $\delta(x,y)$ for holographic recording, as described in the section (2.6).

For the test of the system which uses the complex hologram as a mask, the complex hologram of the reference object is generated by adding holograms as shown in figs. (4.3-2a,b). Then, this is used to modulate the scanning beam. Six separate matching tests are performed for the complex hologram case, both with and without noise.

First, the target object that has the same 3-D image of the reference object is chosen for the test of the matched case without noise. Holograms of the target object are the same as those of the reference object. Thus, the system gives out the strong correlation peak according to Eqs. (2.6-13a,b). The intensity pattern of the system output, $|i_s + j\, i_c|^2$shown in fig. (4.3-3).

Second, for the test of the longitudinally mis-matched case without noise, the target object which is composed of the same 2-D patterns as those in the reference object, but located at different depths as shown in fig. (4.3-4), is chosen. Holograms of the target object are shown in figs. (4.3-5a,b). The intensity pattern of the system output according to Eqs. (2.6-13a, b), $|i_s + j\, i_c|^2$ is shown in fig. (4.3-6). Since the 3-D image of the target object is different from that of the reference object, the system output is not as strong as the matched case.

Third, for the test of the transversely mis-matched case without noise, the target object whose 2-D slides are slightly different from those of the reference object, but located at the same depth as the reference object is shown in fig. (4.3-7). In order to compare discrimination ability among three different modulation schemes, we choose the slides whose spatial distribution is slightly different from that of the reference object.

Holograms of the target object are shown in figs. (4.3-8a,b). The intensity pattern of the system output according to Eqs. (2.6-13a, b), $|i_s + j\, i_c|^2$ is shown in fig. (4.3-9). Since the 3-D image of the target object is different from that of the reference object, the system output is not as strong as the matched case.

Fourth, for the test of the matched case in the presence of noise, the intensity of Gaussian noise with standard deviation, σ=0.25 is added to the same target object that is used in the first case. Images of each slide with noise are shown in figs. (4.3-10a,b). Holograms of the target object are shown in figs. (4.3-11a,b). The intensity pattern of the system output according to Eqs. (2.6-13a, b), $|i_s + j\, i_c|^2$ is shown in fig. (4.3-12). Note that, even though holograms of the target object are severely damaged by noise, the system output still gives the correlation peak as strong as the case without noise.

Fifth, for the longitudinally mis-matched case in the presence of noise, the intensity of Gaussian noise with standard deviation, σ=0.25 is added to the same target object that is used in the second case as shown in fig. (4.3-4). Holograms of the target object are shown in figs. (4.3-13a,b). The intensity pattern of the system output according to Eqs. (2.6-13a, b), $|i_s + j\, i_c|^2$ is shown in fig. (4.3-14). Note that, even in the presence of noise, the system does not give the strong correlation peak for the longitudinally mis-matched case.

Sixth, for the transversely mis-matched case in the presence of noise, the intensity of Gaussian noise with standard deviation, σ=0.25 is added to the same target object that is used in the third case as shown in fig. (4.3-7). Images of each slide with noise are shown in figs. (4.3-15a,b). Holograms of the target object are shown in figs. (4.3-16a,b). The intensity pattern of the system output according to Eqs. (2.6-13a, b), $|i_s + j\, i_c|^2$ is shown in fig. (4.3-17). Note that, even in the presence of noise, the system does not give the strong correlation peak for the transversely mis-matched case. As a conclusion of tests for the system using complex hologram as a mask, we can deduce that the system is very robust against the additive noise in the input object.

For the test of the system which uses the real-only hologram as a mask, the same six separate tests in the complex hologram case are repeated. In these tests, the real-only hologram of the reference object, shown in fig. (4.3-2a), is used as a mask of the system instead of the complex hologram. Fig. (4.3-18) shows the intensity output of the system when the target object's 3-D image is matched with that of the reference object as the first test in the complex hologram case. For the test of the longitudinally mis-matched case through the same procedure of the second test in the complex hologram case, we get the intensity output of the system as shown in fig. (4.3-19). For the test of the transversely mis-matched case through the same procedure of the third test in the complex hologram case, we get the intensity output of the system as shown in fig. (4.3-20). Tests of the system having the real-only hologram as a mask in the presence of noise are repeated. Fig. (4.3-21), fig. (4.3-22) and fig. (4.3-23) show respectively the intensity outputs of the system for the matched case, longitudinally mis-matched case and transversely mis-matched case in the presence of noise. Note that there is very little difference between the real-only hologram and the complex hologram cases, both with and without additive noise. Thus, we can conclude that the system that uses the real-only hologram as a mask is very robust against additive noise in the input image like the system using the complex hologram as a mask.

For the test of the system which uses the phase-only hologram as a pupil, the same tests in the complex hologram case are repeated. In these tests, the phase-only hologram of the reference object is used as a pupil of the system. Fig. (4.3-24) represents the phase-only hologram as a gray level -black denotes zero radian and white denote 2π radian-. Fig. (4.3-25), fig. (4.3-26) and fig. (4.3-27) show respectively the intensity outputs of the system for the matched case, longitudinally mis-matched case and transversely mis-matched case in the absence of noise. The same tests of the system are performed in the presence of noise. Fig. (4.3-28), fig. (4.3-29) and fig. (4.3-30) show respectively intensity outputs of the system for the matched case, longitudinally mis-matched case and

transversely mis-matched case in the presence of noise. Note that the system with the phase-only hologram as a pupil gives the strong correlation peak only when the 3-D image of the target object is matched with that of the reference object, regardless of noise. Thus, we can conclude that the system that uses the phase-only hologram as a mask is very robust about additive noise in the input image like the system using the complex hologram or the real-only hologram as a mask.

4.3.2 Discussion of results

Section 4.3.1 showed the intensity outputs of the system for matched cases and mis-matched cases about three different spatial modulation schemes. These figures show that all three modulation schemes are robust about additive noise in the input image, regardless of spatial modulation schemes.

In addition to the robustness of the system against additive noise, optical efficiency determines the robustness of the system against system noise that is attributed to the detector and the optical components of the system itself. Tables (4.3-1,2) show the peak heights of system outputs and optical efficiencies for each three spatial modulation schemes in the absence of noise and in the presence of noise respectively. In the tables (4.3-1,2), we can see that there is very little difference among the proposed three spatial modulation schemes, except that the peak height of the phase-only spatial modulation scheme is much larger than that of the others. When the output's peak height of the matched case with complex hologram as a spatial modulation scheme is normalized to one, the output's peak height of the phase-only case has a value of 223. This means that the output signal of the phase-only case is 223 times stronger than that of the complex hologram case. Thus, in terms of system noise, the system with the phase-only hologram is robust about system noise. This result is directly related to the optical efficiency of the system. Because the phase-only hologram has 100 % optical efficiency, in other words, it

does not block any light, we get a strong signal compared to two other modulation schemes.

As a conclusion, we can deduce that

1. The 3-D image matching system is very robust about additive noise in the input image regardless of the modulation schemes.

2. The 3-D image matching system with a phase-only hologram is more robust than the two other modulation schemes about system noise that is attributed to the detector and the optical components of the system itself.

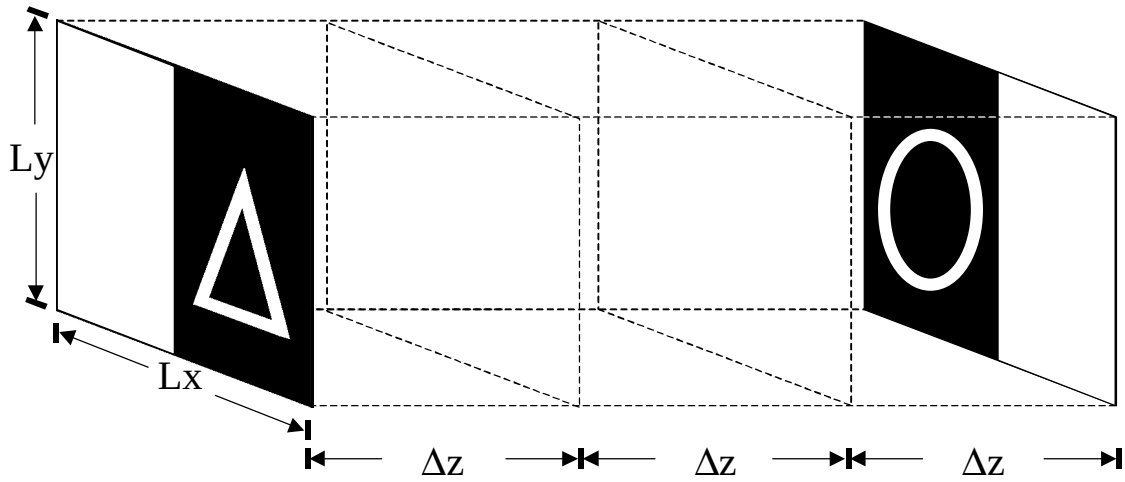

Figure (4.3-1): 3-D reference object R, with $L_x = L_y \ = 1\,cm,\ \triangle \mathrm{z} = 1\,cm.$

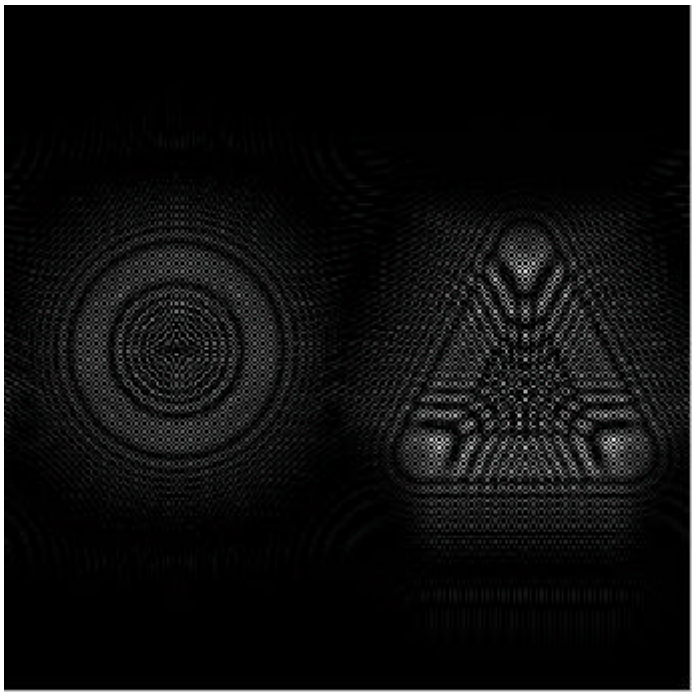

Figure (4.3-2a): Cosine-FZP hologram of 3-D reference object.
(the scanned area is 1 cm $\times$ 1 cm)

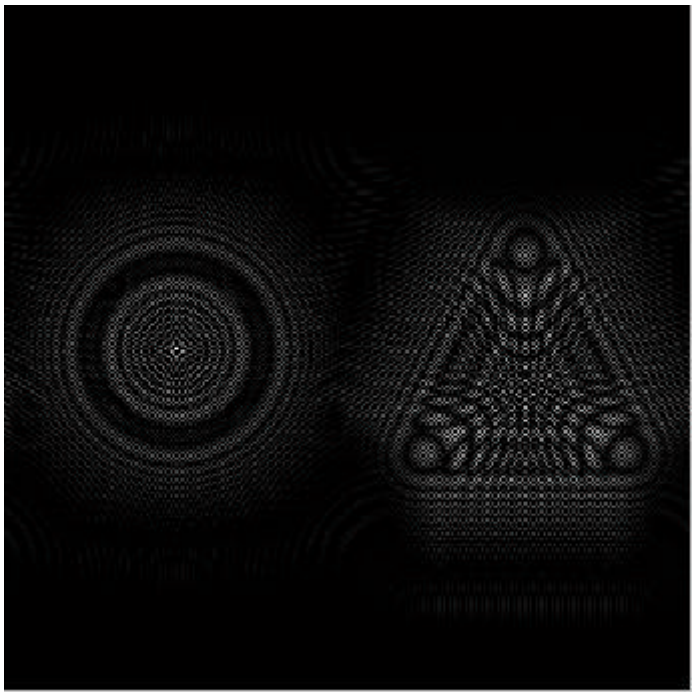

Figure (4.3-2b): Sine-FZP hologram of 3-D reference object.
(the scanned area is 1 cm $\times$ 1 cm)

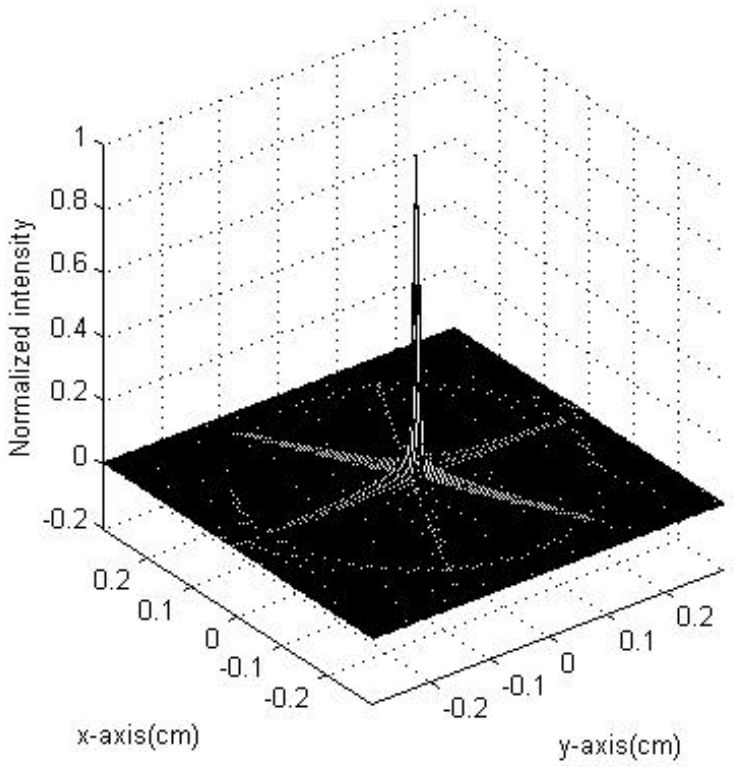

Figure (4.3-3): Correlation output (0.4 cm $\times$ 0.4 cm) when the target object is matched with the reference object.

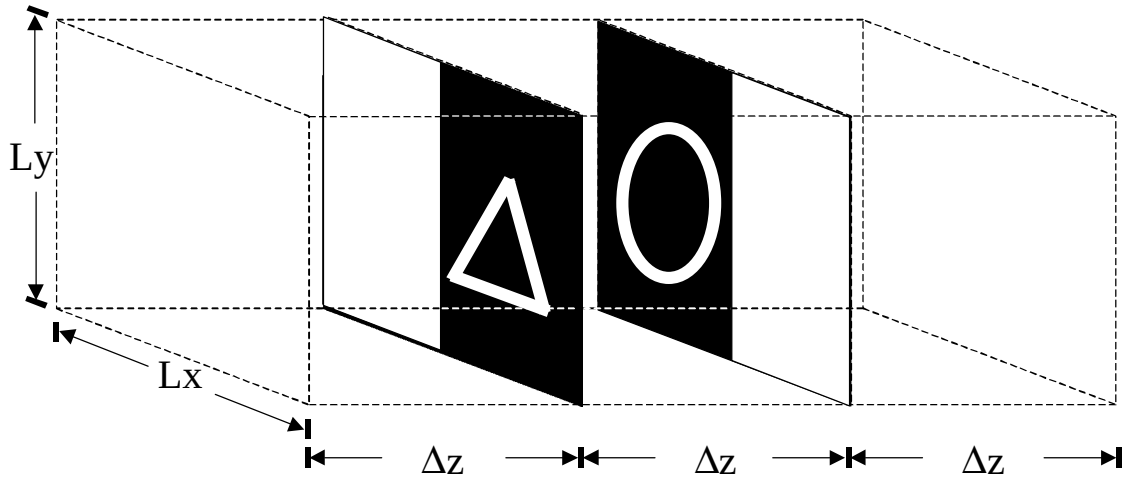

Figure (4.3-4): 3-D target object T.

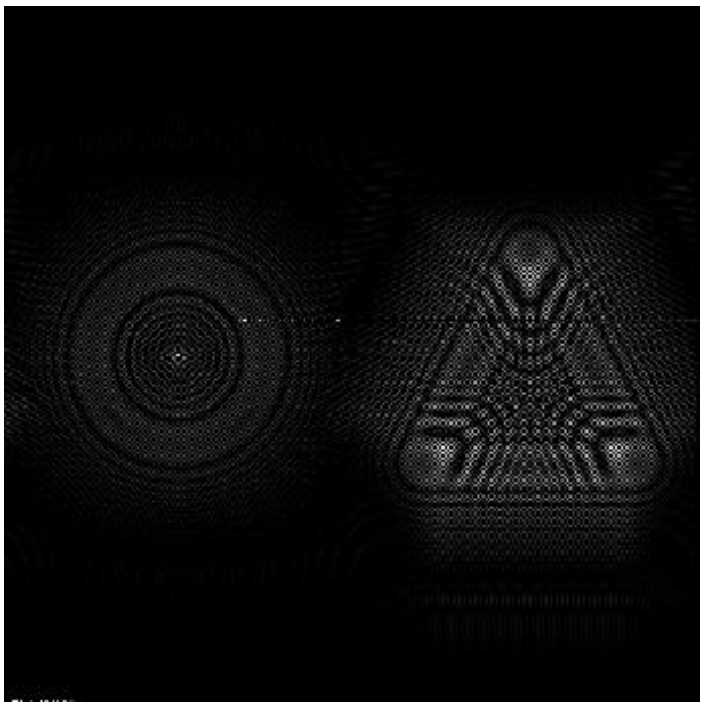

Figure (4.3-5a): Cosine-FZP hologram of the 3-D target object shown in fig. (4.3-4).

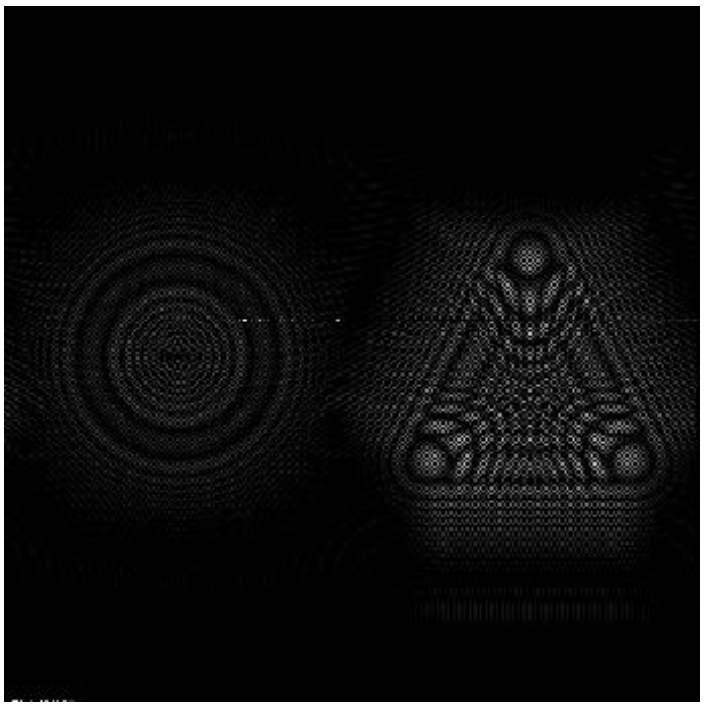

Figure (4.3-5b): Sine-FZP hologram of the 3-D target object shown in fig. (4.3-4).

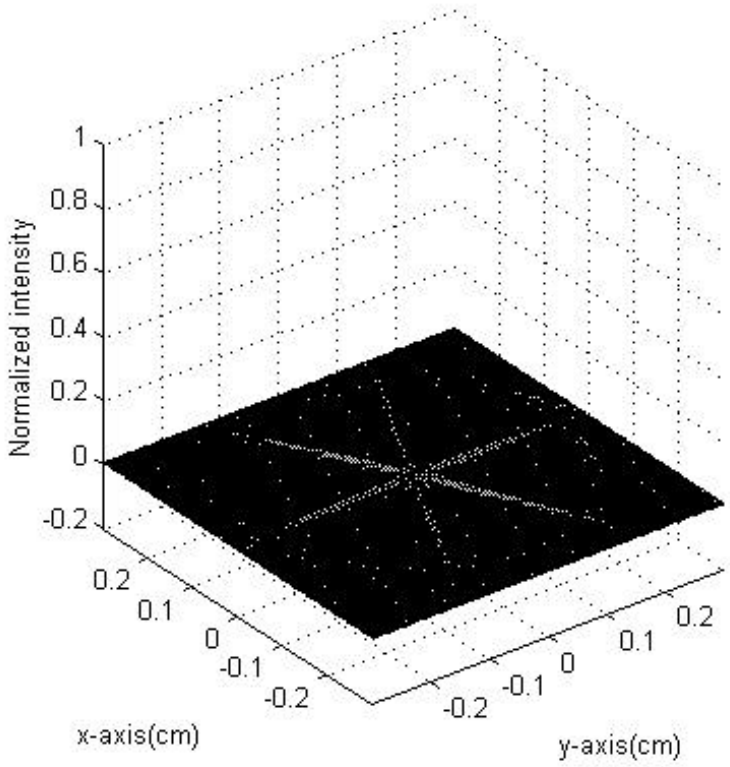

Figure (4.3-6): Correlation output when the target object in fig. (4.3-4) is scanned.

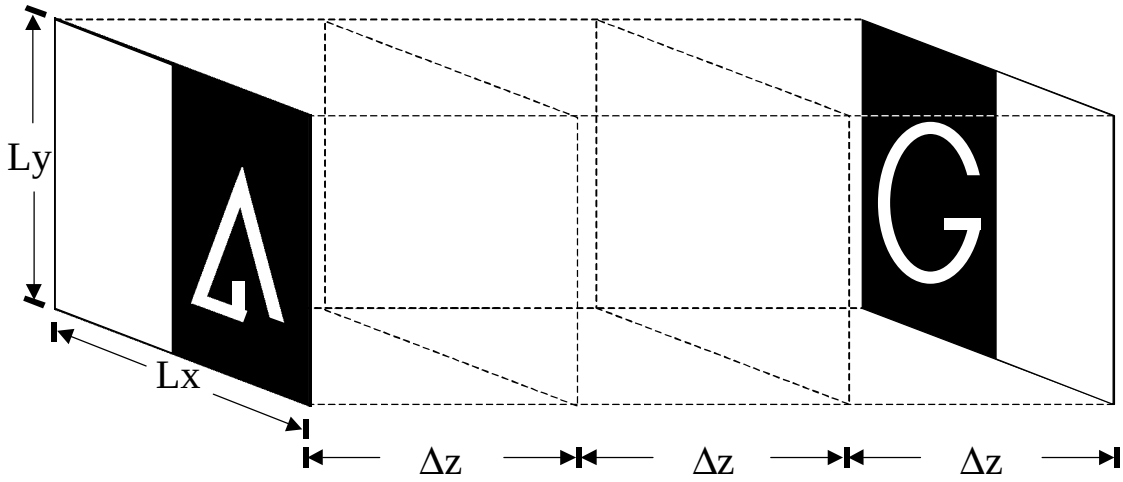

Figure (4.3-7): 3-D target object T.

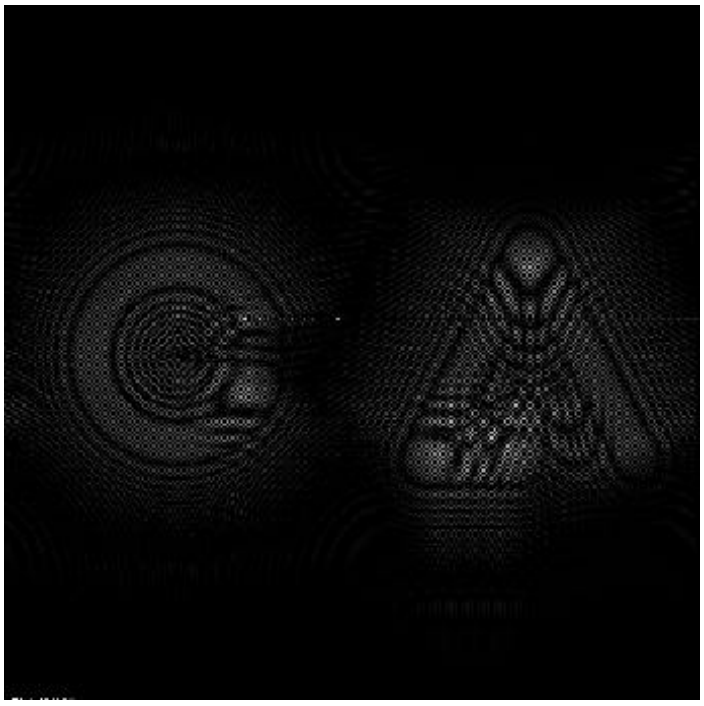

Figure (4.3-8a): Cosine-FZP hologram of the 3-D target object shown in fig. (4.3-7).

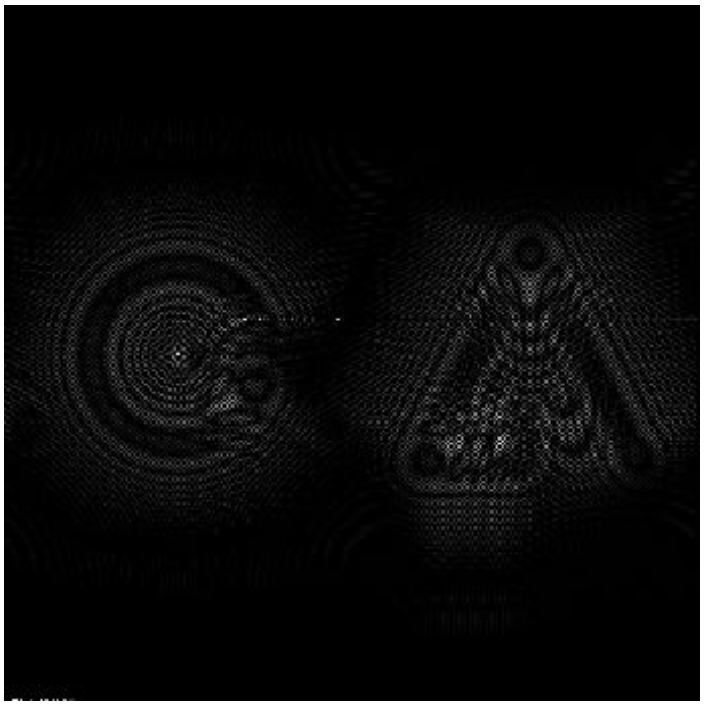

Figure (4.3-8b): Sine-FZP hologram of the 3-D target object shown in fig. (4.3-7).

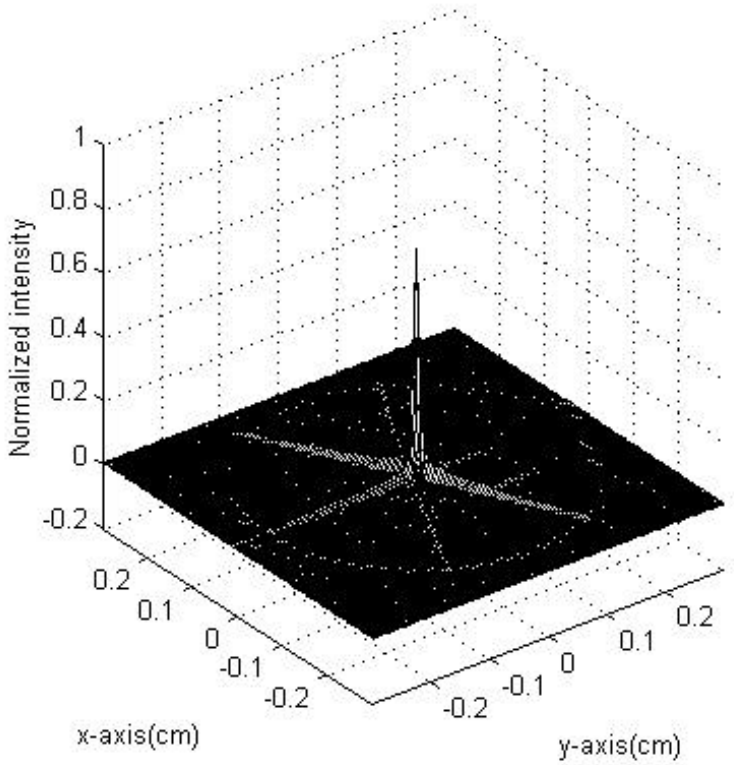

Figure (4.3-9): Correlation output when the target object in fig. (4.3-7) is scanned.

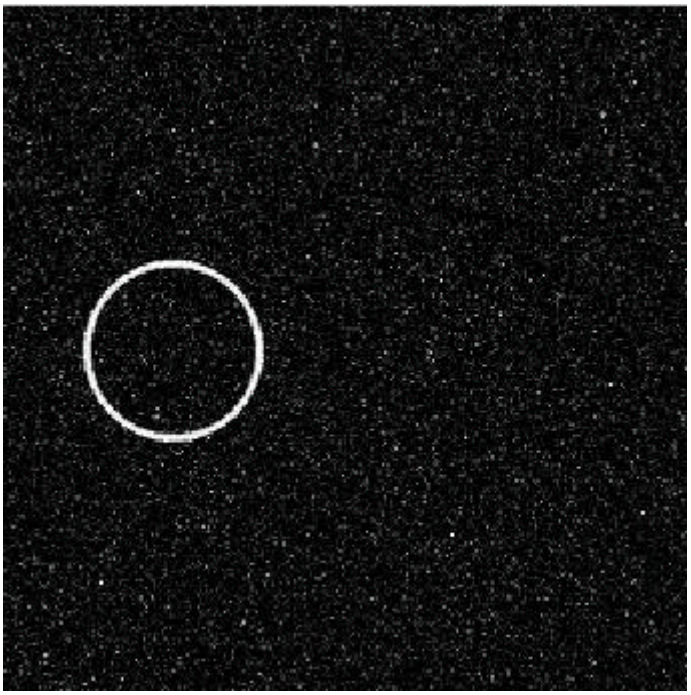

Figure (4.3-10a): The first slide that composes the target object with Gaussian noise having standard deviation, σ=0.25.

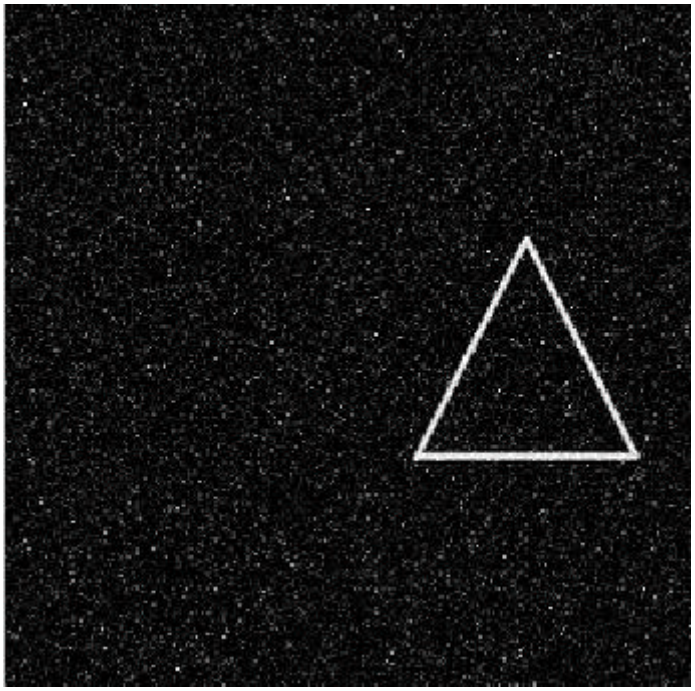

Figure (4.3-10b): The second slide that composes the target object with Gaussian noise having standard deviation, σ=0.25.

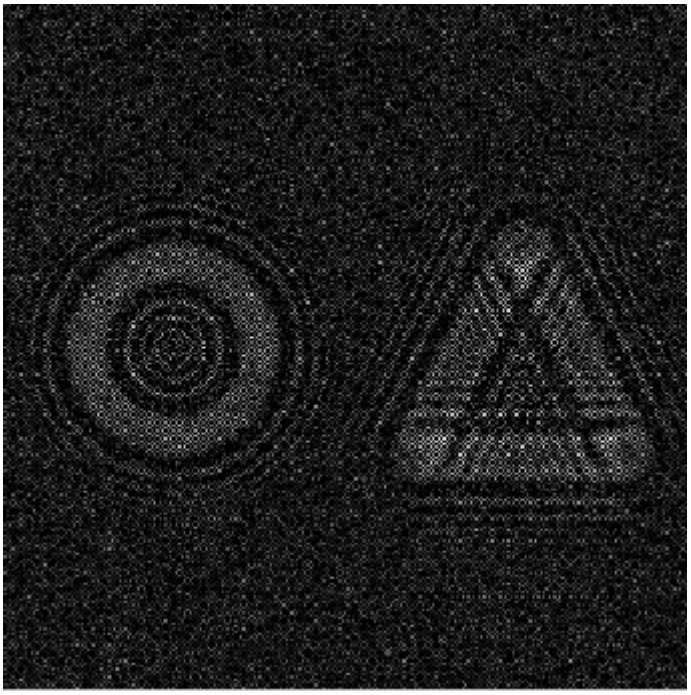

Figure (4.3-11a): Cosine-FZP hologram of the 3-D target object shown in fig. (4.3-1) in the presence of noise.

Figure (4.3-11b): Sine-FZP hologram of the 3-D target object shown in fig. (4.3-1) in the presence of noise.

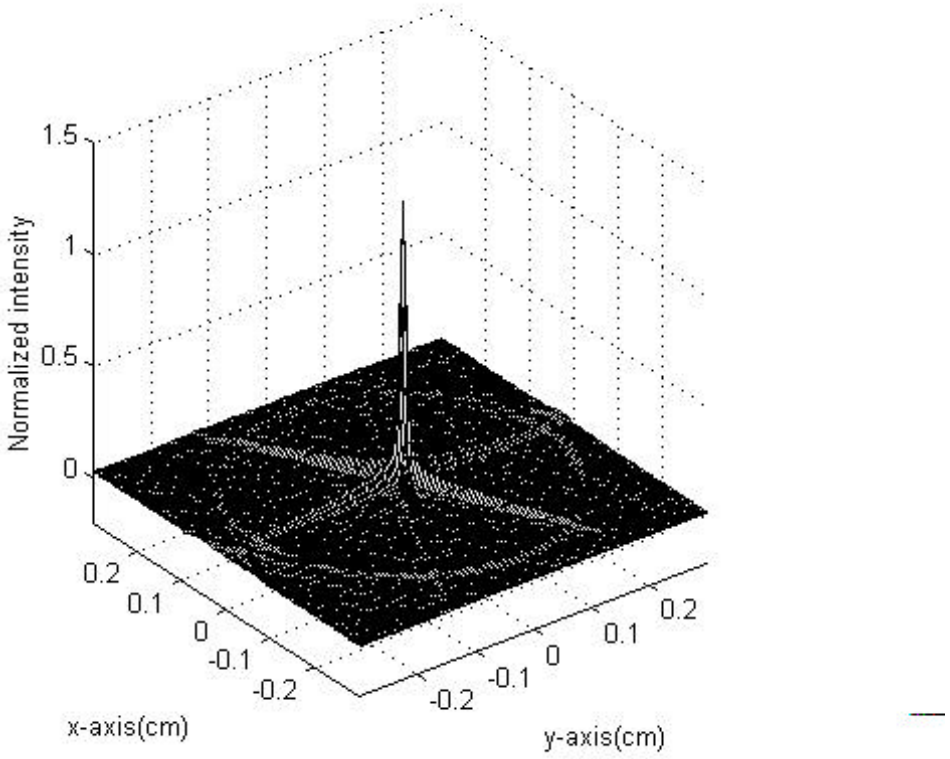

Figure (4.3-12): Correlation output (0.4 cm $\times$ 0.4 cm) when the target object is matched with the reference object, in the presence of noise.

Figure (4.3-13a): Cosine-FZP hologram of the 3-D target object shown in fig. (4.3-4) in the presence of noise.

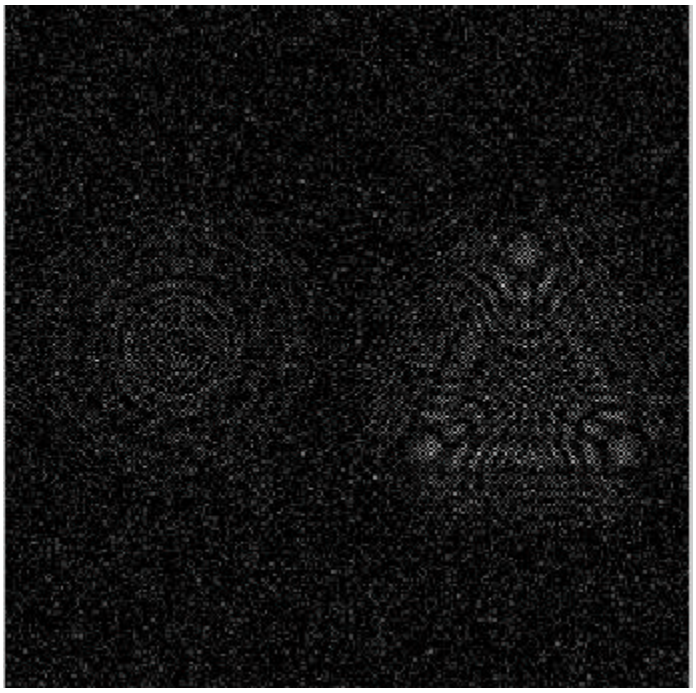

Figure (4.3-13b): Sine-FZP hologram of the 3-D target object shown in fig. (4.3-4) in the presence of noise.

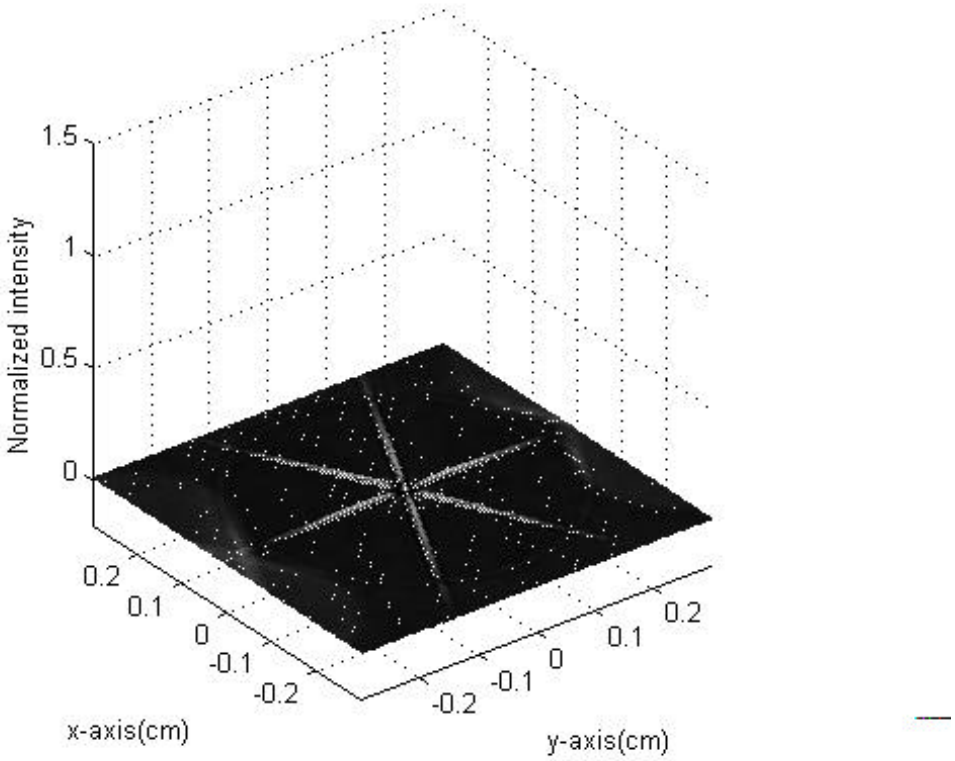

Figure (4.3-14): Correlation output when the target object in fig. (4.3-4) is scanned in the presence of noise.

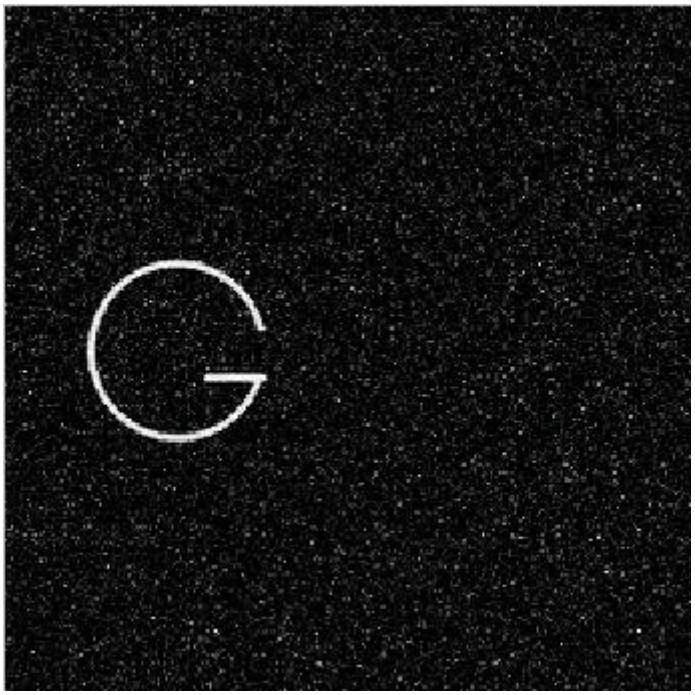

Figure (4.3-15a): The first slide that composes the target object with Gaussian noise having standard deviation, σ=0.25.

Figure (4.3-15b): The second slide that composes the target object with Gaussian noise having standard deviation, σ=0.25.

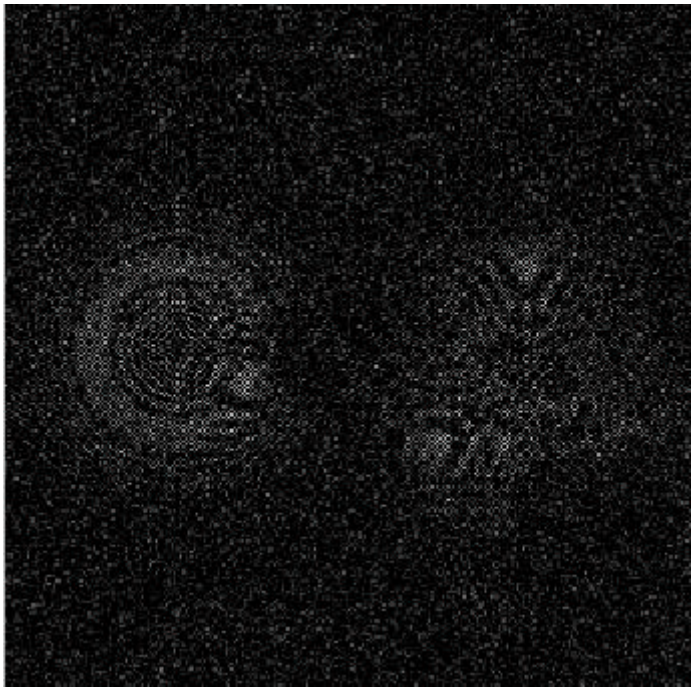

Figure (4.3-16a): Cosine-FZP hologram of the 3-D target object shown in fig. (4.3-7) in the presence of noise.

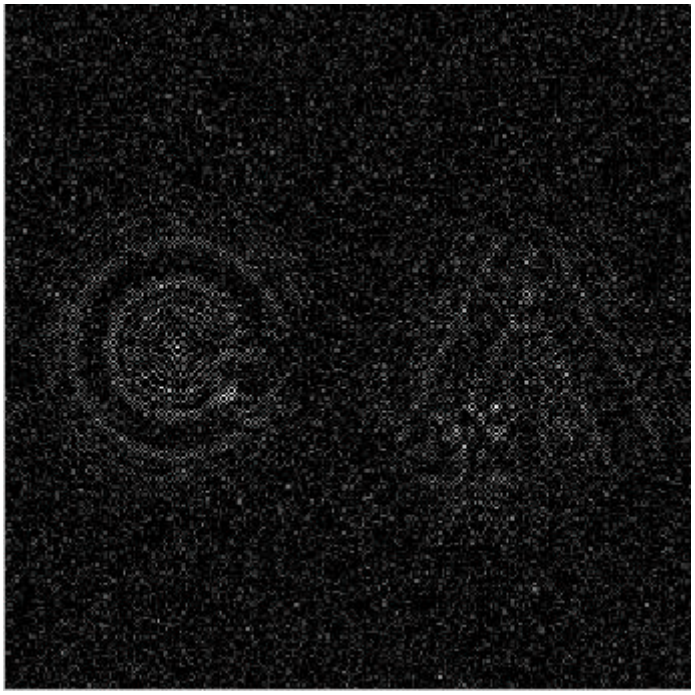

Figure (4.3-16b): Sine-FZP hologram of the 3-D target object shown in fig. (4.3-7) in the presence of noise.

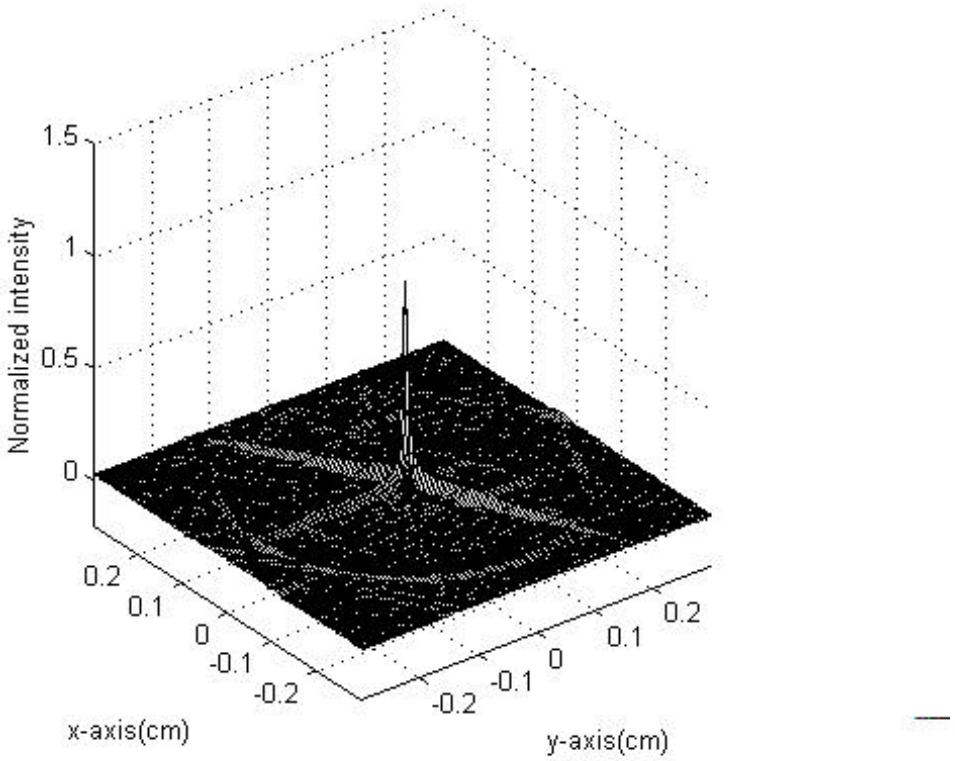

Figure (4.3-17): Correlation output when the target object in fig. (4.3-7) is scanned in the presence of noise.

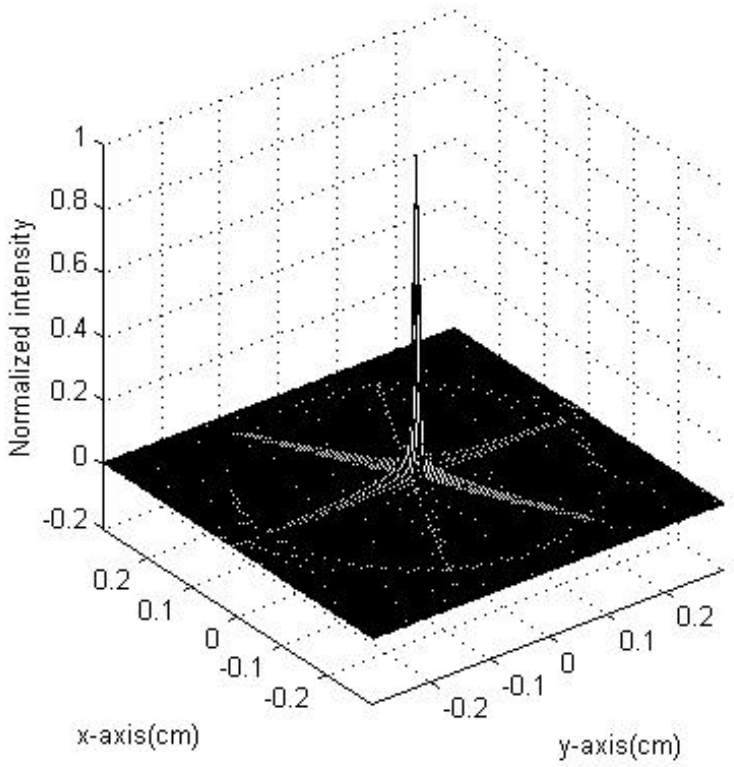

Figure (4.3-18): Correlation output (0.4 cm × 0.4 cm) when the target object is matched with the reference object using real-only hologram as a mask.

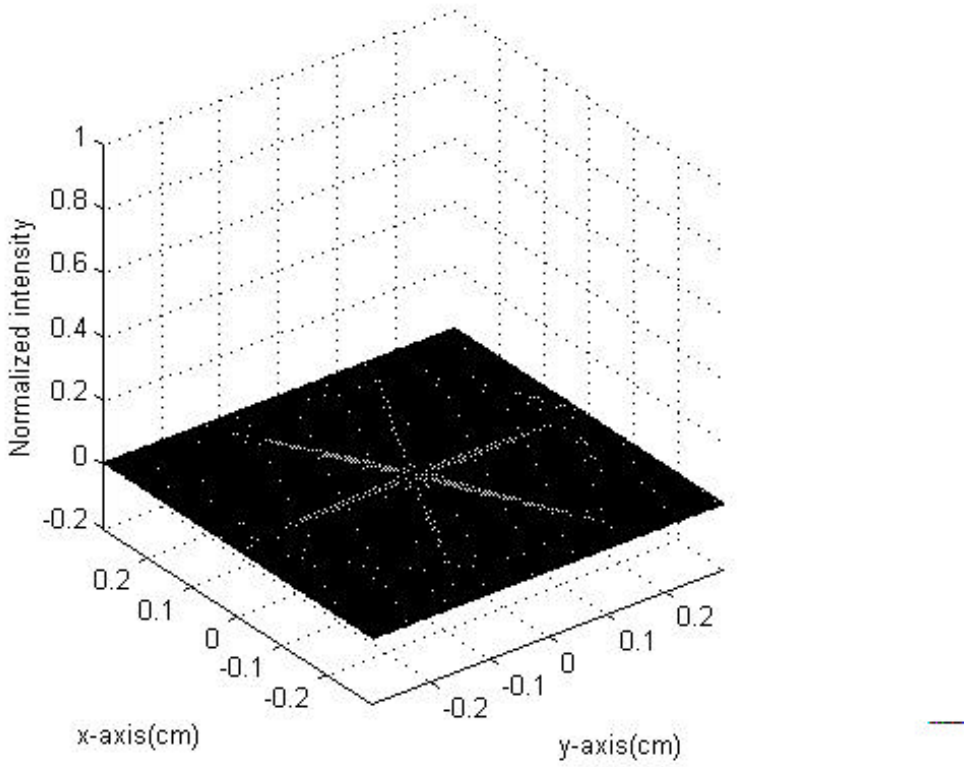

Figure (4.3-19): Correlation output when the target object in fig. (4.3-4) is scanned using real-only hologram as a mask.

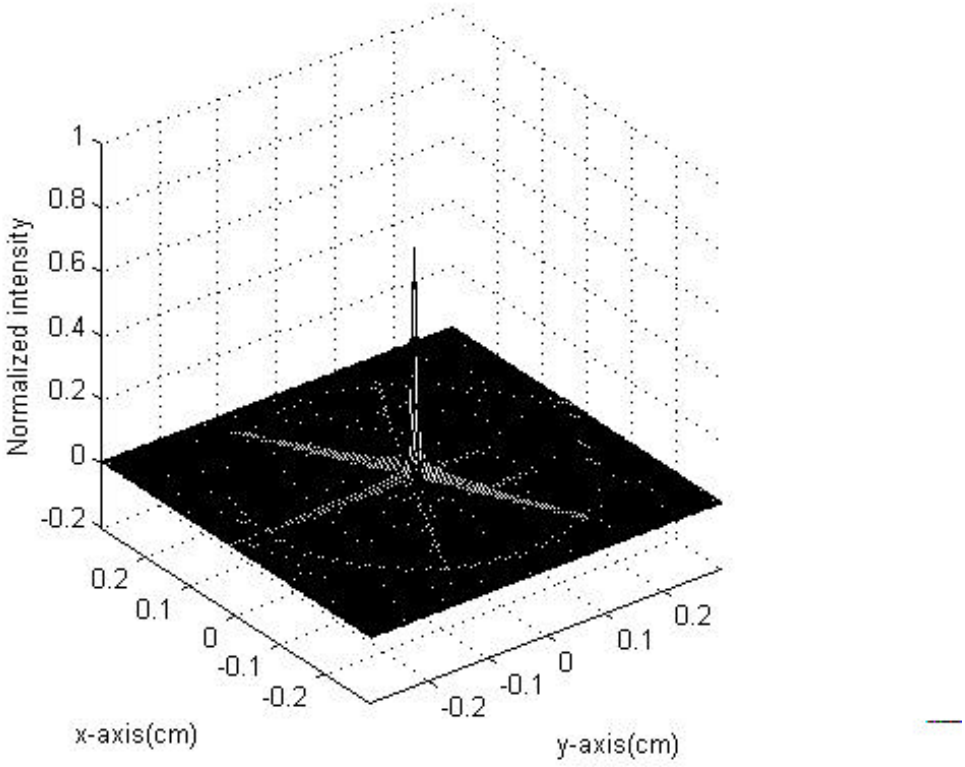

Figure (4.3-20): Correlation output when the target object in fig. (4.3-7) is scanned using real-only hologram as a mask.

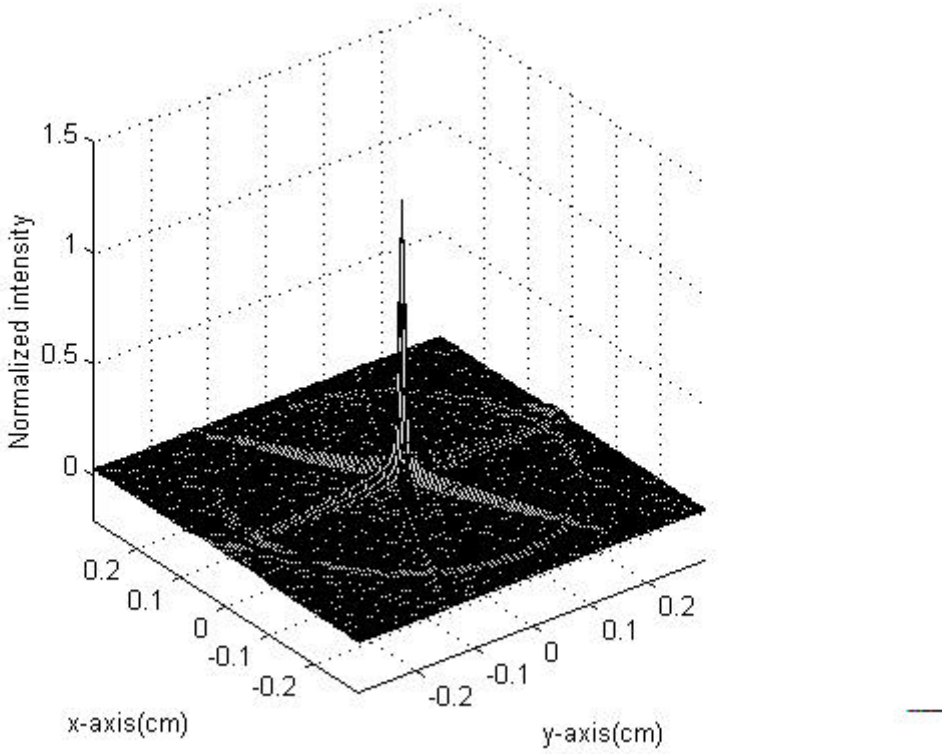

Figure (4.3-21): Correlation output (0.4 cm × 0.4 cm) when the target object is matched with the reference object using real-only hologram as a mask in the presence of noise.

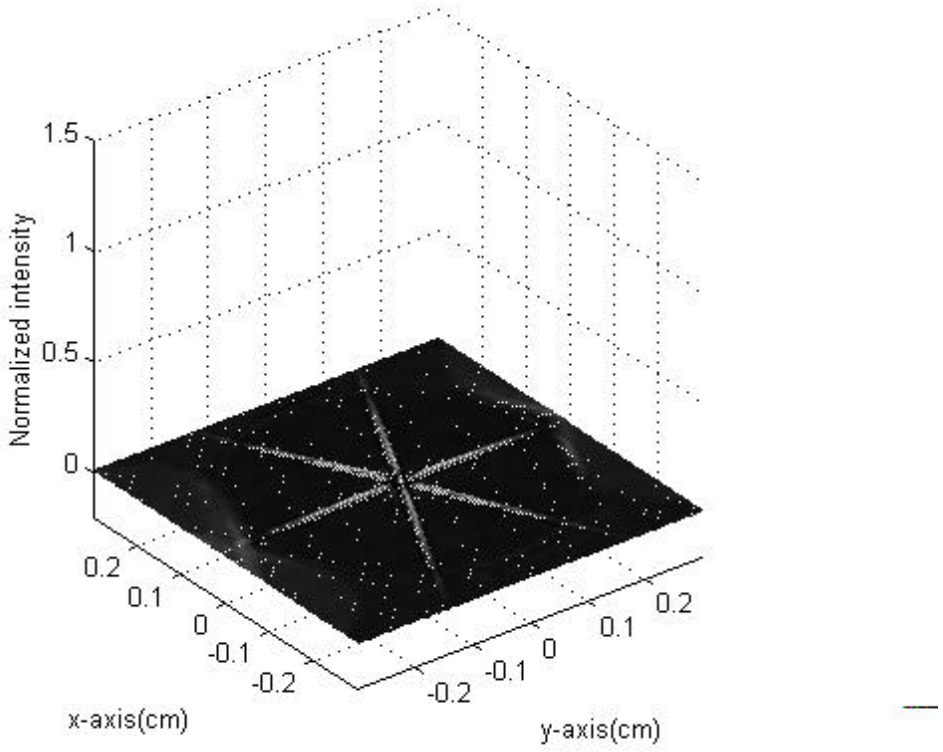

Figure (4.3-22): Correlation output when the target object in fig. (4.3-4) is scanned using real-only hologram as a mask in the presence of noise.

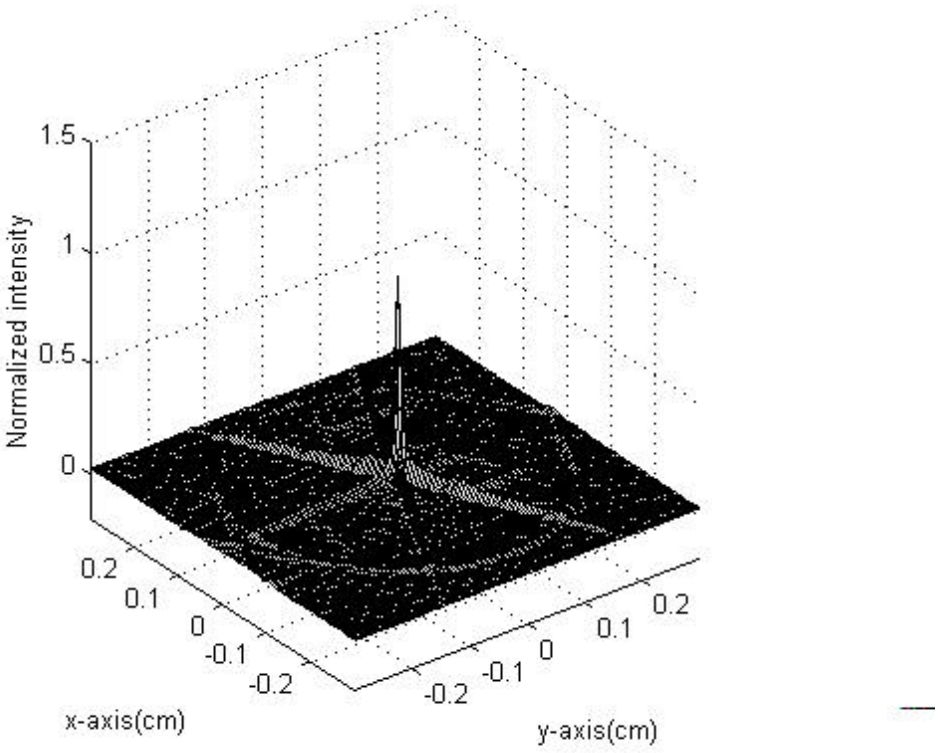

Figure (4.3-23): Correlation output when the target object in fig. (4.3-7) is scanned using real-only hologram as a mask in the presence of noise.

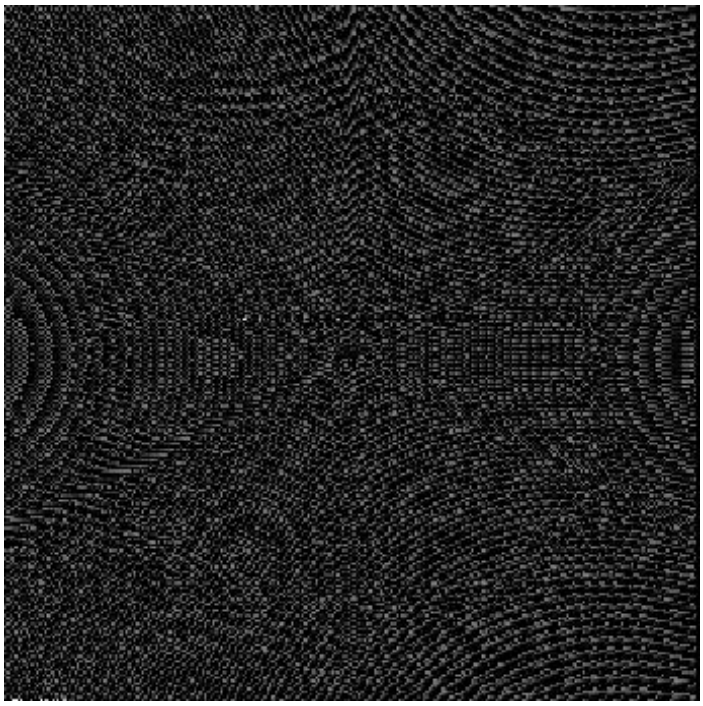

Figure (4.3-24): Phase-only hologram of the 3-D reference object shown in fig. (4.3-1).

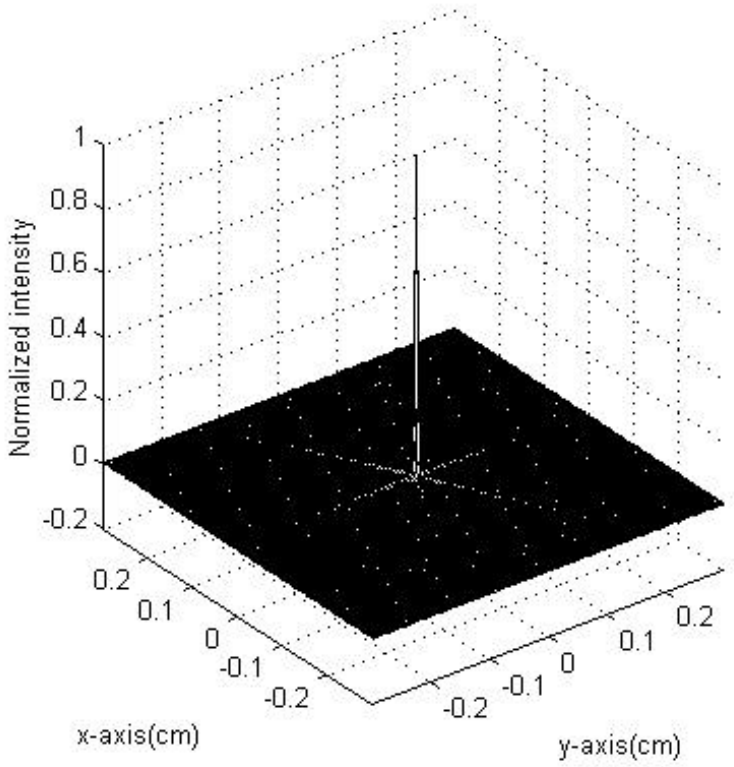

Figure (4.3-25): Correlation output (0.4 cm $\times$ 0.4 cm) when the target object is matched with the reference object using phase-only hologram as a mask.

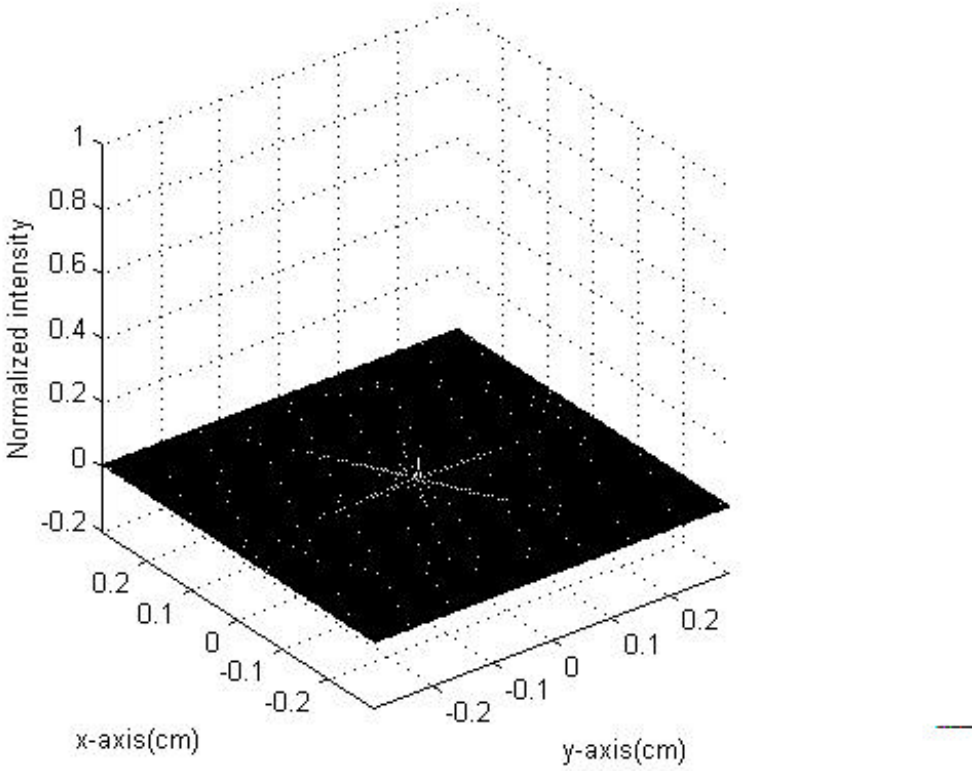

Figure (4.3-26): Correlation output when the target object in fig. (4.3-4) is scanned using phase-only hologram as a mask.

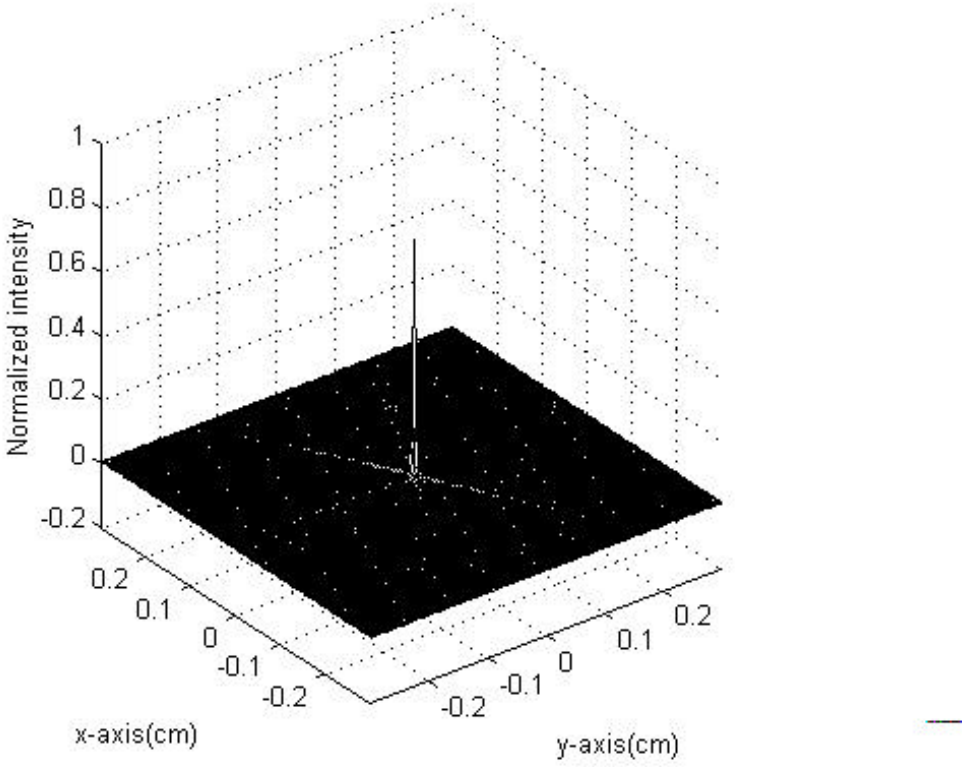

Figure (4.3-27): Correlation output when the target object in fig. (4.3-7) is scanned using phase-only hologram as a mask.

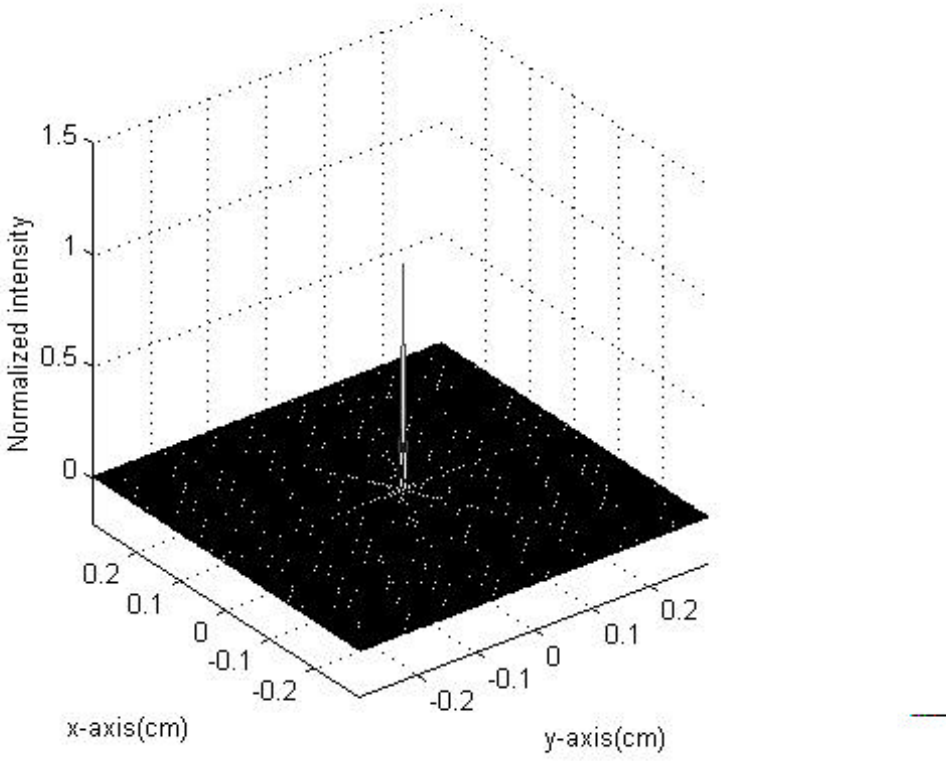

Figure (4.3-28): Correlation output (0.4cm $\times$ 0.4 cm) when the target object is matched with the reference object using phase-only hologram as a mask in the presence of noise.

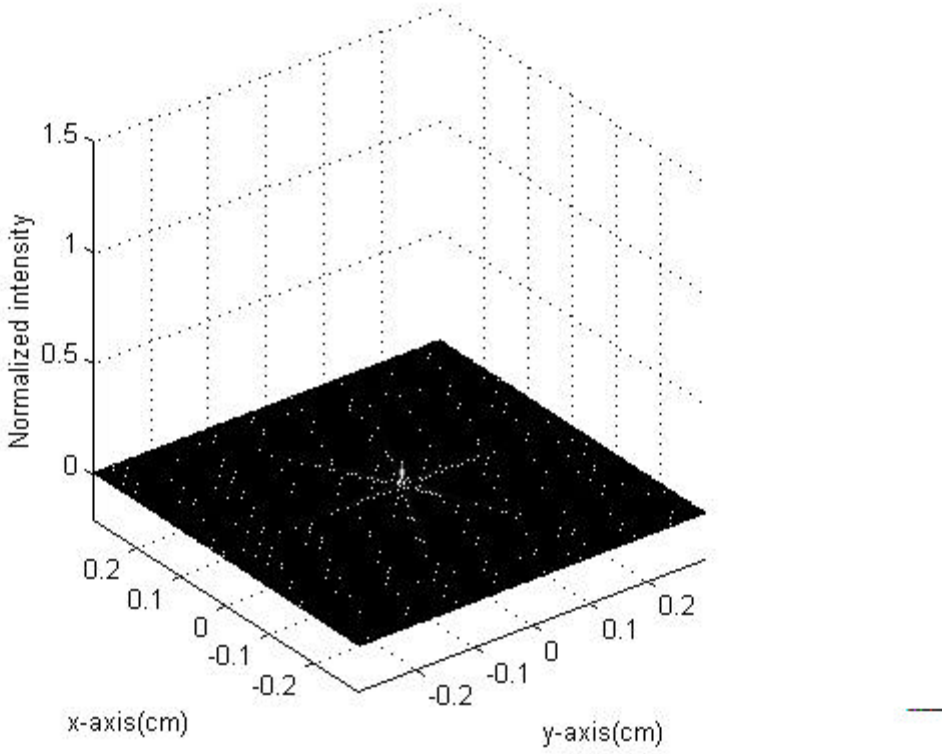

Figure (4.3-29): Correlation output when the target object in fig. (4.3-4) is scanned using phase-only hologram as a mask in the presence of noise.

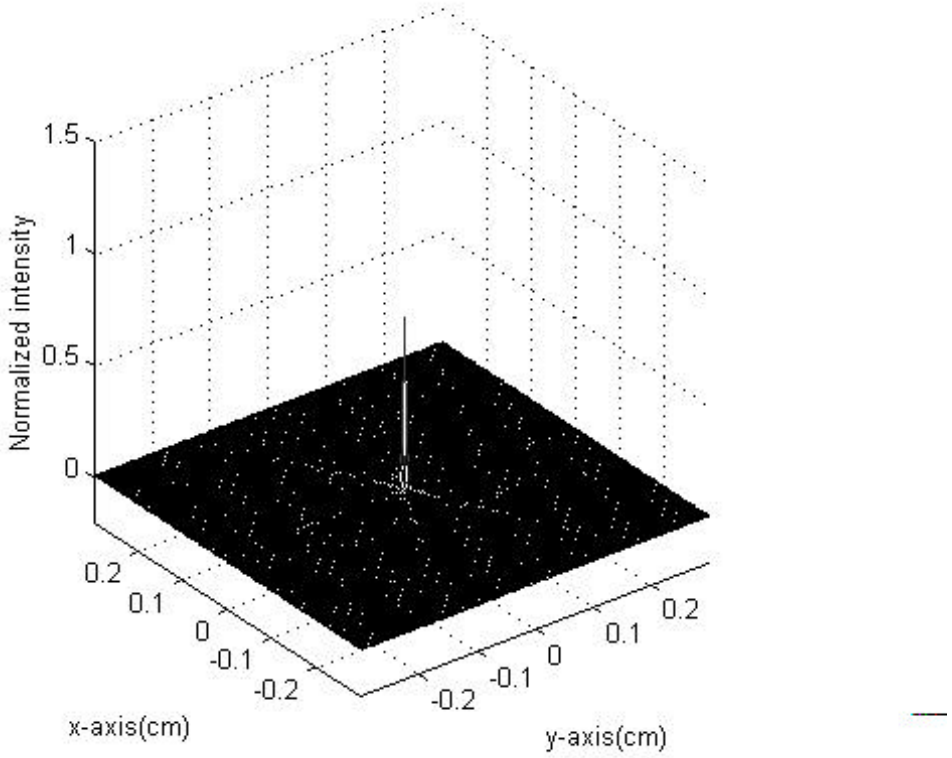

Figure (4.3-30): Correlation output when the target object in fig. (4.3-7) is scanned using phase-only hologram as a mask in the presence of noise.

Table (4.3-1): Matching results for noise-free inputs

Noiseless Case					
Fig.	Modulation scheme	Target object	Peak height	$\Delta(\%)$	$\eta_H(\%)$
4.3-3	Complex Hologram	Matched Obj. (Fig. 4.3-1)	1		5.91
4.3-6	Complex Hologram	Longitudinally Mis-matched Obj. (Fig. 4.3-4)	0.0152	98	3.05
4.3-9	Complex Hologram	Transversely Mis-matched Obj. (Fig. 4.3-7)	0.7088	29	5.69
4.3-18	Real-Only Hologram	Matched Obj. (Fig. 4.3-1)	1		5.91
4.3-19	Real-Only Hologram	Longitudinally Mis-matched Obj. (Fig. 4.3-4)	0.0152	98	3.04
4.3-20	Real-Only Hologram	Transversely Mis-matched Obj. (Fig. 4.3-7)	0.7088	29	5.69
4.3-25	Phase-Only Hologram	Matched Obj. (Fig. 4.3-1)	223		100
4.3-26	Phase-Only Hologram	Longitudinally Mis-matched Obj. (Fig. 4.3-4)	20.87	91	100
4.3-27	Phase-Only Hologram	Transversely Mis-matched Obj. (Fig. 4.3-7)	164.45	26	100

Peak height is normalized to the height of the auto-correlation peak in the absence of noise.
$\Delta(\%)$ is the percentage difference between the peak heights of auto-correlations and those of cross-correlations.
$\eta_H(\%)$ is the Horner efficiency

Table (4.3-2): Matching results for inputs with additive noise

Gaussinan noise with zero mean and standard deviation, σ=0.25					
Fig.	Modulation scheme	Target object	Peak height	$\Delta(\%)$	$\eta_H(\%)$
4.3-12	Complex Hologram	Matched Obj. (Fig. 4.3-1)	1.2825		1.72
4.3-14	Complex Hologram	Longitudinally Mis-matched Obj. (Fig. 4.3-4)	0.0283	98	1.94
4.3-17	Complex Hologram	Transversely Mis-matched Obj. (Fig. 4.3-7)	0.9363	27	1.72
4.3-21	Real-Only Hologram	Matched Obj. (Fig. 4.3-1)	1.2866		1.72
4.3-22	Real-Only Hologram	Longitudinally Mis-matched Obj. (Fig. 4.3-4)	0.0195	98	1.95
4.3-23	Real-Only Hologram	Transversely Mis-matched Obj. (Fig. 4.3-7)	0.9455	26	1.72
4.3-28	Phase-Only Hologram	Matched Obj. (Fig. 4.3-1)	226.29		100
4.3-29	Phase-Only Hologram	Longitudinally Mis-matched Obj. (Fig. 4.3-4)	22.22	90	100
4.3-30	Phase-Only Hologram	Transversely Mis-matched Obj. (Fig. 4.3-7)	171.59	24	100

Peak height is normalized to the height of the auto-correlation peak in the absence of noise.

$\Delta(\%)$ is the percentage difference between the peak heights of auto-correlations and those of cross-correlations.

$\eta_H(\%)$ is the Horner efficiency

Chapter 5: Optical experiments

Section 5.1 presents the experimental results of the 3-D optical matching technique that performs the matching of two 3-D images [3]. The optical system based on optical heterodyne scanning basically performs the 2-D correlation between the hologram of a 3-D reference object and that of a 3-D target. Section 5.2 presents the experimental results of the 3-D location extraction technique [4]. In this technique, we extract the 3-D location of the matched object by using phase information of holograms and the Wigner distribution.

5.1 Experimental results of 3-D image matching

The proposed optical system to demonstrate the 3-D holographic correlation technique is shown in fig. (5.1-1). Illumination is provided by a HeNe Laser, operating at $\lambda = 0.6328\mu m$. The laser beam is collimated by 10 $\times$ beam expanders and the size of the collimated beams is about $15mm$. The frequency shift is provided by acousto-optic frequency shifters. One acousto-optic frequency shifter shifts the frequency of the laser beam by 40 MHz, and the other by 40.01 MHz, and hence $\Omega_1/2\pi$ = 40 MHz and $\Omega_2/2\pi$ = 40.01 MHz. The scanning beams of the system scan the 3-D reference object by the movement of scanning mirrors according to the x-y scanning signal. The 3-D reference object consists of two transparencies, as shown in fig. (5.1-2). The transparencies of a "triangle" and a "rectangle" are located side by side but separated by a depth distance of about 15 cm, with the "triangle" located closer to the 2-D scanning mirror at a distance about 30 cm. Both the "triangle" and the "rectangle" are approximately 0.5 cm by 0.5 cm, have a line width of about 100 μm and are transmissive on an opaque background. The output current from the photo-detector is demodulated through the lock-in amplifier

with respect to the reference signal from the frequency generator. The demodulated output is sent to the Image Processing and Measuring System (IPMS) [40]. The output of the IPMS in the form of an NTSC video signal is sent to a TV monitor for displaying the hologram of the reference object. Fig. (5.1-3) shows the hologram of the reference object. We then generate a transparency according to this hologram and use it as a mask in the 3-D matching stage. A 3-D target object that is exactly the same as the reference object is then placed and scanned in two dimensions. The output of the photodetector is processed in the same manner as in the recording stage as discussed. The result of the processed signal displays effectively the resulting strong correlation peak of the matched 3-D object that is shown in fig. (5.1-4).

In the second experiment, the 3-D target object shown in fig. (5.1-5) is located at the same location as the reference object. However, the 3-D target object now consists of two transparencies that have the same 2-D patterns as the reference object but with different depth locations. The 3-D object is scanned in two dimensions by the optical beams with one of the beams modulated by the holographic information of the reference object. The processed signal displays effectively the resulting correlation between the mis-matched 3-D object and the reference object. The lack of a strong correlation peak in fig. (5.1-6) clearly indicates a mis-match of the two 3-D objects. It is important to point out that the two planar patterns of the object are identical to the reference object and yet the system does not give a strong correlation peak. The reason is that since the output is the correlation of the holograms of the reference object and the target object, the depth information is as important as the planar distributions.

In our last experiment, the 3-D target object shown in fig. (5.1-7) is located at the same location as the reference object. The transparencies of the "cross" and the "circle" are located side by side with same depths as the reference object. Both the "cross" and the "circle" are approximately $0.5\ cm$ by $0.5\ cm$, have a line width of about $100\mu m$, and are transmissive on an opaque background. The 3-D target object is scanned in two

dimensions and the resulting correlation output is shown in fig. (5.1-8). Clearly, no correlation peak is observed as expected.

In conclusion, we have presented experimental results of 3-D optical matching technique that performs the matching of two 3-D images. The optical system based on optical heterodyne scanning basically performed the 2-D correlation between the hologram of a 3-D reference object and that of a 3-D target object. It is important to point out that 2-D correlation of holographic information can match the 3-D aspect of the two 3-D objects because the hologram has the depth information about the 3-D reference object as a form of 2-D fringe pattern. A strong correlation peak results if the two holographic data match. The proposed optical 3-D matching technique is promising for the use of holographic information about the objects in the field of 3-D pattern recognition.

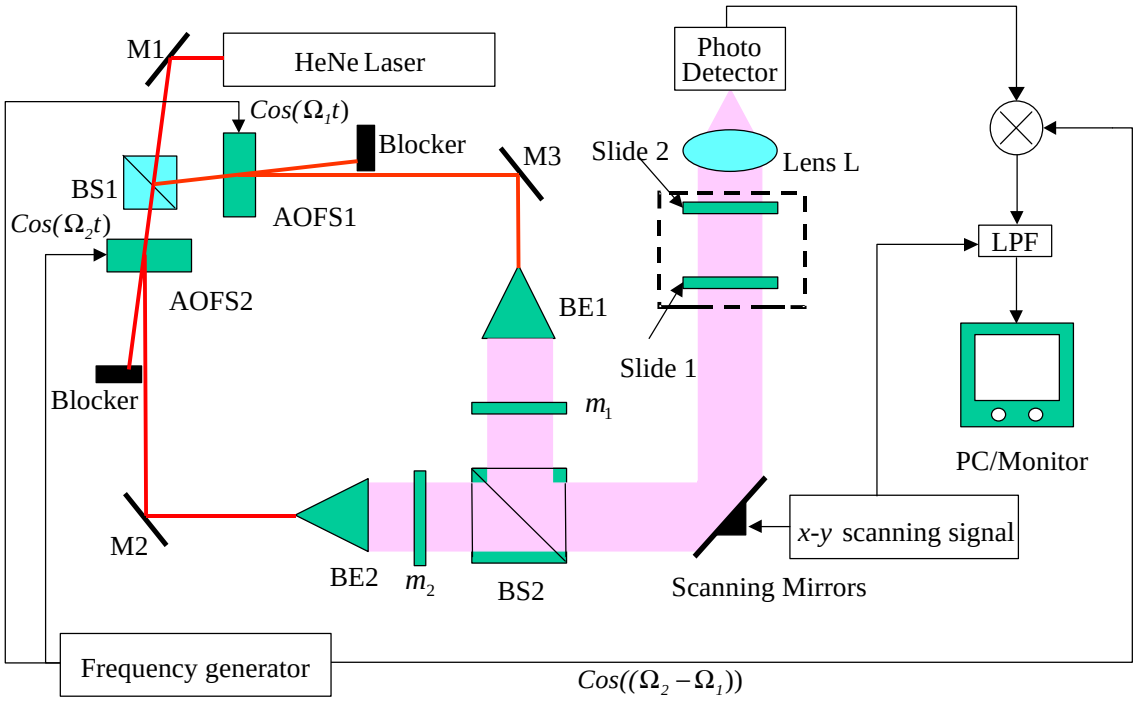

Figure (5.1-1): Optical heterodyne scanning system.
(M1,2,3: mirrors, AOFS1,2: Acousto-optic frequency shifters, BS1,2: Beam splitters, BE1,2,3: Beam expanders, ⊗ electronic multipliers; LPF: lowpass filter)

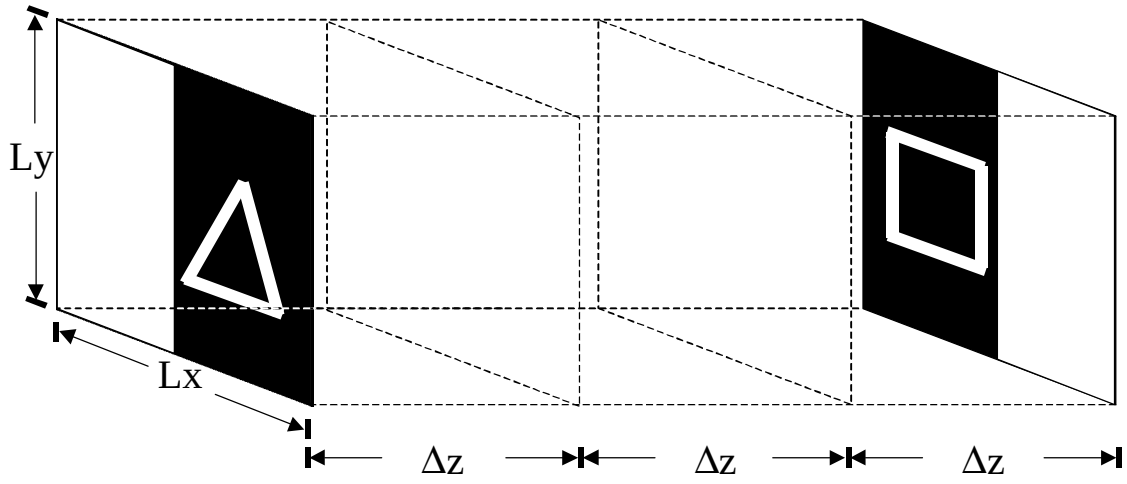

Figure (5.1-2): 3-D reference object I_R, with $L_x = L_y \ = 1\,cm,\ \triangle \text{z} = 5\ cm.$

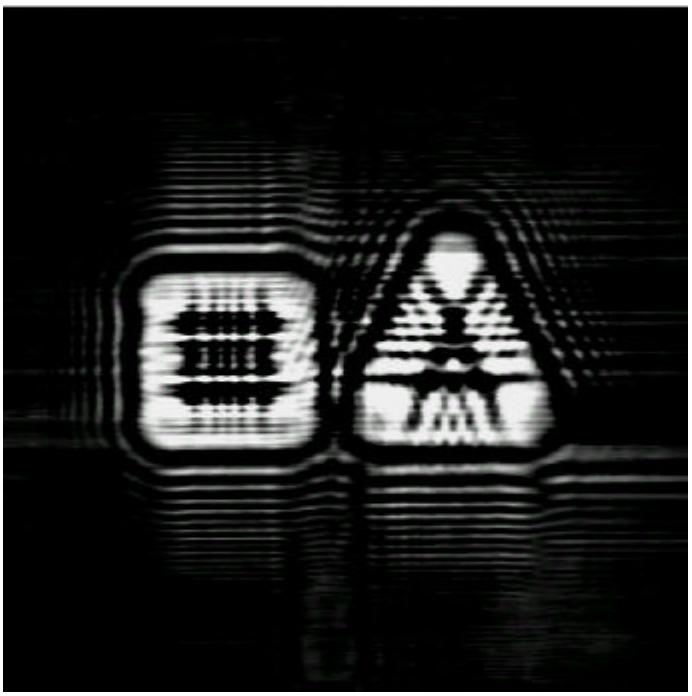

Figure (5.1-3): Hologram of the reference object.

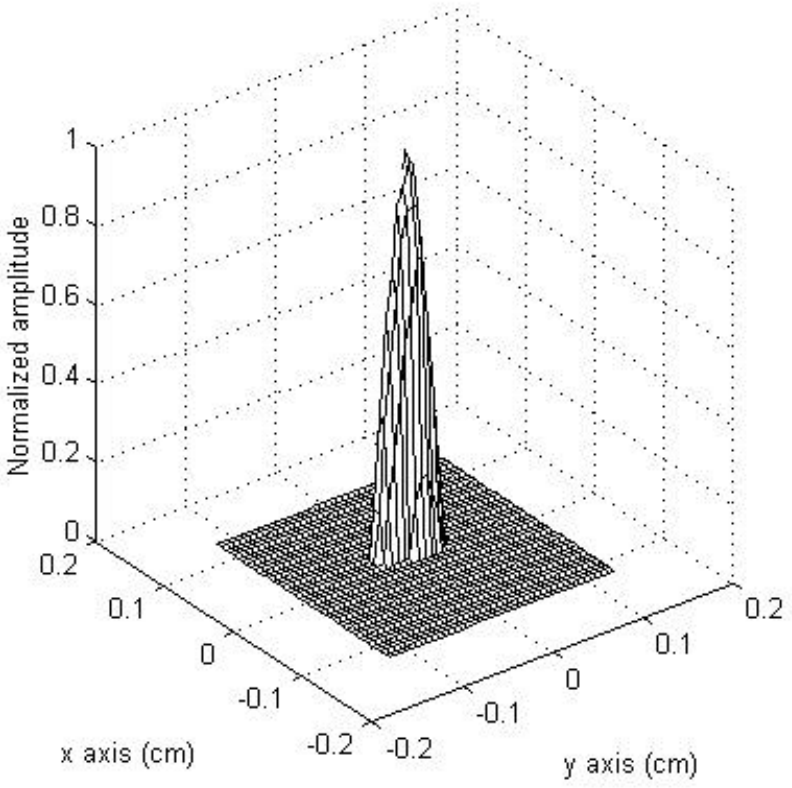

Figure (5.1-4): Correlation output (0.4 cm $\times$ 0.4 cm) when the target object is matched with the reference object.

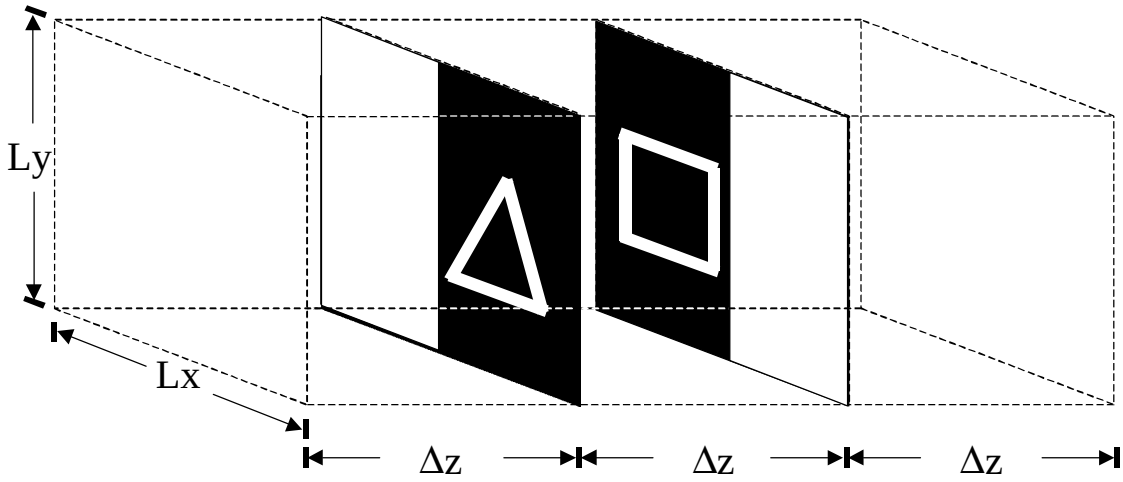

Figure (5.1-5): 3-D target object with the same 2-D patterns but with different depth locations.

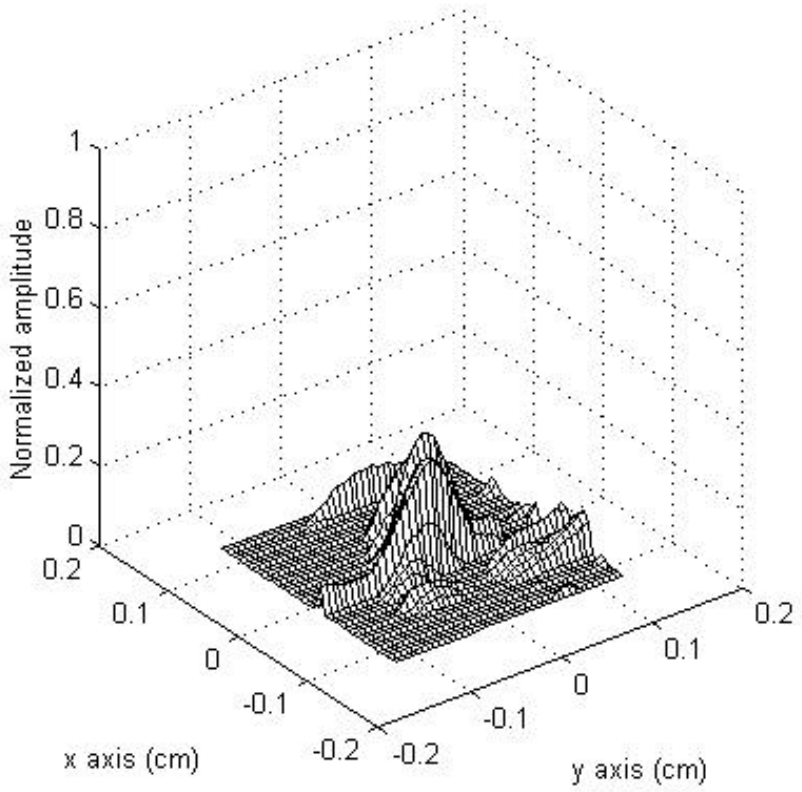

Figure (5.1-6): Correlation output (0.4 cm $\times$ 0.4 cm) when the target object in fig.(5.1-5) is scanned. (no correlation peak observed)

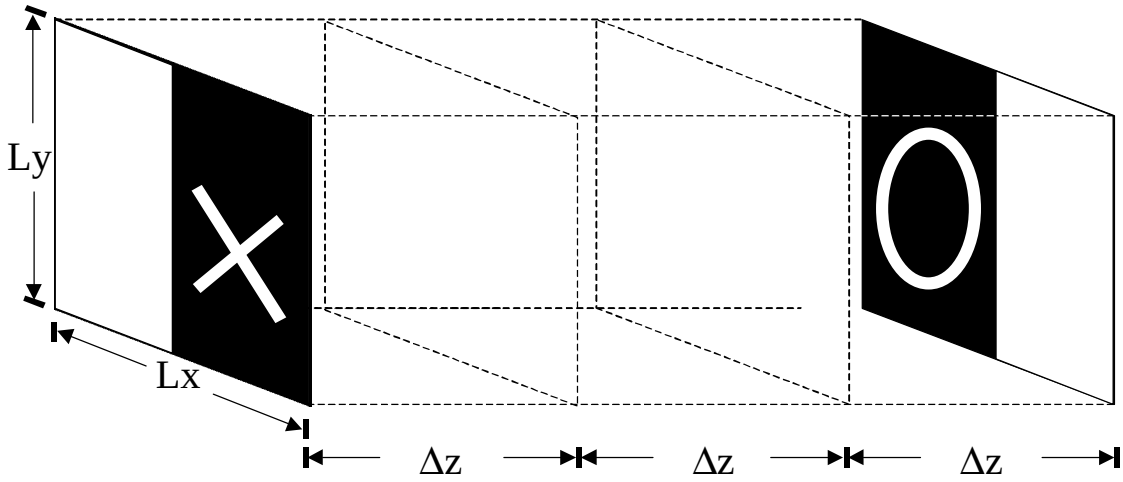

Figure (5.1-7): 3-D target object with the same 2-D patterns but with different depth locations.

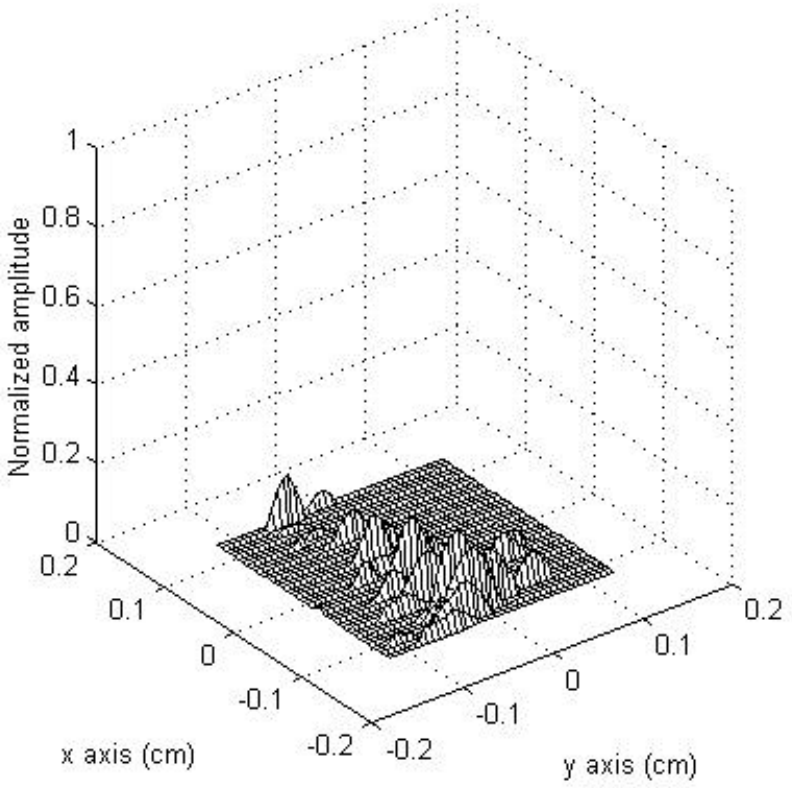

Figure (5.1-8): Correlation output (0.4 cm $\times$ 0.4 cm) when the target object in fig.(5.1-7) is scanned. (no correlation peak observed)

5.2 Experimental results of 3-D location extraction using phase-only holograms and Wigner distribution

A digital signal analysis technique of figure (5.2-1) is proposed to extract 3-D location of the matched object using holographic information and Wigner distribution. First, the complex hologram of a reference object, $R(x,y;z)$, and that of a target object, $T(x,y;z)$, are extracted using an optical heterodyne scanning system and the phase-only hologram in the frequency domain is calculated on a digital computer. The correlation between the phase-only hologram of the reference object and that of the target object is achieved digitally. This is given by

$$c(x,y) = \mathcal{F}^{-1}\{exp[-jarg(\mathcal{F}\{H_R\})]\, exp[jarg(\mathcal{F}\{H_T\})]\} \qquad (5.2\text{-}1)$$

$$= \mathcal{F}^{-1}\{exp[-j(\ arg(\mathcal{F}\{H_R\}) - arg(\mathcal{F}\{H_T\})\ )]\}$$

where H_R=$\int \frac{k_0}{2\pi z} exp[j\frac{k_0}{2z}(x^2 + y^2)] \odot R(x,y;z)dz$ and H_T=$\int \frac{k_0}{2\pi z} exp[j\frac{k_0}{2z}(x^2 + y^2)] \odot T(x,y;z)dz$ respectively represent the complex hologram of the reference object, and that of the target object.

When the 3-D target object is the same as the 3-D reference object but shifted by Δx, Δy and Δz, i.e., $T(x,y;z) = R(x-\Delta x, y-\Delta y; z-\Delta z)$, the hologram of the target object in frequency domain is given by

$$\mathcal{F}\{H_T\} = |\mathcal{F}\{H_R\}| exp\left[j\left\{arg(\mathcal{F}\{H_R\}) + (\Delta x k_x + \Delta y k_y) - \frac{\Delta z}{2k_o}\left(k_x^2 + k_y^2\right)\right\}\right] \qquad (5.2\text{-}2)$$

Note that the argument of the hologram of the target object in frequency domain, $arg(\mathcal{F}\{H_T\})$=$\left\{arg(\mathcal{F}\{H_R\}) + (\Delta x k_x + \Delta y k_y) - \frac{\Delta z}{2k_o}\left(k_x^2 + k_y^2\right)\right\}$, is composed of three

terms. The first term is identical to the phase term of the hologram of the reference object. The second term is the linear phase shift caused by the transverse location shift of the target object about the location of the reference object. Finally, the third term is the fringe term caused by the shift along the depth direction, in which the shifted location along the depth direction, Δz, is contained in a slope of local frequency along the space. Thus, when the three dimensional image of the reference object and that of the shifted target object are matched with each other, the correlation of phase holograms gives a Fresnel zone pattern. This is given by

$$c(x,y) = \mathcal{F}^{-1}\{exp[-j(arg(\mathcal{F}\{H_R\}) - arg(\mathcal{F}\{H_T\}))]\} \tag{5.2-3}$$

$$= \mathcal{F}^{-1}\left\{exp\left[-j\left(arg(\mathcal{F}\{H_R\}) - \left\{arg(\mathcal{F}\{H_R\}) + (\Delta x k_x + \Delta y k_y) - \frac{\Delta z}{2k_o}\left(k_x^2 + k_y^2\right)\right\}\right)\right]\right\}$$

$$= \mathcal{F}^{-1}\left\{exp\left[j\left((\Delta x k_x + \Delta y k_y) - \frac{\Delta z}{2k_o}\left(k_x^2 + k_y^2\right)\right)\right]\right\}$$

$$= \frac{-jk_o}{2\pi\Delta z} exp\left[j\frac{k_o}{2\Delta z}((x-\Delta x)^2 + (y-\Delta y)^2)\right].$$

Note that the phase of the hologram has the 3-D information of an object. Additionally, the phase term of the hologram of the reference object is matched with the first phase term of the phase only hologram of the target object. These cancels each other when the 3-D aspect of the target object is matched with that of the reference object. Thus, the correlation between the phase-only hologram of the reference object and that of the target object gives a Fresnel zone type function only when the 3-D image of the target object is matched with that of the reference object, which has shifted location along Δx, Δy and Δz. Moreover, the information about the 3-D shifted location of the pattern-

matched object is contained in the output correlation as a form of fringe pattern that is the space-frequency characteristic (fringe pattern) of the space signal (the image).

The Wigner distribution is a signal transformation that is convenient for such a space-frequency (or time-frequency) analysis because the Wigner distribution yields the space (time) variation of the frequency components of a signal. Because the local frequency of the chirp signal is a monotonically increasing function along the space, the Wigner distribution of the chirp signal, $f(t) = exp(j\alpha t^2/2)$ gives the line impulse on the space-frequency domain with the slope of the instantaneous frequency on the space-frequency plane. This is given by

$$W_f(t,\omega) = 2\pi\delta(\omega - \alpha t) \tag{5.2-4}$$

The correlation of the phase only hologram for the 3-D image-matched object is a two dimensional chirp signal given by Eq. (5.2-3). Thus, the absolute value of continuous Wigner distribution of the correlation about y for any given x value, $x = x'$, is given by

$$\begin{aligned} \left|W_c(y, k_y; x')\right| = \Bigg| & - j\frac{1}{2\pi}\left(\frac{k_o}{\Delta z}\right)^2 \delta\left(k_y - \frac{k_o}{\Delta z}(y - \Delta y)\right) \\ & \times exp\left[- j\frac{k_o}{2\Delta z}(x' - \Delta x)^2\right]\Bigg| \\ = & \left|\frac{1}{2\pi}\left(\frac{k_o}{\Delta z}\right)^2 \delta\left(k_y - \frac{k_o}{\Delta z}(y - \Delta y)\right)\right|, \end{aligned} \tag{5.2-5}$$

Note that the absolute value of the Wigner distribution of the correlation of phase only holograms is the desired line impulse on the space-frequency plane. This line impulse intersects with the $y-$ axis, and the intersection point is Δy, which is the shifted location

of the 3-D target object along the y-axis. When the 3-D target object is not matched with the 3-D image of the reference object, one can not observe the line impulse in the Wigner distribution. Furthermore, the slope of the line impulse is inversely proportional to the shifted location along the $z-$ axis, that is -$k_o/2\Delta z$. Therefore, if the wave length λ is known ($k_o = 2\pi/\lambda$), the shifted location is known by directly measuring the slope of the line.

In the same manner, the shift along the $x-$ axis can be obtained by the Wigner distribution of the $x-$ axis. This implies that the complete location of the 3-D shifted target object can be directly calculated from the correlation between the phase-only hologram of the reference object and that of the target object. Further it suggests that the Wigner analysis of correlation reveals the 3-D location of the matched 3-D target object.

An experimental set up of optical scanning holography is shown in fig.(5.2-2). Illumination is provided by a He-Ne Laser, operating at $\lambda = 0.6328\mu m$. The two acousto-optic frequency shifters provide frequency up-shifting of the laser beams at $\Omega_2/2\pi = 40.01\,MHz$, and $\Omega_1/2\pi = 40\,MHz$. The collimated beams are $D \sim 15mm$ each. The sinusoidal signals for acousto-optic frequency shifters are generated by the frequency generator which also provides the difference of the frequencies, $(\Omega_2 - \Omega_1)/2\pi$, for electronic mixing. Therefore, the heterodyne frequency of the current from the photo-detector is given by the difference of frequencies of each light beam, 10 KHz.

In the recording stage of the hologram of a reference object, again the two masks are of the forms as follows: $m_1(x,y)$ = $\delta(x,y)$ and $m_2(x,y)$=1. A lens with focal length $f = 400mm$, is used to focus the collimated beam emerging from beam collimator BE1 to about the size of $\lambda f/D \sim 17\,\mu m$ to act as a point source (note that the size of the point source determines the lateral resolution of the scanning system), and the collimated beam emerging from BE2 acts as a plane wave as $m_2(x,y)$=1. Beam splitter BS2 is used to combine the two beams to act as a scanning beam of the system to scan the 3-D reference object that is located $26cm$ away from scanning mirrors. The 3-D reference object

consists of two transparencies, as shown in fig.(5.1-2). The transparencies of a triangle and a rectangle are located side by side, but separated by a depth distance of about 15 cm, with the triangle located closer to the 2-D scanning mirrors. Both the triangle and the rectangle are approximately 0.5 cm by $0.5\ cm$, and have a line width of about 100 μm. They are transmissive on an opaque background. The output current from the photo-detector is demodulated through the mixers based on the reference signal from the frequency generator. These two demodulated outputs pass through two low-pass filters, and are converted to digital signals. These signals are then stored in the computer. Figs. (5.2-3a,b) shows the cosine- and sine- holograms of the reference object, from which a complex hologram is first calculated and the phase-only holographic information in frequency domain are then extracted according to Eq. (4.2-5). The holograms are 800 $\times$ 800 sampled images with 256 gray levels.

In our first experiment, for matching the target object that has the corresponding 3-D image of the reference object but with shifted location, we place a target object with the following specifications: $T(x,y;z) = R(x-\Delta x, y-\Delta y; z-\Delta z)$ with Δx = 0 mm, Δy = 2.5mm, and Δz = 250 mm. In other words, the 3-D target object is identical to the 3-D reference object, but otherwise displaced away from the original 3-D reference object's location. The target object is scanned by the optical heterodyne scanning system. Fig. (5.2-4a,b) shows holograms of the target object. In the computer, the phase-only holographic information of the reference and target object are extracted and finally the correlation between them is calculated. Fig. (5.2-5) shows the Wigner distribution of the correlation along the $y-$direction. The intersection between the line impulse, $\left|\frac{1}{2\pi}\left(\frac{k_o}{\Delta z}\right)^2 \delta\left(k_y - \frac{k_o}{\Delta z}(y-\Delta y)\right)\right|$, and the y-axis gives Δy, i.e., the y-location of the 3-D target object. The slope of the line impulse gives Δz, i.e., the z location of the 3-D target object as expected. The x-location, Δx, can be extracted with the same process along the $x-$direction.

In our second experiment, we choose the target object that consists of two slices and that are identical with slices of the 3-D reference object, but located at different depth locations. The difference of depth location is now $5\,cm$ within the 3-D volume of the object as shown in fig.(5.1-5). Again, this target object is located at the same location as the reference object 26 cm away from the scanning mirrors in the experiment. Figs. (5.2-6a) and (5.2-6b) show the cosine- and sine- holograms of the target object, respectively. Fig.(5.2-7) shows the Wigner distribution of correlation output between the phase-only holographic information of the reference object and that of the target object as shown in Fig. (5.1-5). We cannot observe the line delta in this Wigner distribution because the 3-D pattern of the target object shown in Fig.(5.1-5) is not matched with the reference object.

In the third experiment, we choose the target object as shown in Fig.(5.1-7), in which the depth location of the 2-D patterns are the same as the reference object. The 2-D patterns are different than the reference object but the target object is located at the same location as the reference object, 26 cm away from the scanning mirrors. The cosine- and the sine- holograms of target objects are respectively shown in Fig. (5.2-8a) and Fig. (5.2-8b). The Wigner distribution of the correlation output of this target object is shown in Fig. (5.2-9). In this Wigner distribution, we again do not observe the line delta because the 3-D pattern of the target object is not matched with the reference object.

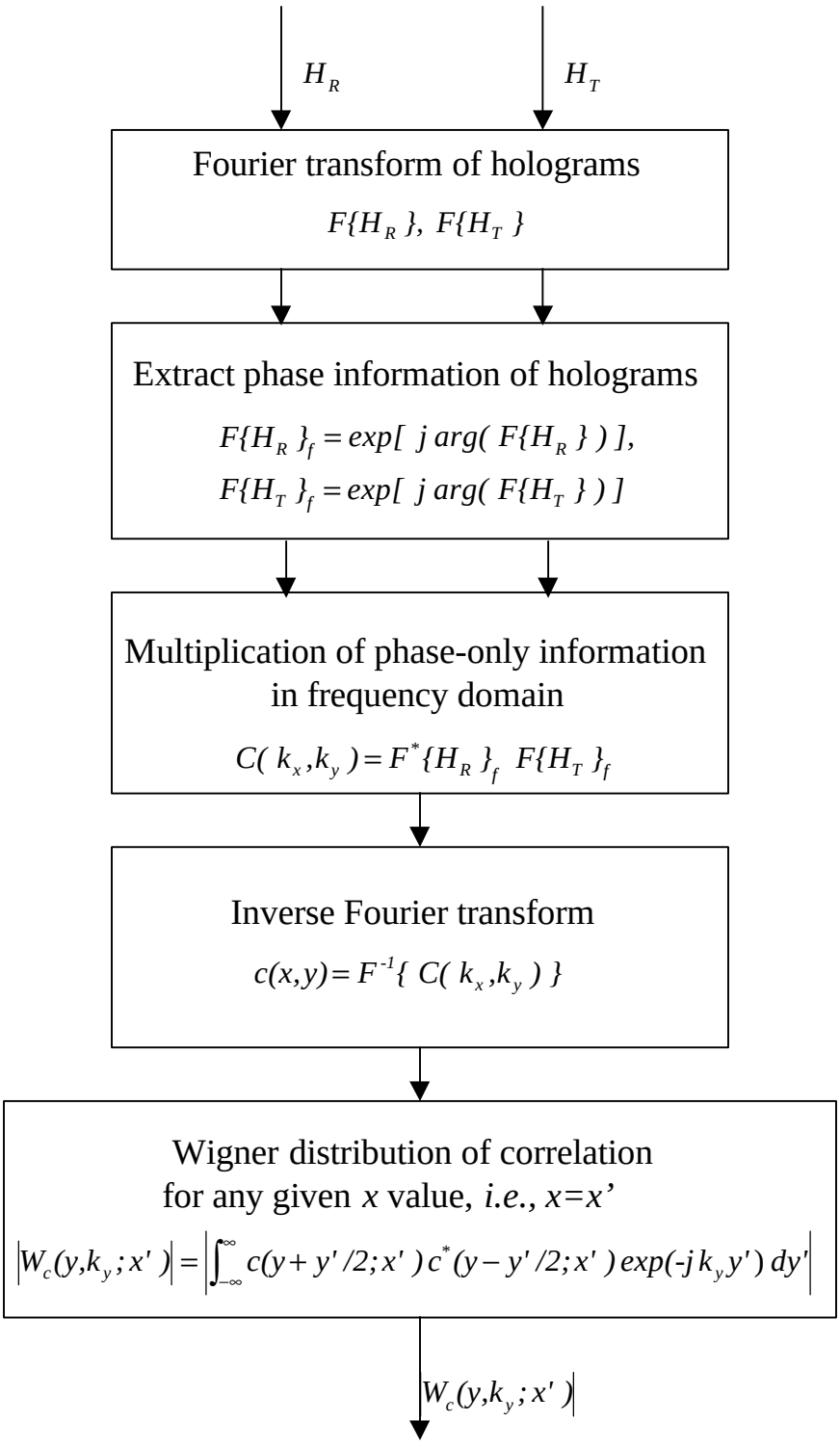

Figure (5.2-1): 3-D image matching using phase-only holographic information of the target and the reference objects and Wigner distribution.

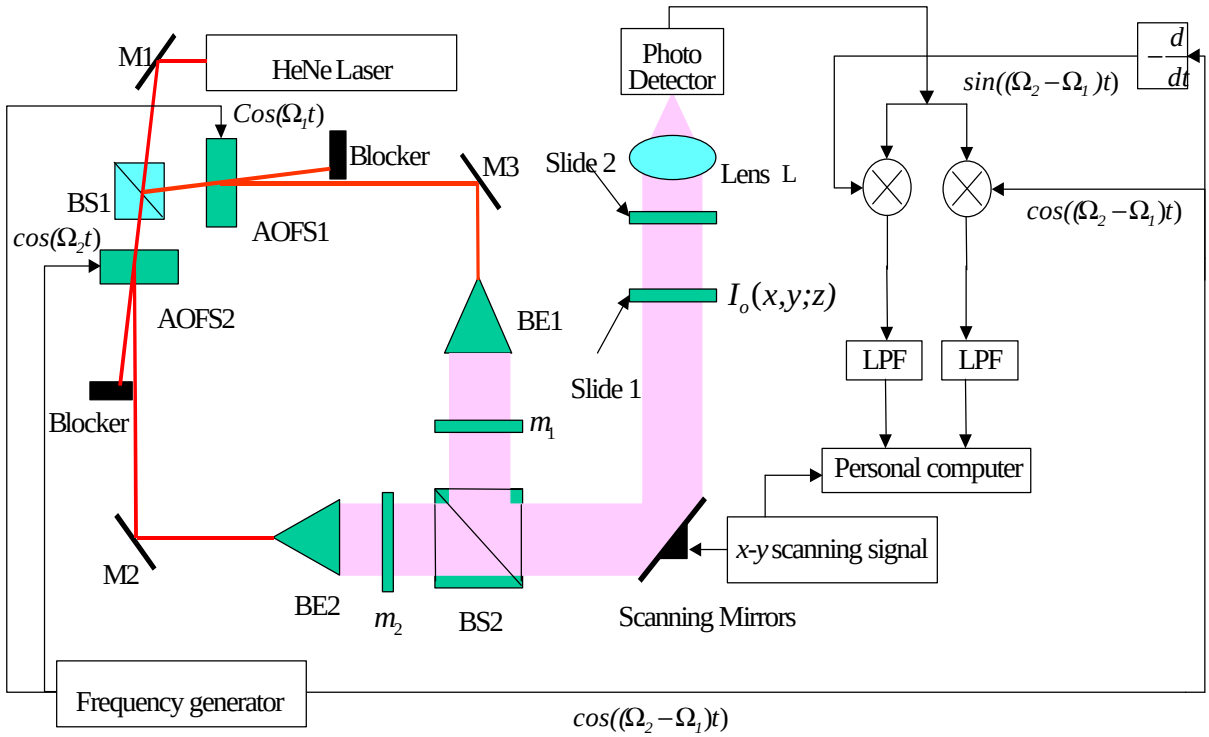

Figure (5.2-2): Optical scanning holography system.
(BS1,2: beam splitters; AOFS1,2: acousto-optic frequency shifters; M1,2,3: mirrors; BE1,2: beam expanders; $-\frac{d}{dt}$: electronic differentiator, $\otimes$ electronic multipliers; LPF: lowpass filters)

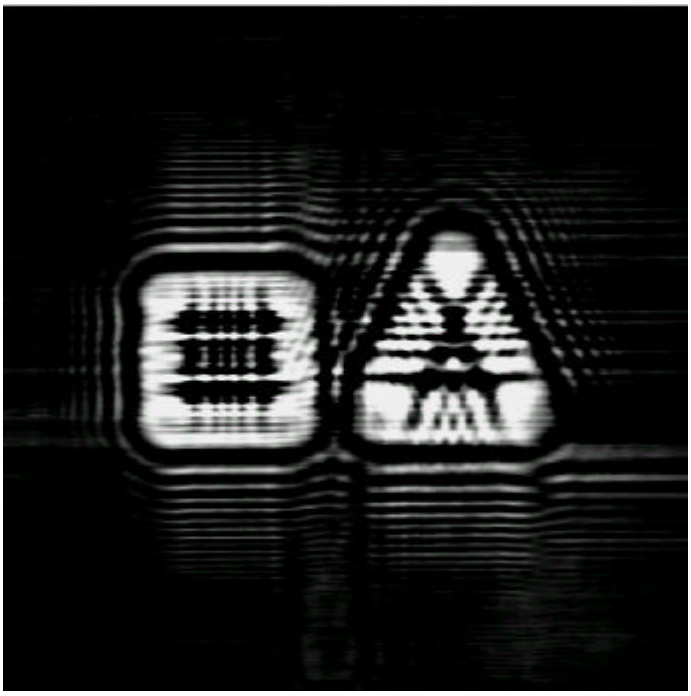

Figure (5.2-3a): Cosine- hologram of the reference object.

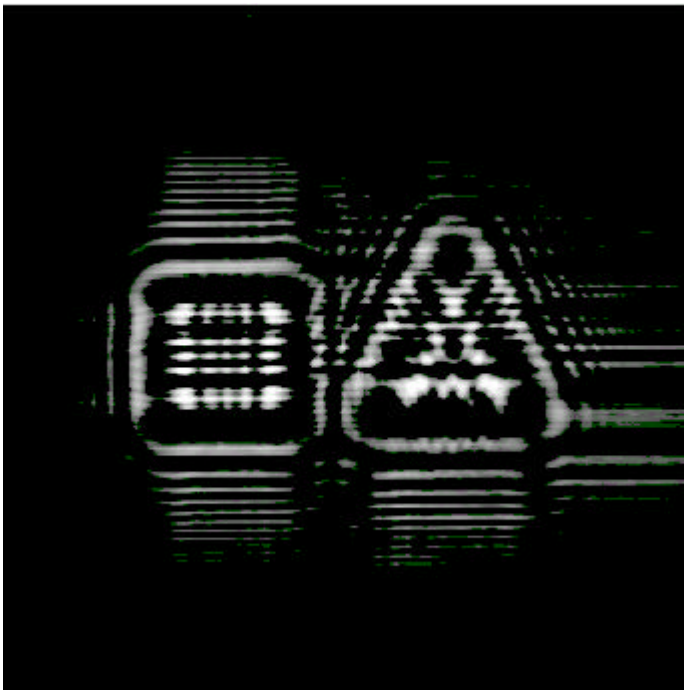

Figure (5.2-3b): Sine- hologram of the reference object.

Figure (5.2-4a): Cosine- hologram of 3-D target object with different depth location but otherwise the target object is the same as the 3-D reference object.

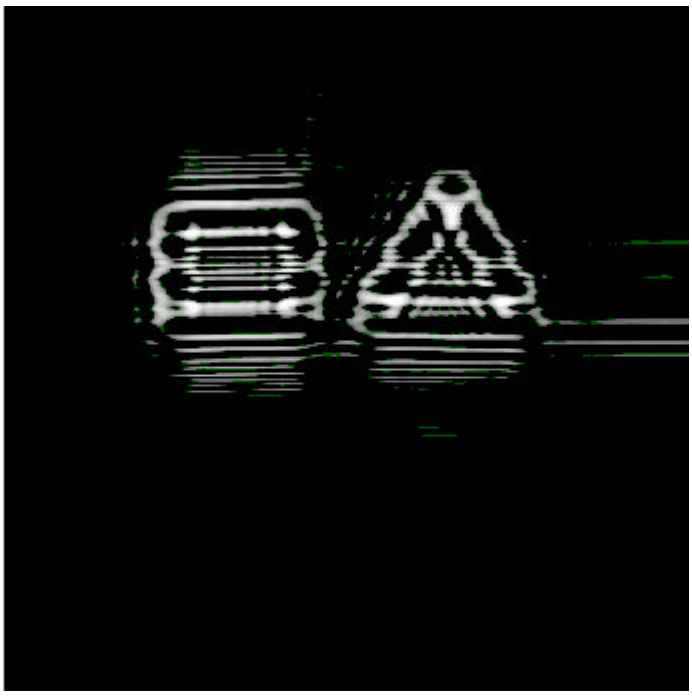

Figure (5.2-4b): Sine- hologram of a 3-D target object with different depth location but otherwise the target object is the same as the 3-D reference object.

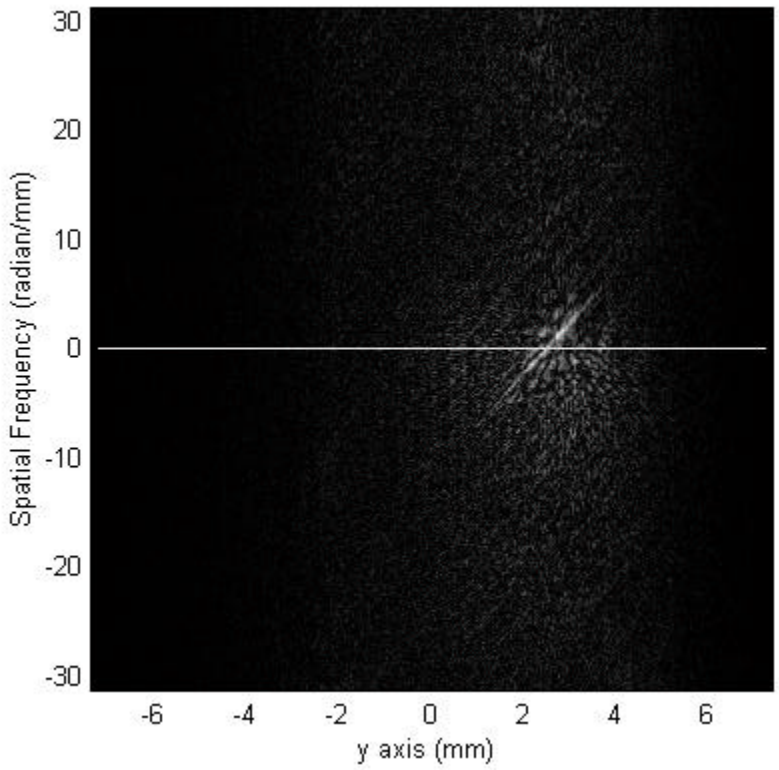

Figure (5.2-5): Wigner distribution of the correlation output when the 3-D target object and the 3-D reference object are displaced along the depth (z-direction) and along the $y-axis$, but otherwise the object and the reference is identical.

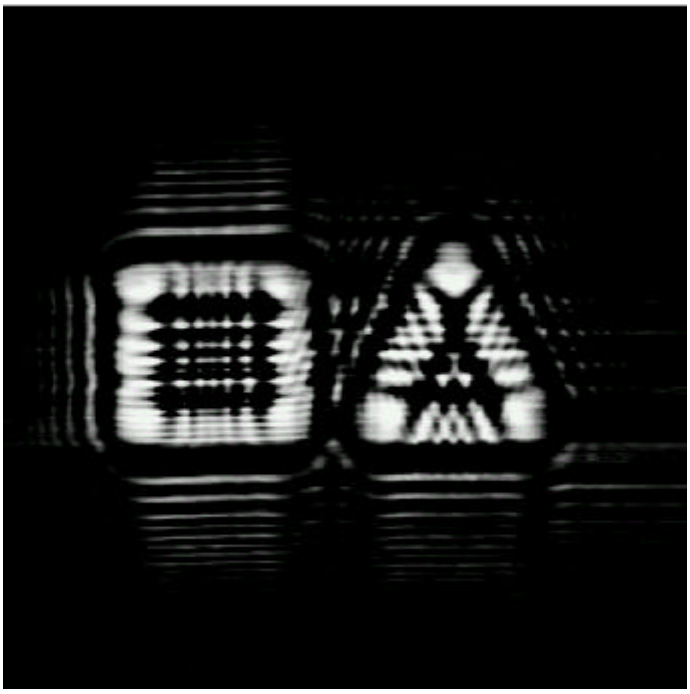

Figure (5.2-6a): Cosine-hologram of the longitudinally mismatched target object.

Figure (5.2-6b): Sine-hologram of the longitudinally mismatched target object.

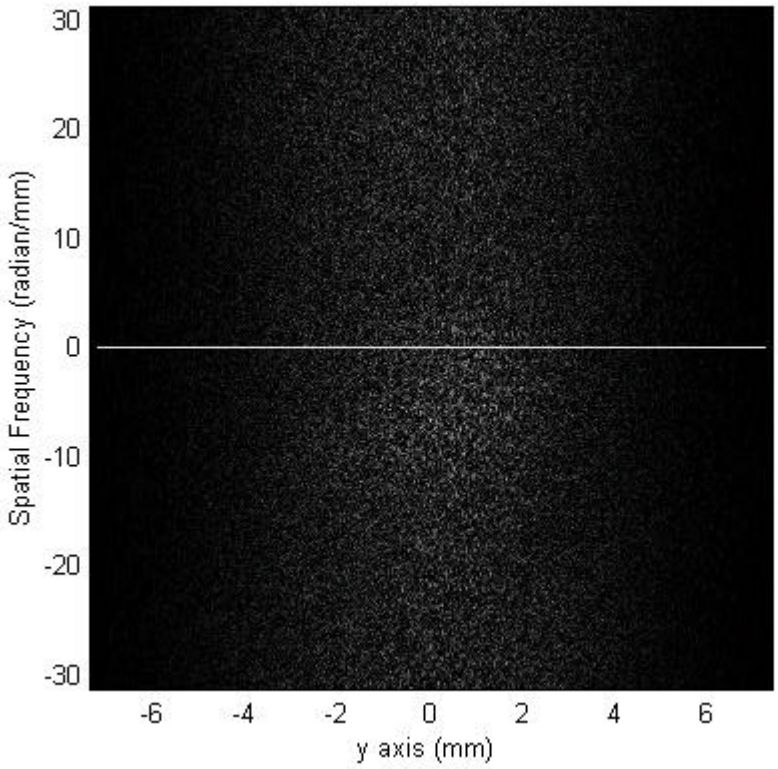

Figure (5.2-7): Wigner distribution of the correlation output when the 3-D target object that is composed of two slices that are identical with the reference object but located at different depths.

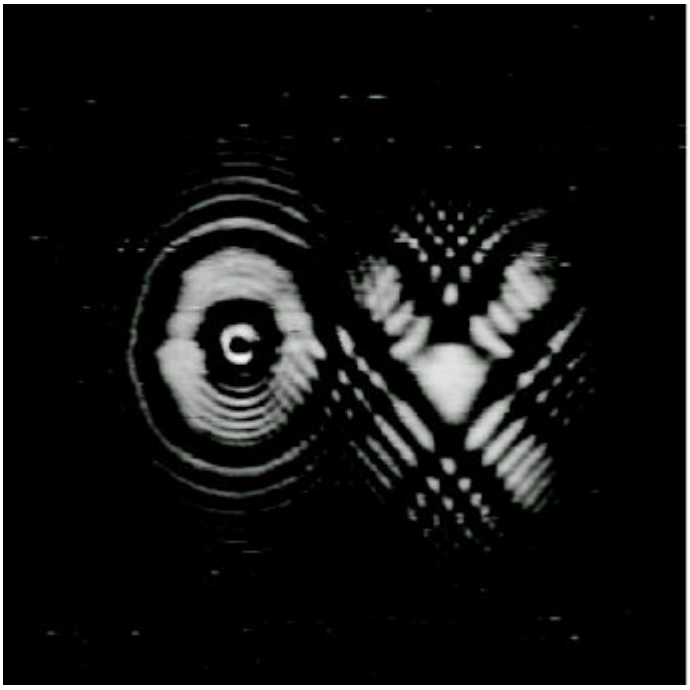

Figure (5.2-8a): Cosine-hologram of the transversely mismatched target object.

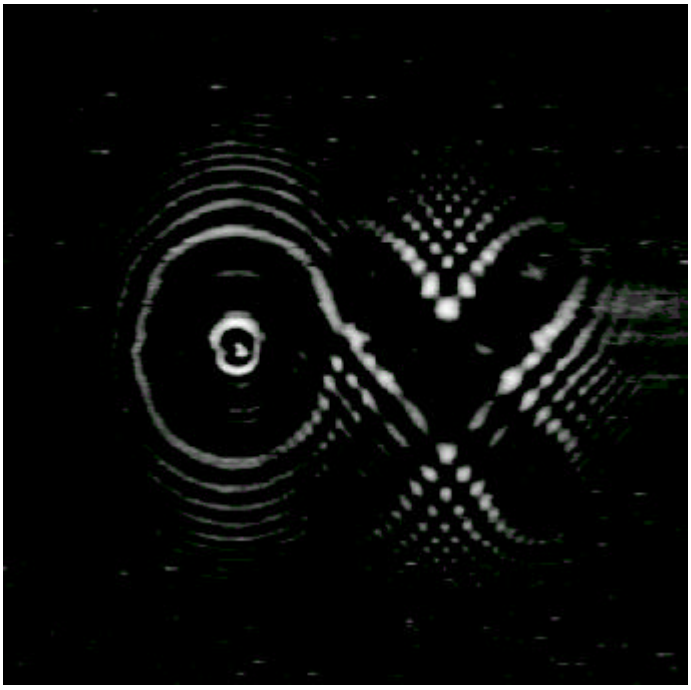

Figure (5.2-8b): Sine-hologram of the transversely mismatched target object.

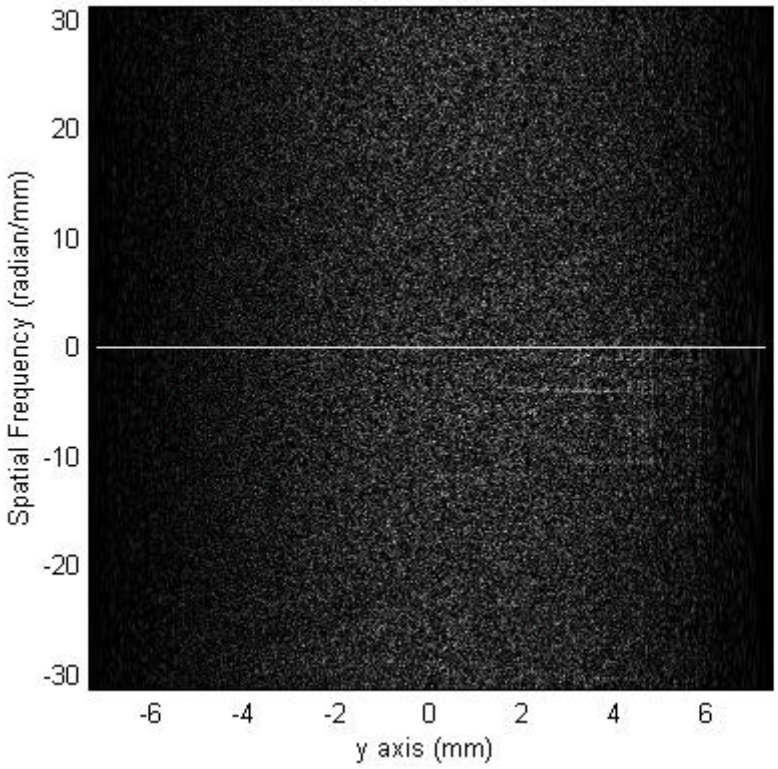

Figure (5.2-9): Wigner distribution of the correlation output when the 3-D target object that is composed of two slices whose depth locations are the same with the reference object but the 2-D patterns are different with the reference object.

Chapter 6: Conclusion

We have presented an optical technique that performs the matching of 3-D images and extracting the 3-D location of the pattern-matched object. 3-D matching and 3-D location extraction endows robust visual capabilities to the pattern recognition system and many applications in 3-D space. The optical system based on the two pupil heterodyne scanning system basically performs the 2-D correlation of the hologram of a 3-D reference object and that of a 3-D target object. It is important to point out that the 2-D correlation of the holograms can match the 3-D aspect of the 3-D objects because the hologram has depth information about the 3-D object as a form of 2-D fringe pattern, as well as transverse information about the 3-D object. A strong correlation peak results if the two holographic data match. However, the correlation output does not give a strong correlation peak when the location of the 3-D target is shifted along the depth direction because the holographic correlation is basically a 2-D correlation process. Two 3-D location extraction techniques were proposed. One proposed technique is that the defocused correlation would first be presented as a complex transparency and illuminated by laser. A z-translated CCD camera would detect the diffraction pattern and give the 3-D coordinates of the shifted correlation. The other technique is to use the Wigner distribution. The Wigner distribution is a signal transformation that yields the spatial frequency contents of a signal at different spatial instants; thus the location that is contained in the fringe pattern is extracted by the Wigner distribution. The proposed optical 3-D matching technique and the analysis techniques for extraction of the location of the matched 3-D object are promising for using holographic information about objects in the field of 3-D pattern recognition and target tracking in 3-D space. Holographic information about a 3-D object is extracted and processed just by 2-D active scanning and the location, contained as a form of fringe pattern, is extracted directly from the correlation pattern using Wigner distribution.

6.1 Summary of original contributions

1. Proposed, for the first time, to utilize the holographic information of objects in the area of 3-D optical pattern recognition.

2. Proposed 3-D optical image matching based on a two-pupil heterodyne scanning system, which extracts the holographic information of a target object, and correlates it with the holographic information of a reference object.

3. Proposed a digital signal processing technique to extract the 3-D location of the 3-D image matched object using the phase-only holographic information of the holograms and Wigner distribution.

4. Experimentally verified the principles of the proposed 3-D optical image matching system.

5. Experimentally verified the principles of the proposed 3-D location extraction technique based on the Wigner distribution.

6. Proposed a real-only hologram mask to improve the feasibility of the proposed system's implementation.

7. Proposed a phase-only hologram mask to improve the robustness of the proposed optical system.

6.2 Future research

Conventional imaging systems are dependent on the viewpoint of an observer. This makes the image matching systems vulnerable to the change of viewpoint. Especially for the object's rotation, conventional matching systems fail. Thus, matching systems are usually used at the feature extraction stage rather than the recognition stage directly. There are a lot of brilliant techniques that endow rotation invariance to 2-D image matching system. The major approaches are divided into two categories. One is the harmonic decomposition technique and the other is the synthesis discriminant function technique [41]. For the future study, we can apply the aforementioned approaches to the proposed 3-D optical image matching technique developed in the dissertation.

Besides that, we propose a new geometry of the optical scanning holography that is inherently rotation invariant, as a future study. Figure (6.2-1) shows the new geometry of the optical scanning holography that is defined in the cylindrical coordinates. The scanning beam scans an object along the perimeter of the cylinder, i.e., scanning of the object is performed about θ and z. The hologram with this geometry has the whole 360^o parallax of the object. Thus, this makes the direct matching of the holograms inherently rotation-invariant. In addition to the rotation-invariant image matching, this proposed geometry has a great potential in 3-D image display. This gives the 360^o-viewing angle to a viewer with a proper reconstruction geometry.

As the basic principles of 3-D image matching presented in this research opens a door of a new area, "Optical 3-D image matching using holographic information", the 360^o-geometry of the optical scanning holography will bring it to another level of 3-D image matching.

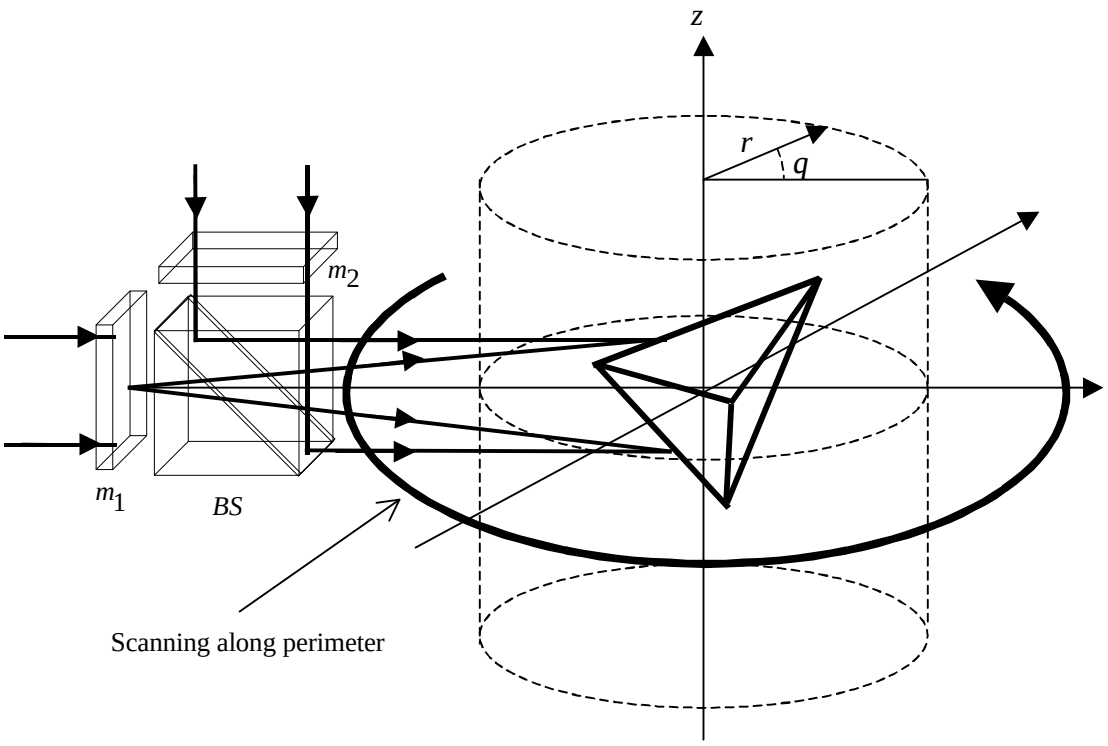

Figure (6.2-1): Proposed geometry for 360^o optical scanning holography.

References

1. Ting-Chung Poon and Taegeun Kim, "Optical image recognition of three-dimensional objects," Appl. Opt. **38**, 370-381, (1999).
2. Taegeun Kim and Ting-Chung Poon, "Extraction of 3-D location of matched 3-D object using power fringe-adjusted filtering and Wigner analysis," Opt. Eng. **38**, 2176-2183, (1999).
3. Taegeun Kim, Ting-Chung Poon , Ming Hsien Wu, Kazunori Shinoda and Yoshiji Suzuki, "Three-dimensional image matching using two-dimensional optical heterodyne scanning", Optical Memory and Neural Networks, Vol.8, No. 3, 139-145.
4. Taegeun Kim and Ting-Chung Poon, "Three-dimensional matching using phase-only holographic information and Wigner Distribution", J. Opt. Soc. Am. (accepted).
5. Anil K. Jain and Patrick J. Flynn, Three-Dimensional Object Recognition Systems (Elsevier Science Publishers 1993 Amsterdam, The Netherlands).
6. Milan Sonka, Vaclav Hlavac and Roger Boyle, Image Processing, Analysis and Machine Vision (Chapman & Hall, 1993, London, Great Britain).
7. Neil Collings,Optical pattern Recognition Using Holographic Techniques (Addison-Wesley, 1988, Great Britain).
8. G.I. Vasilenko and L.M. Tsibul'kin, "Image recognition by holography" (Plenum Publishing Corporation, 1989 NewYork).
9. J.W. Goodman, Introduction to Fourier Optics (McGraw-Hill, 1968, NewYork).
10. E.C. Tam, F.T.S. Yu, D.A. Gregory, and R.D. Juday, "Autonomous real-time object tracking with an adaptive joint transform correlator," Opt. Eng. **29,** 314-320, (1990).
11. A. B. VanderLugt, "Signal detection by complex spatial filtering," IEEE Trans. Info. Theory, IT-10, 139-145, (1964).

12. C.S. Weaver and J.W. Goodman,"A technique for optically convolving two functions," Appl. Opt. **5**, 1248,1249, (1966).
13. Special Issue on "Advances in Recognition Technique," edited by M.A. Karim, and M.S. Alam, Optical Engineering, Jan. Issue, (1998).
14. J. Hofer-Alfeis and R. Bamler, "Three- and four-dimensional convolution by coherent optical filtering," in Transformations in Optical Signal Processing, W.T. Rhodes, J. R. Fienup, and B. E.A. Saleh, eds., Proc. SPIE **373**, 77-87, (1981).
15. Y.B. Karasik, "Evaluation of three-dimensional convolutions by use of two-dimensional filtering." Appl. Opt. **36**, 7397-7401, (1997).
16. J. Rosen, "Three-dimensional electro-optical correlation," J. Opt. Soc. Am. A **15**, 430-436, (1998).
17. L. Onural and M. T. Ozgen, "Extraction of three-dimensional object-location information directly from in-line holograms using Wigner analysis," J. Opt. Soc. Am. A**9**, 252-260, (1992).
18. H. J. Caulfield, "Automated analysis of particle holograms," Opt. Eng. **24,** 462-463, (1985).
19. C. S. Vikram and M. L. Billet, "Far-filed holography at non-image planes for size analysis of small particles," Appl. Phys. B **33.,** 149-153, (1984).
20. C. S. Vikram and M. L. Billet, "On the problem of automated analysis of particle holograms: proposal for direct diffraction measurements without holography," Optik **73,** 160-162, (1986).
21. X.W. Chen, Mohammad A. Karim and Mohammad S. Alam, "Distortion-invariant fractional power fringe adjusted joint transform correlation," Opt. Eng. **37,** 138-143, (1998).
22. Mohammad S. Alam, Xue-Wen Chen, and Mohammad A. Karim, "Distortion-invariant fringe-adjusted joint transform correlation," Appl. Opt. **36,** 7422-7427, (1997).

23. T. A.C.M. Claasen and W.F.G. Mecklenbrauker, "The Wigner distribution- a tool for time-frequency signal analysis. Part 1: Continuous-time signals," Philips J. Res. **35,** 217-250, (1980).
24. T.A.C.M. Claasen and W.F.G. Mecklenbrauker, "The Wigner distribution- a tool for time-frequency signal analysis. Part 2: Discrete-time signals," Philips J. Res. **35,** 276-300, (1980).
25. Ting-Chung Poon and A. Korpel, "Optical Transfer Function of an Acousto-Optic Heterodyning Image Processor," Optics Letters **4**, 317-319, (1979).
26. Ting-Chung Poon. "Scanning Holography and Two-Dimensional Image Processing by Acousto-Optic Two-Pupil Synthesis," J. Opt. Soc. Am. A. **2**, 621-627, (1985).
27. G. Indebetouw, P. Klysubum, Taegeun Kim and Ting-Chung Poon "Imaging properties of scanning holographic microscopy," J. Opt. Soc. Am. A **17**, 380-390, (2000).
28. Ting-Chung Poon, Taegeun Kim, G. Indebetouw, B. Schilling, M.H. Wu, K. Shinoda and Y. Suzuki "Twin-image elimination experiments for three dimensional images in optical scanning holography", Optics-Letters **25**, 215-217, (2000).
29. G. Indebetouw, Taegeun Kim, Ting-Chung Poon and B. Schilling, "Three dimensional location of fluorescent inhomogeneities in turbid media by scanning heterodyne holography," Optics-Letters, **23**, 135-137, (1998).
30. A. W. Lohmann and W. T. Rhodes, "Two-pupil synthesis of optical transfer functions," Appl. Opt. **17**, 1145-1151, (1978).
31. G. Indebetouw and Ting-Chung Poon, "Novel Approaches of Incoherent Image Processing with Emphasis on Scanning Methods," Opt. Eng. **31**, 2159-2167, (1992).
32. A. Korpel, *Acousto-Optic*s (Marcel Dekker, Inc., New York,1997).

33. J. W. Goodman, *Introduction to Fourier Optics* (McGraw Hill, New York, 1968).
34. F.T.S. Yu, *Optical Information Processing* (Wiely, New York, 1983).
35. P.P. Banerjee and Ting-Chung Poon, *Principles of Applied Optics* (Richard D. Irwin, Inc., 1991).
36. Ting-Chung Poon, M. Wu, K. Shinoda, and Y. Suzuki, "Optical Scanning Holography," Proceedings of the IEEE, **84**, 753-764, (1996).
37. Joseph L. Horner and Peter D. Gianino, "Phase-only matched filtering," Appl. Opt. **23**, 812-816, (1984).
38. Joseph L. Horner, "Light utilization in optical correlators," Appl. Opt. **21**, 4511-4514, (1982).
39. A.V. Oppenheim and J.S. Lim, "The Importance of Phase in Signals," Proc. IEEE **69,** 529-541, (1981).
40. Image Processing and Measuring System (IPMS), Model DVS-3010/SS, Hamamatsu Photonics K.K., Japan and Hamamatsu Corp., Bridgewater, NJ, 1991.
41. B.V.K. Vijaya Kumar, "Tutorial survey of composite filter designs for optical correlators," Appl. Opt. **31**, 4773-4801, (1992).

Vita

Taegeun Kim was born in Seoul, Korea, on November 23, 1972. He received the B.S. degree in Electronic Engineering from Kyung Hee University, Seoul, Korea in 1996. He then joined the Electrical and Computer Engineering Department at Virginia Polytechnic Institute and State University (Virginia Tech.) where he received the M.S., and Ph.D. degrees in Electrical and Computer Engineering in 1997, and 2000, respectively. He joined the Optical Image Processing Laboratory in 1996, where he has been a research assistant. His research interests include holography, electro/acousto optics, 3-D display, optical 3-D pattern recognition, digital image processing, optical information processing. He is a member of OSA and SPIE.